Volume 2, Issue 3, September 2022

CHEMICAL SYNTHESIS

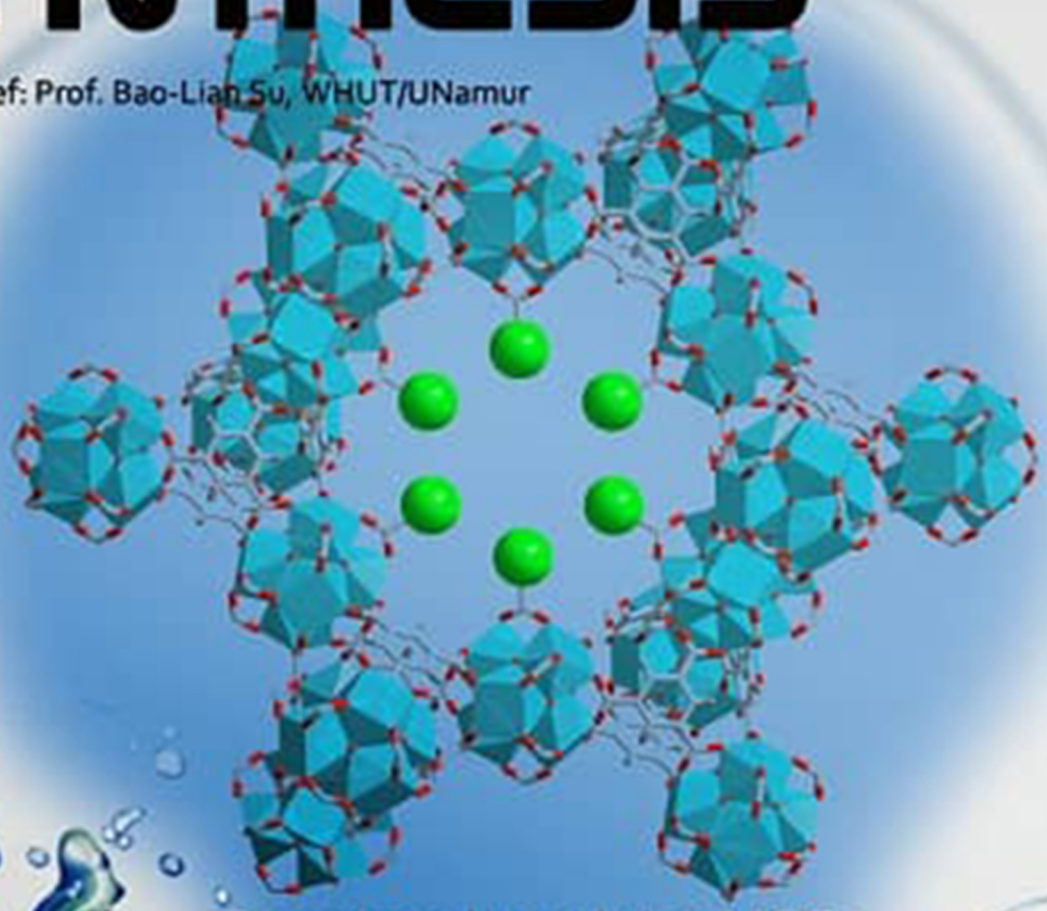

Functional modular MOFs

Customization of functional MOFs by a modular design strategy for target applications

Yaguang Peng, Qiang Tan, Hongliang Huang*, Qinggong Zhu, Xinchen Kang*, Chongli Zhong, Buxing Han*

Open Access
ISSN 2769-5247 (Online)
www.chesynjournal.com

EDITORIAL BOARD

GENERAL INFORMATION

About the Journal

Chemical Synthesis (*CS*) is an international peer-reviewed, open access, online journal. *Chemical Synthesis* is an open access peer-reviewed journal publishing original research involving all areas of the chemical sciences. The journal aims to be the premier resource of seminal and insightful research and showcases for researchers in both academia and industry, providing a platform of inspiration for the future of chemistry. *Chemical Synthesis* intends to serve as the preeminent international chemistry journal and has the ambition to be among the first choices of chemists for publication of their discoveries.

The scope of the journal focuses on the breadth of the chemical synthetic sciences, covering fields from synthetic methodologies, property studies by theoretical calculations or instrumental approaches at molecular and/or nano levels of the obtained products (materials) to the applications in catalysis, energy conversion and storage, biomedicals, pharmaceuticals, environment protection and remediation, etc.

Information for Authors

Manuscripts should be prepared in accordance with Author Instructions.
Please check www.chesynjournal.com/pages/view/author_instructions for details.
All manuscripts should be submitted online at https://oaemesas.com/login?JournalId=cs.

Copyright

Permissions

For information on how to request permissions to reproduce articles/information from this journal, please visit www.chesynjournal.com.

Disclaimer

The information and opinions presented in the journal reflect the views of the authors and not of the journal or its Editorial Board or the Publisher. Publication does not constitute endorsement by the journal. Neither the *CS* nor its publishers nor anyone else involved in creating, producing or delivering the *CS* or the materials contained therein, assumes any liability or responsibility for the accuracy, completeness, or usefulness of any information provided in the *CS*, nor shall they be liable for any direct, indirect, incidental, special, consequential or punitive damages arising out of the use of the *CS*. The *CS*, nor its publishers, nor any other party involved in the preparation of material contained in the *CS* represents or warrants that the information contained herein is in every respect accurate or complete, and they are not responsible for any errors or omissions or for the results obtained from the use of such material. Readers are encouraged to confirm the information contained herein with other sources.

Publisher

OAE Publishing Inc.
245 E Main Street st112, Alhambra, CA 91801, USA
Website: www.oaepublish.com

Contacts

E-mail: editorialoffice@chesynjournal.com
Website: www.chesynjournal.com

Chemical Synthesis

CONTENTS

Volume 2 / Issue 3 / September 2022

Yamamoto. *Chem Synth* 2022;2:14
DOI: 10.20517/cs.2022.12

Chemical Synthesis

Feature Article

Open Access

From Lewis acids to peptide chemistry

Hisashi Yamamoto*

Peptide Research Center, Chubu University, Kasugai, Aichi 487-8501, Japan.

Correspondence to: Prof. Hisashi Yamamoto, Peptide Research Center, Chubu University, 1200 Matsumoto-cho, Kasugai, Aichi 487-8501, Japan. E-mail: yamamoto.hisashi@gmail.com

How to cite this article: Yamamoto H. From Lewis acids to peptide chemistry. *Chem Synth* 2022;2:14. https://dx.doi.org/10.20517/cs.2022.12

Received: 17 May 2022 **First Decision:** 25 Jun 2022 **Revised:** 12 Jul 2022 **Accepted:** 13 Jul 2022 **Published:** 19 Jul 2022

Academic Editor: Bao-Lian Su **Copy Editor:** Peng-Juan Wen **Production Editor:** Peng-Juan Wen

Keywords: Peptides, protection free, non-racemization

INTRODUCTION

Despite the importance of peptide synthesis in medicinal chemistry, the current organic synthetic methods for peptides were developed almost 50 years ago. Completely new synthetic methodologies are therefore clearly necessary for modern organic synthesis. This article summarizes several new aspects in this regard from our laboratory.

In the 1970s, we initiated research into Lewis acids, an amazing area of organic chemistry. Lewis acids coordinate to various functional groups in substrates. After coordination, the reactivity of the functional group changes significantly. This new chemistry of Lewis acid catalysts opened a new door for initiating numerous new reactions for organic synthesis. For example, after coordination by a Lewis acid, the carbonyl group reactivity changes completely[1]. We have published numerous studies and revealed several leading principles of these new reactions[2]. However, the changes in reactivity are only for one functional group of a given substrate. This chemistry is known as a "reagent-controlled" or "catalyst-controlled" reaction. In fact, most of the organic reactions known to humans originate from reagent-controlled reactions. In contrast, most biological reactions in the human body proceed through multiple functional groups of the same substrate. This multi-functional interaction is known as a "substrate-controlled" reaction. We are interested in substrate-controlled reactions and have reported a number of reactions, including the asymmetric epoxidation of olefinic alcohols[3,4].

In 2010, I decided to change my research area and initiate research toward peptide synthesis. The history of peptide synthesis really began in the 1960s. At that time, Dr. Merrifield reported an amazingly useful solid phase peptide synthesis (SPPS), and since then, the method has been broadly used in research labs and industry. However, this method presents several serious problems that make the application of peptides as a new modality for the drug market very challenging. The issues of SPPS are as follows: linear synthesis; racemization; prevention of analysis during synthesis; exceedingly low yields; costly purification. These problems have also been discussed by major pharmaceutical companies in the important journal, *J Org Chem*[5]. In little over a decade, we succeeded in developing a completely new methodology for peptide synthesis [Figure 1]. In fact, most of our new methodology depends on substrate-controlled reactions, in spite of Merrifield's method that depends on reagent-controlled reactions.

Let me give you some examples of the differences between the two methodologies. Most of the SPPS method depends on reagent-controlled reactions. Specifically, the method depends on carboxylic acid activation. Numerous activation reagents have been developed, and in fact, many are commercially available. Our substrate-controlled reactions depend on tantalum-catalyzed reactions [Figure 2]. Ta metal has a strong affinity to oxygen but a weaker affinity to nitrogen. This unique property plays an important role in this transformation and no other metal ions work for this purpose[6-8].

Starting with this peptide synthesis, we decided to develop a completely new and transformative methodology from the previous SPPS methodology.

Importance of convergent synthesis

We have successfully changed from a linear to a convergent synthetic route [Figure 3]. This is related to the later described protecting group-free strategy, where the protecting group-free protocols for both the head and tail amino acid and carboxylic acid groups are successfully activated to realize the simultaneous synthesis from three components (m + n + o). As a result, not only can 50-peptide insulin be synthesized but also the 100-peptide limit is closer to being achieved[9].

Amide to amide transformation is reasonably rare in organic synthesis. In this case, an amide bond is activated by the Boc group of an amino acid to thus generate a new longer peptide. The method can also be used for peptide bond formation as a convergent methodology [Figure 4][10].

Use of safe solvents

In order to use solvents safe for humans, we have developed a supersilyl method that increases the lipophilicity of peptides and have successfully used ordinary solvents, such as ethyl acetate, toluene, and acetonitrile [Figure 5][10].

Reduction in use of resin materials

Since this is a solution method, the expensive solid resin is not used. In fact, solid phase peptide synthesis is based on resin, which has a rather large molecular weight and, moreover, is difficult to analyze after the reaction.

Protecting group-free synthesis

Using various inexpensive metal reactants, the first protection group-free peptide synthesis was enabled by metal ions of silicon and aluminum [Figure 6]. In both cases, the metal ion plays two roles in organic synthesis, namely, carboxylic acid activation and amino group protection[10].

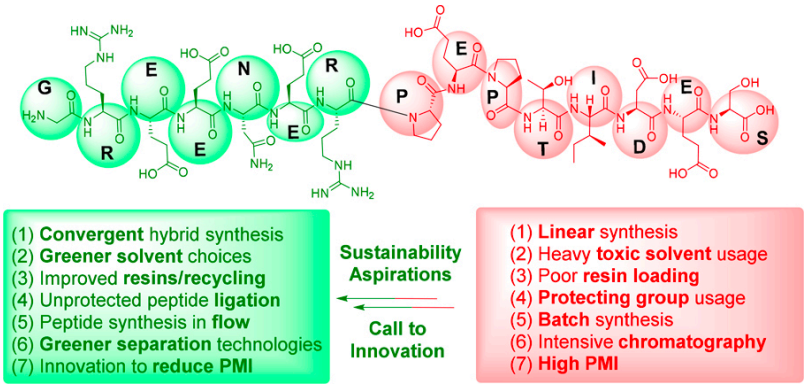

Figure 1. Necessary improvements for modern peptide synthesis (reproduced from Ref. 5[5]).

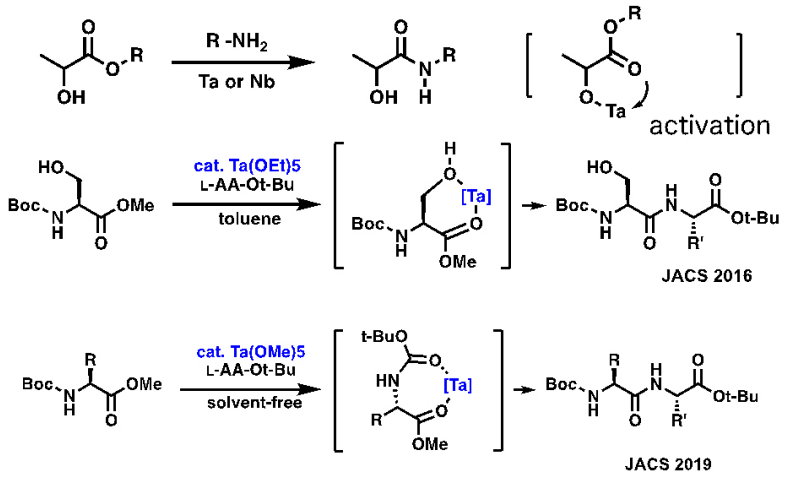

Figure 2. Substrate-controlled reactions using Ta catalysts.

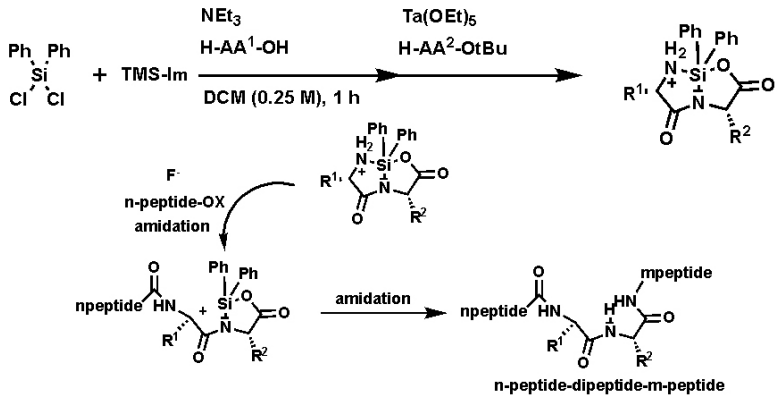

Figure 3. Convergent synthesis of peptides.

Flow synthesis

Using protecting Fmoc groups in our flow synthesis, a high purity tetrapeptide was obtained with a 90% yield in three steps [Figure 7]. Flow synthesis fulfilled the role of providing a component in the above-mentioned convergent synthesis. The pentafluorophenyl ester plays the following important roles in our

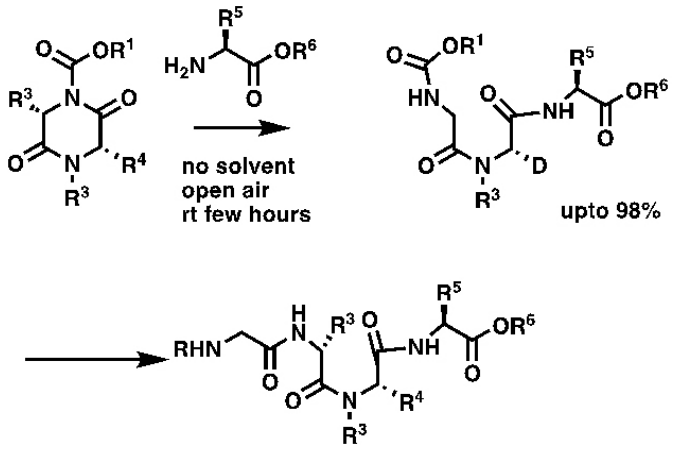

Figure 4. New method using diketopiperazines.

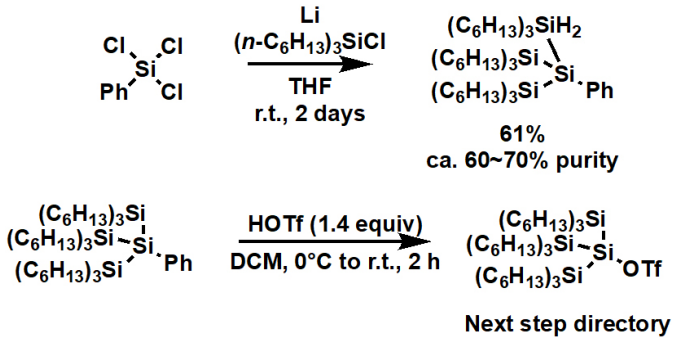

Figure 5. Supersilyl as the key to high hydrophobicity.

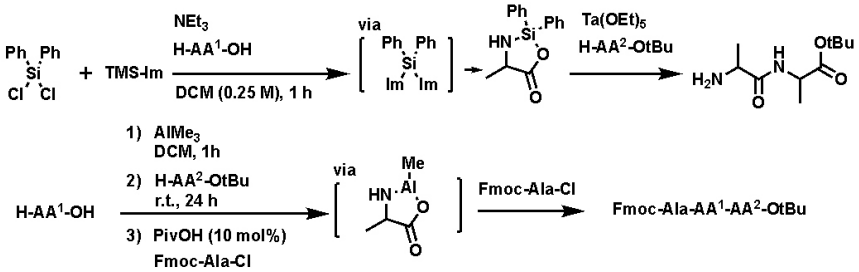

Figure 6. Concept of non-peptide synthesis.

peptide synthesis. First, it enables a high reactivity of activation of carboxylic acid. Second, it enables the reaction proceeds in three minutes at room temperature. Finally, it allows a substrate ratio of 1:1 to be used for the process[10].

Environmentally benign purification

Since this basically is not a carboxylic acid activation method, racemization does not require consideration, and because a hydrophilic supersilyl method is used, an ordinary simple short path column is sufficient [Figure 8][10].

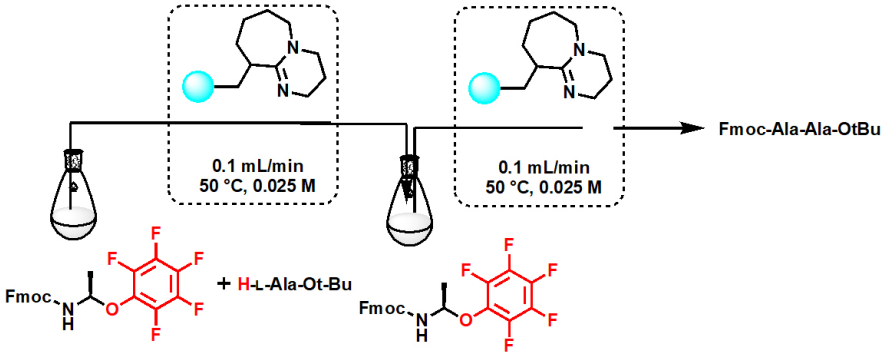

Figure 7. Flow peptide synthesis.

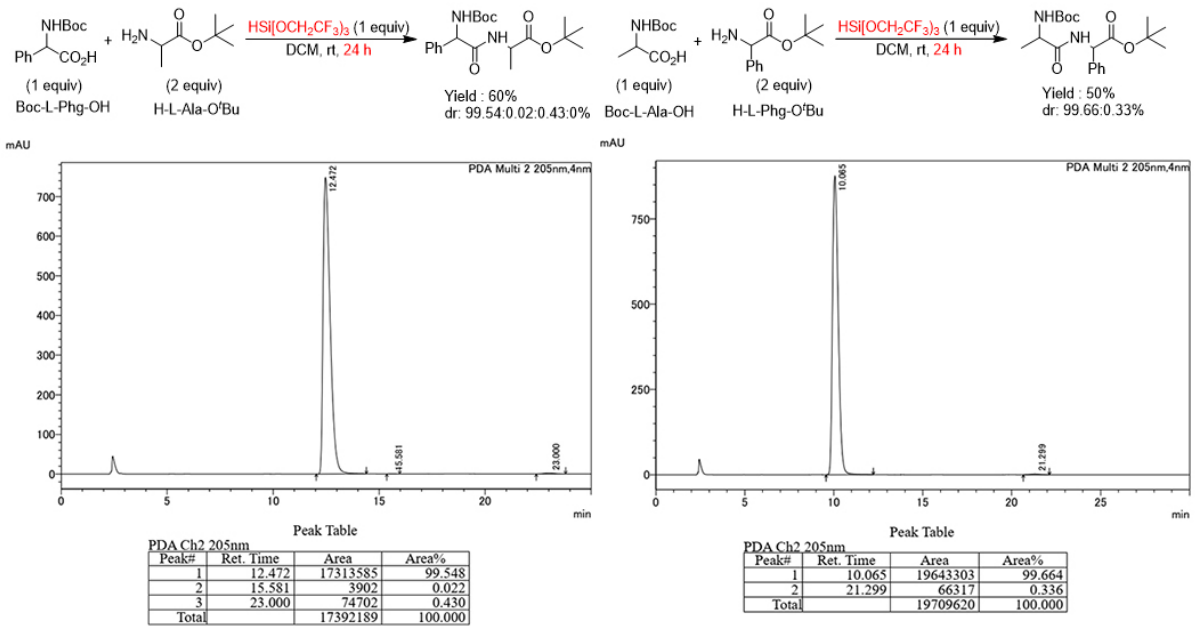

Figure 8. Non-racemization process using silicone reagent.

Reduction of process mass intensity

Because the reactants are very inexpensive and have low molecular weight, the number of steps is small, and high concentration reactions are possible, the process mass intensity is exceedingly small.

Henceforth, we can confirm the social implementation of this new synthesis method through joint research with companies and simultaneously make daily efforts to make the method more elegant. In particular, we have started to develop a catalytic reaction with less than a 1% catalyst loading without using stoichiometric reagents and further focus on developing a higher quality process using data-driven chemistry.

CONCLUSION AND OUTLOOK

Even with these findings, there remain significant opportunities for new innovation. I believe peptide synthesis is truly a science of tomorrow, and I hope more young scientists join this amazing area.

DECLARATIONS

Author's contribution

The author contributed solely to the article.

Availability of data and materials

Not applicable.

Financial support and sponsorship

None.

Conflicts of interest

The author declared that there are no conflicts of interest.

Ethical approval and consent to participate

Not applicable.

Consent for publication

Not applicable.

REFERENCES

1. Maruoka K, Ito M, Yamamoto H. Unprecedented nucleophilic addition of organolithiums to aromatic aldehydes and ketones by complexation with aluminum tris(2,6-diphenylphenoxide). *J Am Chem Soc* 1995;117:9091-2. DOI
2. Yamamoto H, Futatsugi K. "Designer acids": combined acid catalysis for asymmetric synthesis. *Angew Chem Int Ed Engl* 2005;44:1924-42. DOI PubMed
3. Bhadra S, Yamamoto H. Substrate directed asymmetric reactions. *Chem Rev* 2018;118:3391-446. DOI PubMed
4. Sawano T, Yamamoto H. Substrate-directed catalytic selective chemical reactions. *J Org Chem* 2018;83:4889-904. DOI PubMed
5. Isidro-Llobet A, Kenworthy MN, Mukherjee S, et al. Sustainability challenges in peptide synthesis and purification: from R&D to production. *J Org Chem* 2019;84:4615-28. DOI PubMed
6. Tsuji H, Yamamoto H. Hydroxy-directed amidation of carboxylic acid esters using a tantalum alkoxide catalyst. *J Am Chem Soc* 2016;138:14218-21. DOI PubMed
7. Muramatsu W, Hattori T, Yamamoto H. Substrate-directed lewis-acid catalysis for peptide synthesis. *J Am Chem Soc* 2019;141:12288-95. DOI PubMed
8. Muramatsu W, Yamamoto H. Peptide bond formation of amino acids by transient masking with silylating reagents. *J Am Chem Soc* 2021;143:6792-7. DOI PubMed
9. Hattori T, Yamamoto H. Synthesis of silacyclic dipeptides: peptide elongation at both N- and C-termini of dipeptide. *J Am Chem Soc* 2022;144:1758-65. DOI PubMed
10. Yamamoto H. Unpublished.

Peng *et al. Chem Synth* 2022;2:15
DOI: 10.20517/cs.2022.15

Chemical Synthesis

Research Article

Open Access

Customization of functional MOFs by a modular design strategy for target applications

Yaguang Peng[1,2], Qiang Tan[1], Hongliang Huang[1,*], Qinggong Zhu[2], Xinchen Kang[2,3,*], Chongli Zhong[1], Buxing Han[2,3,*]

[1]State Key Laboratory of Separation Membranes and Membrane Processes, School of Chemical Engineering and Technology, Tiangong University, Tianjin 300387, China.
[2]Beijing National Laboratory for Molecular Sciences, Key Laboratory of Colloid, Interface and Thermodynamics, CAS Research/Education Center for Excellence in Molecular Sciences, Institute of Chemistry, Chinese Academy of Sciences, Beijing 100190, China.
[3]School of Chemistry, University of Chinese Academy of Sciences, Beijing 100049, China.

[*]**Correspondence to:** Prof./Dr. Hongliang Huang, State Key Laboratory of Separation Membranes and Membrane Processes, School of Chemical Engineering and Technology, Tiangong University, No. 399 BinShuiXi Road, Tianjin 300387, China. E-mail: huanghongliang@tiangong.edu.cn; Prof./Dr. Xinchen Kang, Beijing National Laboratory for Molecular Sciences, Key Laboratory of Colloid, Interface and Thermodynamics, CAS Research/Education Center for Excellence in Molecular Sciences, Institute of Chemistry, Chinese Academy of Sciences, No. 2 Zhongguancun North First Street, Beijing 100190, China. E-mail: kangxinchen@iccas.ac.cn; Prof./Dr. Buxing Han, Beijing National Laboratory for Molecular Sciences, Key Laboratory of Colloid, Interface and Thermodynamics, CAS Research/Education Center for Excellence in Molecular Sciences, Institute of Chemistry, Chinese Academy of Sciences, No. 2 Zhongguancun North First Street, Beijing 100190, China. E-mail: hanbx@iccas.ac.cn

How to cite this article: Peng Y, Tan Q, Huang H, Zhu Q, Kang X, Zhong C, Han B. Customization of functional MOFs by a modular design strategy for target applications. *Chem Synth* 2022;2:15. https://dx.doi.org/10.20517/cs.2022.15

Received: 13 Jun 2022 **First Decision:** 8 Jul 2022 **Revised:** 20 Jul 2022 **Accepted:** 21 Jul 2022 **Published:** 28 Jul 2022

Academic Editors: Bao-Lian Su, Teng Ben **Copy Editor:** Peng-Juan Wen **Production Editor:** Peng-Juan Wen

Abstract

Herein, we propose a versatile "functional modular assembly" strategy for customizing MOFs that allows installing the desired functional unit into a host material. The functional unit could be switched according to different applications. MOF-808, a highly stable Zr-MOF containing dangling formate groups, was selected as a host material for demonstration. Functional molecules with carboxyl connectors can be directly inserted into MOF-808 to form functional modular MOFs (FM-MOFs) through single substitution, while for those without carboxyl connectors, a pre-designed convertor was grafted firstly followed by the functional molecules in a stepwise manner. A series of tailor-made FM-MOFs were generated and show excellent performance toward different applications, such as adsorption, catalysis, fluorescent sensing, electrochemistry, and the control of surface wettability. On the other hand, the functional units on the FM-MOFs can switch freely and completely via full interconversion, as well as partly to construct multivariate MOFs (MTV-MOFs). Therefore, this strategy provides a

benchmark for rapid customization of functional MOFs for diverse applications that can realize the rapid modular design of materials.

Keywords: Metal-organic frameworks, functionality, modular design strategy, customization

INTRODUCTION

Porous materials have been attracting intense attention owing to their wide range of potential applications[1,2]. Rational design and functional targeting synthesis of porous materials on demand by the introduction of functional groups or molecules are essential for practical application[3,4]. It is relatively difficult to insert and modify functional groups in the structures of conventional porous solids such as zeolites and activated carbons, especially at the molecular level, whereas metal-organic frameworks (MOFs), newly developed porous crystalline materials constructed by metal clusters and organic linkers, are acknowledged to be relatively easy in this regard[5-9]. Because of their highly diversified structure, tailorable porosity, and tunable functionality, MOFs show great potential in various areas including adsorption[10-12], catalysis[13,14], chemical sensing[15,16], and electrochemistry[17,18]. Endowed with these fantastic features, MOFs are an ideal platform to customize functional materials on demand. Currently, various functional methods have been used in different kinds of MOF materials for a given system[19-21]. However, these functional approaches sometimes have poor versatility and are difficult to extend to other host MOFs or functional molecules[22]. In some cases, time- and resource-intensive processes are needed to find and design requisite host materials, functional parts, and their appropriate connection modes in each unit operation. Besides, it is also relatively difficult to impart some complex but useful functional molecules into MOF structures through direct postsynthetic substitution or sophisticated organic synthesis. Considering the variety and complexity of practical demands, a general strategy that allows the versatile and facile customization of MOFs according to a wide variety of applications is highly desirable yet remains a challenge to date.

To tackle the above-mentioned question, we here propose a "functional modular assembly" (FMA) strategy for customizing MOFs - a versatile conceptual approach that allows installing desired functional units into a host MOF material, opening up the possibility of assembling modular devices according to practical requirements. Such a novel strategy should possess the following features: (i) the functional module on the host MOF can be installed and switched freely, acting as a "plug and socket", and thus a proper functional unit can be inserted for a targeted application; (ii) to enrich modular diversity, the accessible functional molecules should be modularized as much as possible; (iii) the assembly step of installing functional modules onto host MOF should be accomplished in a simple manner, thereby facilitating target customization of MOFs in a facile and efficient way; and (iv) the host MOF material should be stable enough to be used in different conditions. In addition, as most MOFs are moisture sensitive and unstable in aqueous media, developing stable hydrophobic MOFs is necessary for practical applications[23,24].

To fulfill this goal, the proper connection mode between host material and modules is firstly needed. Considering the reversibility of coordination bonds in MOFs, postsynthetic substitution appears to be a reliable and simple approach to implementing installing and switching functional modules in MOFs. Moreover, combining different functional modules into one host MOF through multi-substitution may also open up the possibility of constructing multivariate MOFs (MTV-MOFs) for a target application. In this work, as a proof-of-concept experiment, we demonstrate that such a "functional modular assembly" strategy can be achieved on the highly robust MOF-808. This Zr-MOF was chosen as a host material for the following two reasons: (i) exceptional water/chemical stability; and (ii) the dangling formate groups on Zr_6 clusters are prone to be substituted by other ligands with carboxyl groups in a simple way, making it easy to

graft functional molecules/active fragments onto the host material. These interesting features of MOF-808 stimulate us to try to use the carboxyl group as a connector to assemble functional modular MOFs (FM-MOFs). Functional molecules with a carboxyl connector can be directly inserted into MOF-808 through single substitution. For functional molecules without a connector, we insert a pre-designed convertor and modules in a stepwise manner by tandem postsynthetic modification. That is, the convertor has two different terminals that can combine modules and MOF-808, respectively. Theoretically, a wide range of accessible functional molecules could be used as modules in the assembly process, thus generating practically numerous distinct new MOFs for functional targeting customization. To prove the feasibility of our strategy, several applications from completely different fields including adsorption, catalysis, fluorescent sensing, electrochemistry, and the control of surface wettability were selected as examples. Such tailor-made FM-MOFs exhibit excellent performance toward different target applications. Moreover, the functional units on our FM-MOFs can fully interconvert via a simple solvothermal method, readily implementing the installing and switching of modules in MOFs freely. Interestingly, we also found that two functional modules can be assembled into MOF-808 through partial conversion to construct multivariate FM-MOFs. Overall, this functional modular assembly strategy enables MOFs to achieve the goals of multi-modules, multi-objectives, switchable modules, and interfunctional coordination, providing a general and simple route for the rapid targeting customization of functional MOFs on demands.

RESULTS AND DISCUSSION

Customization of FM-MOFs by single substitution

A schematic illustration of the construction of FM-MOFs is shown in Scheme 1. Theoretically, in the assembly process, various desired functional modules could be imparted into the host framework to customize FM-MOFs according to arbitrary target applications. Thus, it is imperative to ensure that the various functional molecules can be modularized as much as possible. Considering that labile formate groups on MOF-808 are easy to be substituted, a carboxyl group can serve as a connector to impart functional molecules into MOF-808. To specify this concept, several applications including Hg^{2+} capture, Ag^{+} recovery, proton conductivity, detection of nitro explosives, and the control of surface wettability were taken as examples. We subsequently used thioglycollic acid (M1, M refers to module), propiolic acid (M2), oxalic acid (M3), pyrenecarboxylic acid (M4), and perfluorooctanoic acid (M5) to assemble series of FM-MOFs based on MOF-808 according to respective target applications [Figure 1 and Supplementary Figure 1]. Supplementary Figure 2 shows the PXRD patterns of MOF-808 and its functional derivatives. It is obvious that the related peaks of these assembled FM-MOFs are in good agreement with that of pristine MOF-808, confirming that the crystal structure of these materials remains intact after functional modules insertion. N_2 adsorption-desorption isotherms of FM-MOFs measured at 77 K display a typical I isotherm, suggesting the reservation of microporous features after introducing functional units into the framework, despite a decrease in their BET surface areas [Supplementary Figure 3]. The scanning electron microscopy (SEM) images demonstrate that our FM-MOFs possess octahedral morphology, with no apparent morphology change observed compared with MOF-808 [Supplementary Figure 4]. Individually, given that the thiolate ligand possesses a strong coordination ability to Hg^{2+}, thioglycollic acid (M1) was used as a functional modular to construct FM-MOF-1 for Hg^{2+} capture. The successful insertion of M1 into MOF-808 was also proved by Fourier transform infrared (FT-IR) spectroscopy, ^{1}H nuclear magnetic resonance (NMR) spectroscopy, and elemental analysis. The FT-IR spectra of FM-MOF-1 reveal that there is a new peak at 2564 cm^{-1} [Supplementary Figure 5], which can be attributed to the S-H stretching of free -SH groups. Supplementary Figure 6 shows the ^{1}H NMR spectra of FM-MOF-1 and MOF-808 after dissolving the samples in KOH/D_2O solution. Obviously, the peak intensity at δ = 8.3 ppm corresponding to the hydrogen of formate of FM-MOF-1 significantly decreased and a new peak at δ = 2.8 ppm for the hydrogen signal of $-CH_2-$ in M1 appeared, indicating that formate ligands on Zr_6 clusters were substituted by M1 molecules. All

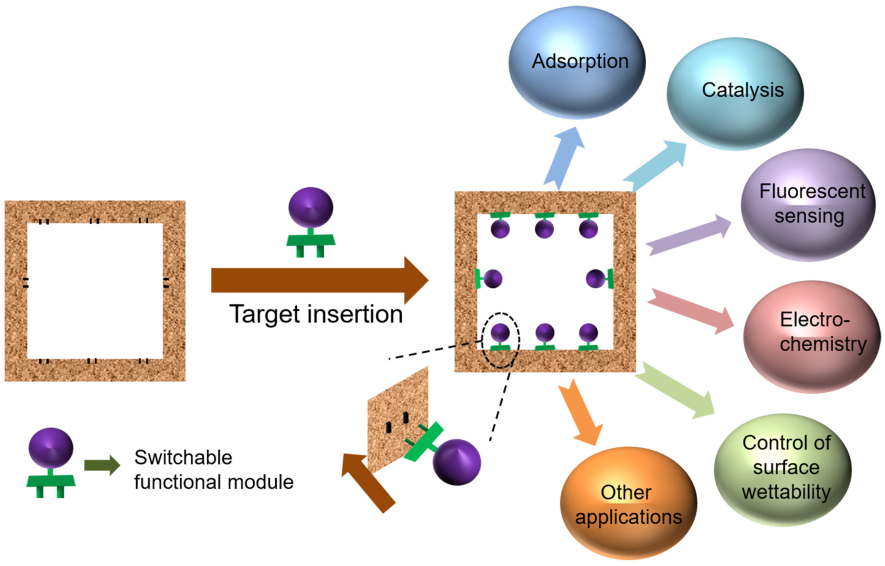

Scheme 1. Illustration of customization of FM-MOFs toward different applications.

these observations demonstrate that M1 was successfully inserted into the framework of MOF-808. To evaluate the effectiveness of FM-MOF-1 for Hg^{2+} capture, adsorption kinetics and isotherms were measured. As shown in Figure 1B and Supplementary Figure 7, an extremely quick process was observed for FM-MOF-1. Over 99% of Hg^{2+} was removed within 5 min. Supplementary Figure 8 shows the adsorption isotherms of FM-MOF-1 towards Hg^{2+}. By fitting with Langmuir model, the saturated Hg^{2+} removal capacity of FM-MOF-1 was estimated to be 758 mg g^{-1}, suggesting the great potential of FM-MOF-1 for Hg^{2+} capture. Similarly, considering the strong affinity of the terminal alkynyl group toward Ag^{+}, propiolic acid (M2) was selected as another functional module to assemble FM-MOF-2 for silver recovery. FT-IR and ^{1}H NMR spectra were used to demonstrate the successful insertion of M2 into the framework of MOF-808 [Supplementary Figures 9 and 10]. Supplementary Figure 11 shows the adsorption kinetics of FM-MOF-2 towards Ag^{+}; the removal efficiency increased sharply during the initial stage and then approached equilibrium after 2 h of contact. The adsorption isotherm revealed that FM-MOF-2 exhibits high silver uptake [Figure 1C]. By fitting with Langmuir model, the saturated Ag^{+} uptake capacity was calculated to be 806 mg g^{-1}, surpassing most reported porous materials [Supplementary Table 1][25-34]. This is also the first study of introducing alkynyl groups into the MOF framework for Ag^{+} recovery. Besides, to construct the proton-conducting MOF, we used oxalic acid as the functional module to assemble FM-MOF-3. The detailed characterizations are provided in the Supplementary Materials [Supplementary Figures 12-14]. Proton conductivities were then checked on a pressed plate at varying relative humidity (RH) from 33% to 100% at 298 K for FM-MOF-3. As shown in Supplementary Figure 15, all of the Nyquist plots display circular arcs at high frequencies. The proton conductivity of FM-MOF-3 increased with the elevated moisture [Figure 1D], suggesting water molecules play a vital role in the proton transportation of this MOF. Meanwhile, FM-MOF-3 exhibited a striking proton conductivity of 1.2 10^{-2} S cm^{-1} at 298 K and 100% RH, whereas the original MOF-808 displayed an inferior proton conductivity of 2.2 10^{-6} S cm^{-1} under the same condition [Supplementary Figure 16]. It should be noted that only a few MOFs featuring high proton conductivity over 10^{-2} S cm^{-1} have been reported[35-37]. Moreover, to achieve the goals of detecting nitro explosives and controlling surface wettability, conjugated pyrenecarboxylic acid (M4) and perfluorooctanoic acid (M5) were utilized as modules to construct FM-MOF-4 and FM-MOF-5, respectively. The related characterizations can be found in the Supplementary Materials [Supplementary Figures 17-20]. To investigate the explosive sensing ability of FM-MOF-4, fluorescence quenching titrations were conducted by

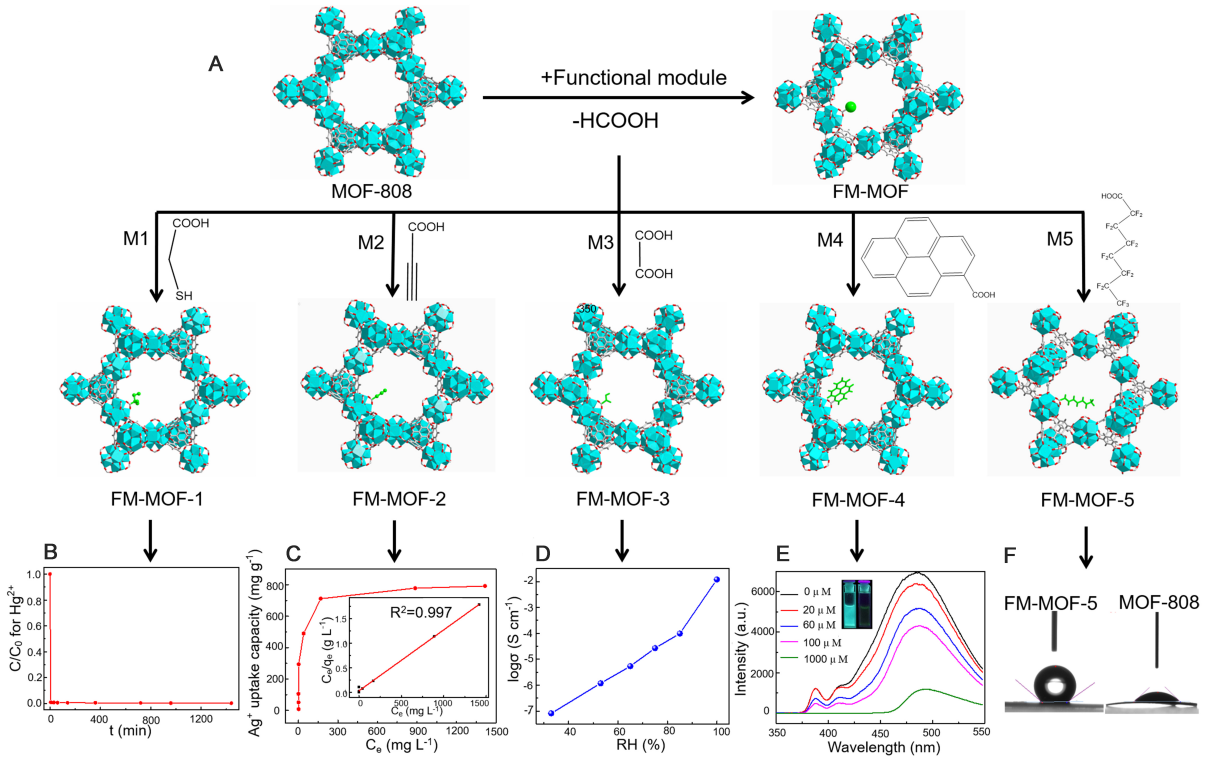

Figure 1. Customization of FM-MOFs through single substitution. (A) Schematic illustration of constructing FM-MOFs by functional modules with carboxyl connector. (B) Hg^{2+} adsorption kinetics of FM-MOF-1 at the initial concentration of 10 ppm. (C) Ag^{+} adsorption isotherm for FM-MOF-2. The inset shows the linear regression by fitting the experimental data with the Langmuir model. (D) Humidity dependence of the proton conductivities in FM-MOF-3 at room temperature. (E) The effect on the emission spectra of FM-MOF-4 dispersed in DMF upon incremental addition of a TNP solution (1 mM). The inset shows the original fluorescence and the decreased fluorescence upon the addition of TNP solution (1 mM). (F) Contact angle images of FM-MOF-5 and MOF-808.

the increasing amount of nitro aromatics. As shown in Figure 1E, fast and significant fluorescence quenching was observed with an increase in the amount of TNP (2,4,6-trinitrophenol). The fluorescence quenching could be discerned at a low concentration (0.5 μM; Supplementary Figure 21) and reached nearly 83% when the concentration of TNP increases to 1 mM. By contrast, other nitro compounds have little effect on the fluorescence intensity [Supplementary Figure 22]. These results demonstrate that FM-MOF-4 could selectively and sensitively detect TNP over other nitro explosives. On the other hand, the surface wettability of FM-MOF-5 and MOF-808 was also examined by contact angle measurements. As shown in Figure 1F, the contact angle of water on MOF-808 was estimated to be 37°, whereas FM-MOF-5 gave the water contact angle at as high as 142°. The surface character of MOF-808 transformed from hydrophilic to hydrophobic after M5 insertion into the framework, confirming the coating of perfluoroalkyl groups on the surface of material can dramatically enhance its hydrophobicity. This hydrophobic behavior of FM-MOF-5 was also illustrated by water vapor adsorption experiment: the water uptakes of MOF-808 reduced significantly after the incorporation of M5 [Supplementary Figure 23].

Customization of FM-MOFs through tandem postsynthetic modification

The above proof-of-concept experiments revealed that functional molecules with carboxyl groups can be used as modules to insert into MOF-808 directly according to numerous target applications. However, to expand the scope of our strategy, some useful functional molecules without carboxyl groups should also be modularized. To solve this problem, we installed a pre-designed convertor into MOF-808 before functional modules insertion through a tandem postsynthetic modification [Figure 2]. Such convertors should have

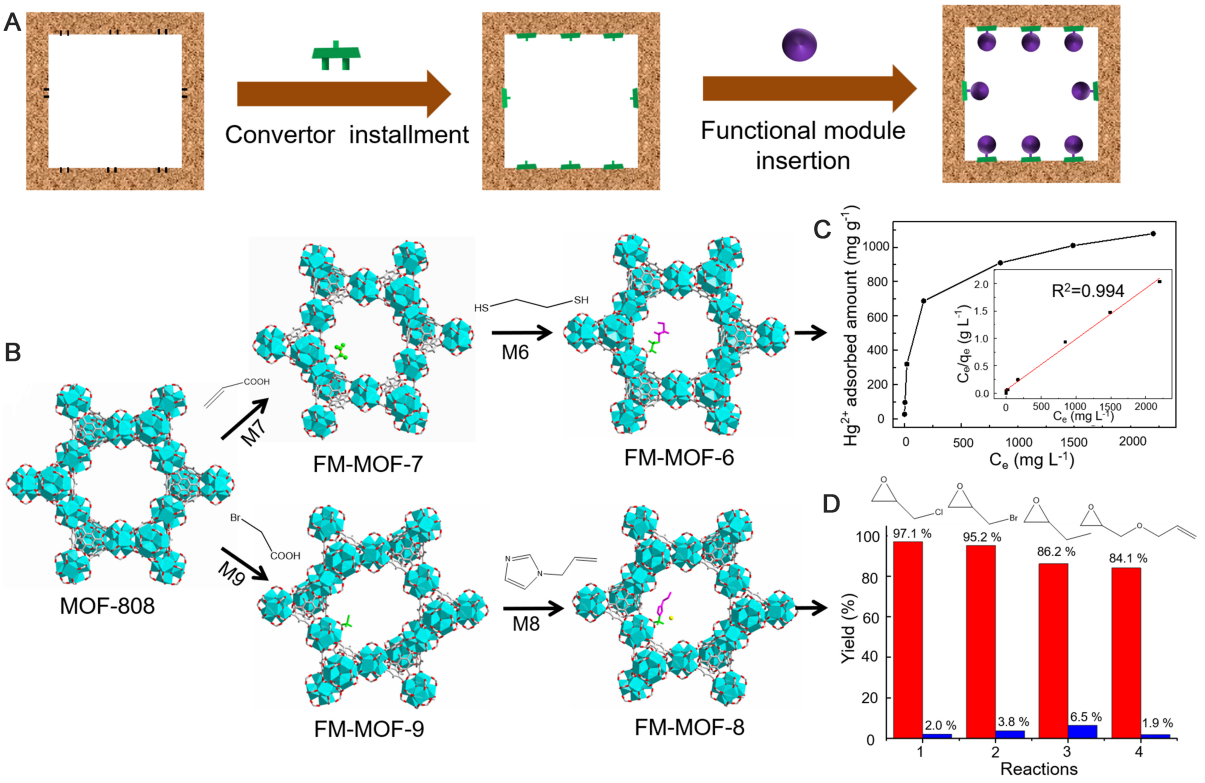

Figure 2. Customization of FM-MOFs through tandem postsynthetic modification. (A and B) Scheme illustration of FM-MOFs and their pore structures. (C) Hg^{2+} adsorption isotherm of FM-MOF-6. The inset shows the linear regression by fitting the experimental data with the Langmuir model. (D) Yields of various cyclic carbonates prepared from the cycloaddition of CO_2 with related epoxides catalyzed by FM-MOF-8 (red) and FM-MOF-9 (blue).

two terminals that can combine modules and the host framework, respectively. Here, the aforementioned Hg^{2+} capture and CO_2 conversion were taken as target applications to fully illustrate this. Firstly, we tried to use thioglycollic acid (M1) to construct FM-MOF-1 for mercury adsorption. Considering a functional unit with more chelating sites is needed to achieve higher Hg^{2+} uptake capacity, 1,2-ethanedithiol (M6) containing higher sulfur content yet without carboxyl group compared with M1 was adopted. To impart M6 on MOF-808, we chose propenoic acid (M7) as a convertor and inserted it into the host framework firstly to construct FM-MOF-7, where the accessible vinyl groups could allow for further chemical modifications. As shown in Supplementary Figures 24-28, FM-MOF-7 was characterized by PXRD, N_2 adsorption, SEM, FT-IR, and ^{1}H NMR. FT-IR spectra reveal the appearance of a new characteristic peak at 1639 cm^{-1} compared with MOF-808, which can be attributed to the C=C stretching band of vinyl groups [Supplementary Figure 27]. ^{1}H NMR spectra demonstrate that the peak at 8.3 ppm assigned to the formate groups disappeared and several strong peaks around 5.0-7.0 ppm corresponding to the vinyl groups emerged, indicating the successful insertion of M7 into MOF-808 [Supplementary Figure 28]. FM-MOF-7 was then treated with 1,2-ethanedithiol (M6) to obtain FM-MOF-6 through the thiol-ene "click" reaction between thiol compounds and the vinyl groups in FM-MOF-7. The resulting material was also carefully characterized by PXRD, N_2 adsorption, FT-IR, SEM, and NMR [Supplementary Figures 29-33]. Compared with FM-MOF-7, FT-IR spectra of FM-MOF-6 show a new peak at 2555 cm^{-1} despite the absence of the band at 1639 cm^{-1}, indicating the elimination of vinyl groups and the appearance of free-standing thiol group after modification [Supplementary Figure 32]. The thio-ene transformation was also confirmed by the disappearance of the peaks around 5.0-7.0 ppm corresponding to the hydrogen signals of vinyl groups in the ^{1}H NMR spectrum of FM-MOF-6 and the concomitant emergence of new peaks around 2.0 and 3.0

ppm attributed to the different hydrogen of -CH_2- in M6 [Supplementary Figure 33]. To assess the overall capacity of FM-MOF-6 towards Hg^{2+}, the adsorption isotherm was then measured. As shown in Figure 2C, FM-MOF-6 displayed extremely high Hg^{2+} uptake. By fitting with Langmuir model, the saturated adsorption capacity of FM-MOF-6 for Hg^{2+} was determined to be 1077 mg g^{-1}, which is about 1.4 times higher than that of FM-MOF-1, surpassing various MOF adsorbents Supplementary Table 2[38-48]. In addition, we also investigated the adsorption kinetics of FM-MOF-6 toward Hg^{2+}. As shown in Supplementary Figure 34, a quick purification process was observed. The removal efficiency displayed a steep profile at the initial stage and then tended to equilibrium with about 99.84% of Hg^{2+} ions being removed. The excellent performance of FM-MOF-6 in mercury capture can be traced to the strong binding interactions between the Hg and sulfur species in FM-MOF-6, as evidenced by the enlarged S 2p binding energy of XPS analysis and the absence of S-H stretching mode in FT-IR spectra after Hg^{2+} adsorption [Supplementary Figures 35-37]. These results demonstrate the superiority of the utilization of FM-MOF-6 as a promising candidate for mercury capture from aqueous solutions.

On the other hand, the cycloaddition of CO_2 with epoxides into cyclic carbonates is an attractive strategy for addressing anthropogenic CO_2 emission issues, and imidazole-based functional molecules are regarded as efficient catalysts for this purpose. Considering the issues of homogeneous catalysts in product purification and catalyst recycling, it is advisable to graft imidazole-based functional molecules onto host materials for use as heterogeneous catalysts. Here, we chose 1-allylimidazole (M8) as a functional module to construct FM-MOF-8. Because of the absence of carboxylic connector in M8, a suitable convertor was needed. Therefore, bromoacetic acid (M9), which contains both a carboxylic connector and an accessible bromomethyl group for further chemical modification, was selected to assemble FM-MOF-9 first. The detailed characterizations are provided in Supplementary Figures 38-42. FM-MOF-9 was then treated with 1-allylimidazole (M8) through a tandem postsynthetic modification to obtain FM-MOF-8, as characterized by PXRD, N_2 adsorption, SEM, FT-IR, and NMR [Supplementary Figures 43-47]. Interestingly, the two incorporated modules of M8 and M9 in FM-MOF-8 combined together to form an imidazolium-based ionic liquid (IL) unit. Because of the proper distribution of formate groups in MOF-808, theoretically, such IL unit in FM-MOF-8 would also disperse uniformly within the pore, thus avoiding agglomeration and providing more accessible catalytic sites compared to the conventional dipping method. To evaluate the effectiveness of FM-MOF-9 as a catalyst, experiments were carried out. As shown in Figure 2D, the reaction yields catalyzed by FM-MOF-8 from related epoxides were determined to be 97.1% for epichlorohydrin, 95.2% for epibromohydrin, 86.2% for 1,2-epoxybutane, and 84.1% for allyl glycidyl ether, indicating that FM-MOF-8 exhibited a highly efficient catalytic performance for a variety of epoxides. It should be noted that the good performance of FM-MOF-8 was achieved without using any co-catalysts, whereas most reported MOF catalysts employ other substances, such as TBAB, to improve activity, which is considered uneconomical and complicated[49]. In contrast, FM-MOF-9 showed an extremely low activity, with a yield of < 10% under similar conditions, manifesting that the grafted M8 played a key role during the catalytic process. The above two proof-of-concept experiments fully demonstrated the reliability of this tandem postsynthetic modification for inserting functional modules without a carboxyl connector into MOF-808, which greatly expands the scope of FM-MOFs for functional targeting customization.

Switching modules on FM-MOFs

Another important aspect to consider is whether the functional modules on FM-MOFs could be freely switched in a simple manner, which allows for changing user-defined units in accordance with different needs, thereby affording matrix recycling and cost saving. The mutual transformation among FM-MOF-2, FM-MOF-7, and FM-MOF-9 was taken as a representative sample to confirm this [Figure 3]. These FM-MOFs were added into the solution containing the corresponding functional module, and the detailed experiments can be found in the Supplementary Materials. This conversion process was repeated several

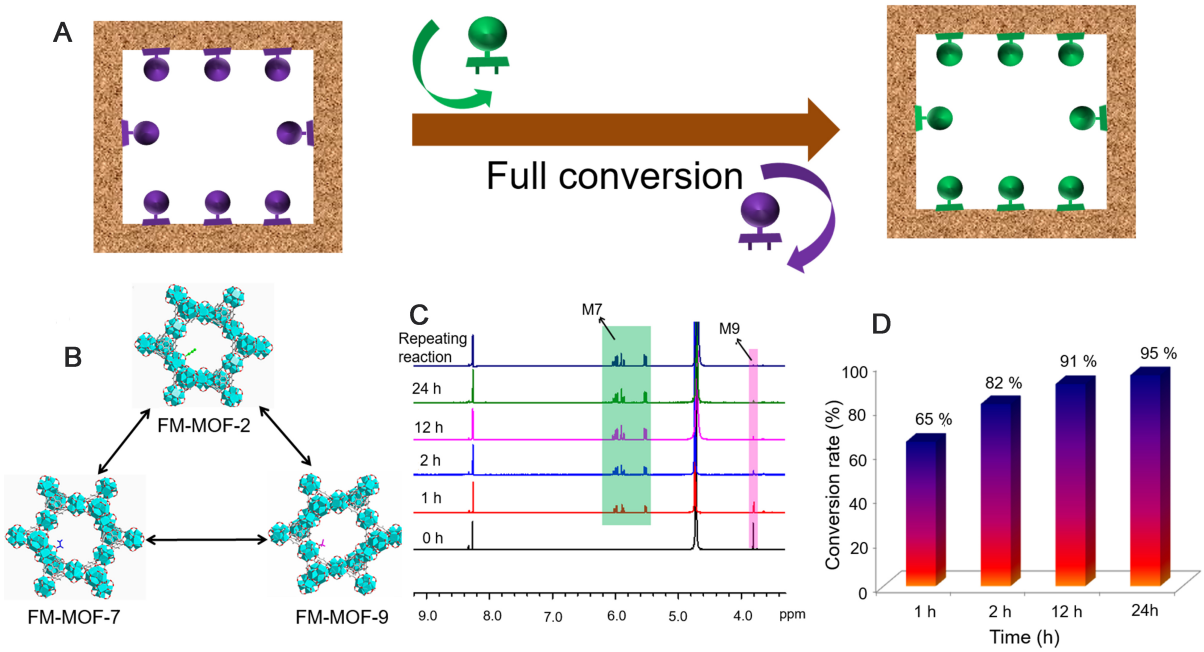

Figure 3. Full conversion process among FM-MOFs: (A and B) scheme illustration of mutual transformation among FM-MOFs and the associated pore structures of FM-MOF-2, FM-MOF-7, and FM-MOF-9; (C) the conversion process characterized by ^{1}H NMR spectra; and (D) the conversion rate from FM-MOF-9 to FM-MOF-7 with the increase of time.

times, and the as-transformed FM-MOFs were determined by ^{1}H NMR analysis. As shown in Supplementary Figures 48-53, for all three FM-MOFs, the signals of the original functional module disappeared, whereas the peaks attributed to the new unit emerged, demonstrating full switching of functional modules on MOF-808. Besides, PXRD measurements indicate no apparent loss of crystallinity during the conversion process [Supplementary Figures 54-59]. To further illustrate this, we also symmetrically investigated the conversion process from FM-MOF-9 to FM-MOF-7 with the increase of time. As shown in Figure 3C and D, the conservation rate reached 65% in the initial 1 h and steadily increased over time. After 24 h of reaction, the ^{1}H NMR spectrum reveals that δ at 3.8 ppm corresponding to the hydrogen signals of -CH_2- in M9 significantly decreased, whereas several new peaks around 5-7 ppm attributed to the vinyl group in M7 enhanced dramatically, achieving a high conservation of 95%. The peak of M9 further reduced when we repeated this conservation process several times, demonstrating essentially full conversion from FM-MOF-9 to FM-MOF-7.

Interestingly, we found that two functional modules could coexist in one host matrix during the switching process, which would form multivariate MOFs (MTV-MOFs) via partial conversion [Figure 4]. For full illustration, Hg^{2+} detection was selected as target application. We combined a mercury capture module and fluorophore moiety into MOF-808 through partial conservation and supposed that the resulting MTV-MOF would show improved performance in mercury detection. As such, the aforementioned FM-MOF-1 was immersed in DMF solution containing M4 for a period of time to obtain FM-MOF-1-4 (see Supplementary Figures 60-62). Compared to FM-MOF-1, the ^{1}H NMR spectra of this MTV-MOF reveal that δ at 2.8 ppm corresponding to M1 decreased and new peaks assigned to the hydrogen signals of pyrene in M4 emerged [Figure 4C]. The relevant signals of M1 in FM-MOF-1 and FM-MOF-1-4 were also integrated against that of the BTC ligand, resulting in peak ratios of 6:7 and 6:2, respectively, demonstrating that 71% of M1 was substituted by M4 during module switching process [Supplementary Figures 63 and 64]. FM-MOF-1-4 was then used to sense a trace quantity of Hg^{2+} in aqueous solutions. As shown in Figure 4D, obvious

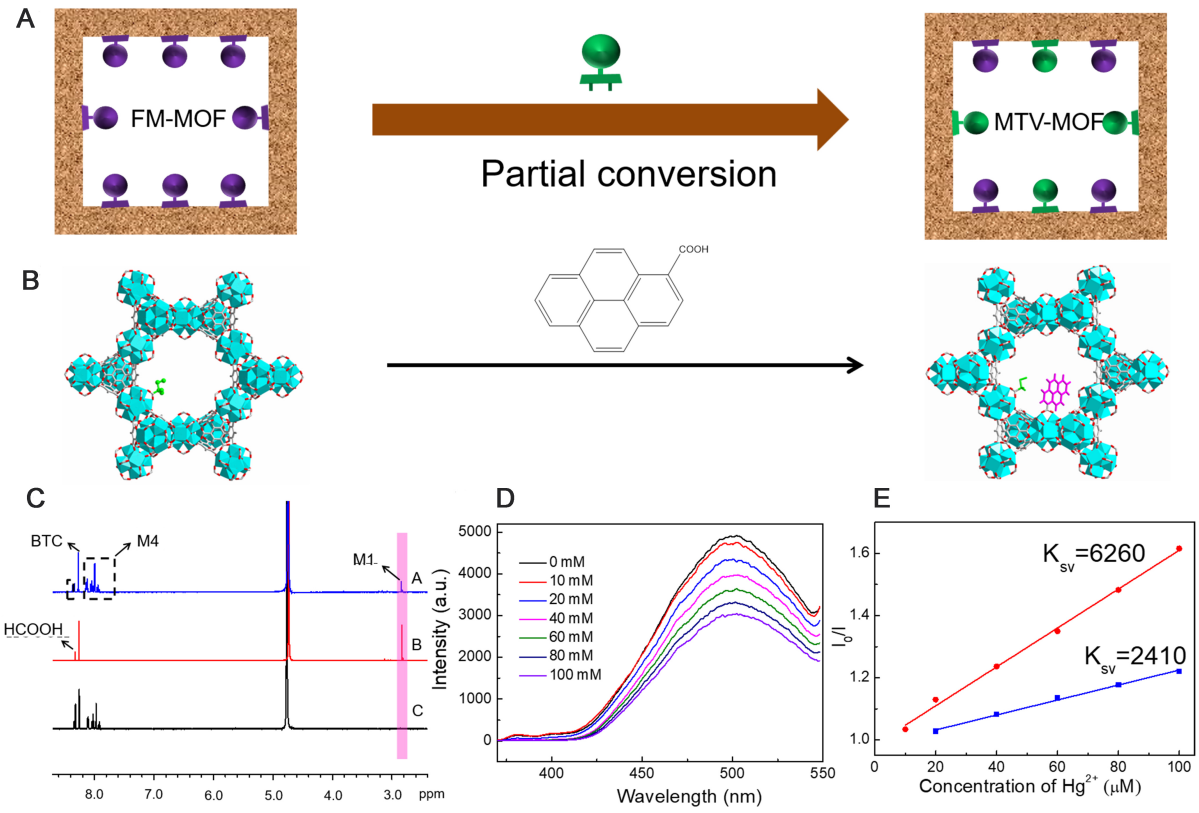

Figure 4. Partial conversion process among FM-MOFs: (A) scheme illustration of constructing MTV-MOF through a partial conversion process; (B) constructing FM-MOF-1-4 from FM-MOF-1; (C) ^{1}H NMR spectra of (A) FM-MOF-1-4, (B) FM-MOF-1, and (C) FM-MOF-4 in D_2O/KOH solution; (D) effect on the emission spectra of FM-MOF-1-4 with different concentration of Hg^{2+} in aqueous solution; and (E) Stern-Volmer plots of Hg^{2+} in aqueous solution for FM-MOF-1-4 (red) and FM-MOF-4 (blue).

fluorescence quenching was observed as the concentration of Hg^{2+} increased from 10 to 100 μM, specially, the quenching effect of Hg^{2+} was quantified by the Stern-Volmer equation ($I_0/I = 1 + K_{sv}[M]$), where I_0 and I are emission intensity of MOF material before and after reaction with Hg^{2+}, K_{sv} is the Stern-Volmer quenching effect constant of Hg^{2+}, and [M] is the concentration of Hg^{2+}. As shown in Figure 4E, FM-MOF-1-4 showed a distinguishable K_{sv} value for Hg^{2+} at 6260 M^{-1}, which is 2.6 times higher than that of FM-MOF-4 at 2410 M^{-1}. It is worth noting that FM-MOF-1 exhibited very weak fluorescence, and no visible quenching effect was observed towards Hg^{2+}. With M4 anchored in the pores, the thiol group within MOF and the fluorophore part of pyrene can cooperatively interact to significantly improve sensing performance. Specifically, the thiol groups of M1 in MOF captured traces of Hg^{2+}, and then the fluorophore pyrene of M4, which is in close proximity, responded to mercury ions. This process allows two functional modules to work in a cooperative manner. The above representative sample, therefore, demonstrates the feasibility of constructing MTV-MOF via partial conversion, which may further enhance the performance of MOFs. In principle, two arbitrary functional modules can exist in one host MOFs, thus constructing numerous of MTV-MOFs for target applications.

CONCLUSION

We propose a versatile "functional modular assembly" strategy for customizing MOFs, which allows installing the desired functional unit into a host material, and the unit can be switched flexibly according to different requirements. Functional molecules with connectors could be used as modules to insert into MOF structures through single substitution directly. To enrich modular diversity, molecules without connectors

could also be modularized by inserting pre-designed convertors into MOFs ahead through tandem postsynthetic modifications. Therefore, a wide range of available functional molecules, both with and without connectors, could be modularized during such an assembly process. Thus, a series of tailor-made FM-MOFs were generated and showed excellent performance toward entirely different fields, covering adsorption, catalysis, fluorescent sensing, electrochemistry, and the control of surface wettability. Moreover, the functional units on our FM-MOFs can be freely switched via full interconversion. Interestingly, we also found that two functional modules could coexist in one host matrix through partial conversion, opening up the possibility to construct multivariate MOFs (MTV-MOFs). Our strategy, therefore, provides a versatile and simple route for the rapid targeting customization of functional MOFs according to diverse applications, achieving the goals of multi-modules, multi-objectives, switchable units, and interfunctional cooperation for FM-MOFs.

DECLARATIONS

Authors' contributions

Planned the study, analyzed the data and prepare the manuscript: Peng Y, Tan Q, Huang H
Performed manuscript correcting: Kang X, Zhu Q, Zhong C, Han B

Availability of data and materials

Not applicable.

Financial support and sponsorship

This work is supported by Beijing Natural Science Foundation (2222043) and National Natural Science Foundation of China (21978212).

Conflict of interest

All authors declared that there are no conflicts of interest.

Ethical approval and consent to participate

Not applicable.

Consent for publication

Not applicable.

REFERENCES

1. Slater AG, Cooper AI. Porous materials. Function-led design of new porous materials. *Science* 2015;348:aaa8075. DOI PubMed
2. Kitagawa S. Future porous materials. *Acc Chem Res* 2017;50:514-6. DOI PubMed
3. Wu J, Xu F, Li S, et al. Porous polymers as multifunctional material platforms toward task-specific applications. *Adv Mater* 2019;31:e1802922. DOI PubMed
4. Siegelman RL, Kim EJ, Long JR. Porous materials for carbon dioxide separations. *Nat Mater* 2021;20:1060-72. DOI PubMed
5. Kirchon A, Feng L, Drake HF, Joseph EA, Zhou HC. From fundamentals to applications: a toolbox for robust and multifunctional MOF materials. *Chem Soc Rev* 2018;47:8611-38. DOI PubMed
6. Cui Y, Li B, He H, Zhou W, Chen B, Qian G. Metal-organic frameworks as platforms for functional materials. *Acc Chem Res* 2016;49:483-93. DOI PubMed
7. Li B, Chrzanowski M, Zhang Y, Ma S. Applications of metal-organic frameworks featuring multi-functional sites. *Coordin Chem Rev* 2016;307:106-29. DOI
8. Deng H, Doonan CJ, Furukawa H, et al. Multiple functional groups of varying ratios in metal-organic frameworks. *Science* 2010;327:846-50. DOI PubMed

9. Han Y, Li JR, Xie Y, Guo G. Substitution reactions in metal-organic frameworks and metal-organic polyhedra. *Chem Soc Rev* 2014;43:5952-81. DOI PubMed
10. Li J, Wang X, Zhao G, et al. Metal-organic framework-based materials: superior adsorbents for the capture of toxic and radioactive metal ions. *Chem Soc Rev* 2018;47:2322-56. DOI PubMed
11. Peng Y, Huang H, Zhang Y, et al. A versatile MOF-based trap for heavy metal ion capture and dispersion. *Nat Commun* 2018;9:187. DOI PubMed PMC
12. Peng Y, Zhang Y, Tan Q, Huang H. Bioinspired construction of uranium ion trap with abundant phosphate functional groups. *ACS Appl Mater Interfaces* 2021;13:27049-56. DOI PubMed
13. Shen Y, Pan T, Wang L, Ren Z, Zhang W, Huo F. Programmable logic in metal-organic frameworks for catalysis. *Adv Mater* 2021;33:e2007442. DOI PubMed
14. Newar R, Akhtar N, Antil N, et al. Amino acid-functionalized metal-organic frameworks for asymmetric base-metal catalysis. *Angew Chem Int Ed Engl* 2021;60:10964-70. DOI PubMed
15. Cui Y, Yue Y, Qian G, Chen B. Luminescent functional metal-organic frameworks. *Chem Rev* 2012;112:1126-62. DOI PubMed
16. Wang B, Lv XL, Feng D, et al. Highly stable Zr(IV)-based metal-organic frameworks for the detection and removal of antibiotics and organic explosives in water. *J Am Chem Soc* 2016;138:6204-16. DOI PubMed
17. Li H, Li C, Wang Y, et al. Selenium confined in ZIF-8 derived porous carbon@MWCNTs 3D networks: tailoring reaction kinetics for high performance lithium-selenium batteries. *Chem Synth* 2022;2:8. DOI
18. Kang X, Wang B, Hu K, et al. Quantitative electro-reduction of CO_2 to liquid fuel over electro-synthesized metal-organic frameworks. *J Am Chem Soc* 2020;142:17384-92. DOI PubMed PMC
19. Li N, Chang Z, Zhong M, et al. Functionalizing MOF with redox-active tetrazine moiety for improving the performance as cathode of Li-O_2 batteries. *CCS Chem* 2021;3:1297-305. DOI
20. Cho W, Lee HJ, Choi G, Choi S, Oh M. Dual changes in conformation and optical properties of fluorophores within a metal-organic framework during framework construction and associated sensing event. *J Am Chem Soc* 2014;136:12201-4. DOI PubMed
21. Deria P, Bury W, Hupp JT, Farha OK. Versatile functionalization of the NU-1000 platform by solvent-assisted ligand incorporation. *Chem Commun (Camb)* 2014;50:1965-8. DOI PubMed
22. Zhu W, Xiang G, Shang J, et al. Versatile surface functionalization of metal-organic frameworks through direct metal coordination with a phenolic lipid enables diverse applications. *Adv Funct Mater* 2018;28:1705274. DOI
23. Jayaramulu K, Geyer F, Schneemann A, et al. Hydrophobic metal-organic frameworks. *Adv Mater* 2019;31:e1900820. DOI PubMed
24. Mukherjee S, Datta K, Fischer RA. Hydrophobicity: a key factor en route to applications of metal-organic frameworks. *Trends in Chemistry* 2021;3:911-25. DOI
25. Hou H, Yu D, Hu G. Preparation and properties of ion-imprinted hollow particles for the selective adsorption of silver ions. *Langmuir* 2015;31:1376-84. DOI PubMed
26. Yao Y, Gao B, Wu F, Zhang C, Yang L. Engineered biochar from biofuel residue: characterization and its silver removal potential. *ACS Appl Mater Interfaces* 2015;7:10634-40. DOI PubMed
27. Zhang M, Zhang Y, Helleur R. Selective adsorption of Ag^+ by ion-imprinted O-carboxymethyl chitosan beads grafted with thiourea-glutaraldehyde. *Chemical Engineering Journal* 2015;264:56-65. DOI
28. Wang L, Wang K, Huang R, Qin Z, Su Y, Tong S. Hierarchically flower-like WS_2 microcrystals for capture and recovery of Au (III), Ag (I) and Pd (II). *Chemosphere* 2020;252:126578. DOI PubMed
29. Pan X, Fu L, Wang H, Xue Y, Zu J. Synthesis of novel sulfydryl-functionalized chelating adsorbent and its application for selective adsorption of Ag(I) under high acid. *Separation and Purification Technology* 2021;271:118778. DOI
30. Fard Z, Malliakas CD, Mertz JL, Kanatzidis MG. Direct extraction of Ag^+ and Hg^{2+} from cyanide complexes and mode of binding by the layered $K_2MgSn_2S_6$ (KMS-2). *Chem Mater* 2015;27:1925-8. DOI
31. Ma L, Wang Q, Islam SM, Liu Y, Ma S, Kanatzidis MG. Highly Selective and Efficient Removal of Heavy Metals by Layered Double Hydroxide Intercalated with the MoS4(2-) Ion. *J Am Chem Soc* 2016;138:2858-66. DOI PubMed
32. Zhou Y, Gao B, Zimmerman AR, Cao X. Biochar-supported zerovalent iron reclaims silver from aqueous solution to form antimicrobial nanocomposite. *Chemosphere* 2014;117:801-5. DOI PubMed
33. Asiabi H, Yamini Y, Shamsayei M, Molaei K, Shamsipur M. Functionalized layered double hydroxide with nitrogen and sulfur co-decorated carbondots for highly selective and efficient removal of soft Hg^{2+} and Ag^+ ions. *J Hazard Mater* 2018;357:217-25. DOI PubMed
34. Das R, Giri S, King Abia AL, Dhonge B, Maity A. Removal of noble metal ions (Ag^+) by mercapto group-containing polypyrrole matrix and reusability of its waste material in environmental applications. *ACS Sustainable Chem Eng* 2017;5:2711-24. DOI
35. Wu H, Yang F, Lv X, et al. A stable porphyrinic metal-organic framework pore-functionalized by high-density carboxylic groups for proton conduction. *J Mater Chem A* 2017;5:14525-9. DOI
36. Xue WL, Deng WH, Chen H, et al. MOF-directed synthesis of crystalline ionic liquids with enhanced proton conduction. *Angew Chem Int Ed Engl* 2021;60:1290-7. DOI PubMed
37. Sharma A, Lim J, Jeong S, et al. Superprotonic conductivity of MOF-808 achieved by controlling the binding mode of grafted sulfamate. *Angew Chem Int Ed Engl* 2021;60:14334-8. DOI PubMed
38. Yee KK, Reimer N, Liu J, et al. Effective mercury sorption by thiol-laced metal-organic frameworks: in strong acid and the vapor phase. *J Am Chem Soc* 2013;135:7795-8. DOI PubMed

39. Hou YL, Yee KK, Wong YL, et al. Metalation triggers single crystalline order in a porous solid. *J Am Chem Soc* 2016;138:14852-5. DOI PubMed
40. Luo F, Chen JL, Dang LL, et al. High-performance Hg^{2+} removal from ultra-low-concentration aqueous solution using both acylamide- and hydroxyl-functionalized metal-organic framework. *J Mater Chem A* 2015;3:9616-20. DOI
41. Zhao M, Huang Z, Wang S, Zhang L, Zhou Y. Design of l-cysteine functionalized UiO-66 MOFs for selective adsorption of Hg(II) in aqueous medium. *ACS Appl Mater Interfaces* 2019;11:46973-83. DOI PubMed
42. Shi M, Lin D, Huang R, Qi W, Su R, He Z. Construction of a mercapto-functionalized Zr-MOF/melamine sponge composite for the efficient removal of oils and heavy metal ions from water. *Ind Eng Chem Res* 2020;59:13220-7. DOI
43. Liang L, Chen Q, Jiang F, et al. In situ large-scale construction of sulfur-functionalized metal-organic framework and its efficient removal of Hg(ii) from water. *J Mater Chem A* 2016;4:15370-4. DOI
44. Liang L, Liu L, Jiang F, et al. Incorporation of In_2S_3 nanoparticles into a metal-organic framework for ultrafast removal of hg from water. *Inorg Chem* 2018;57:4891-7. DOI PubMed
45. Jiang SY, He WW, Li SL, Su ZM, Lan YQ. Introduction of molecular building blocks to improve the stability of metal-organic frameworks for efficient mercury removal. *Inorg Chem* 2018;57:6118-23. DOI PubMed
46. Li J, Duan Q, Wu Z, et al. Few-layered metal-organic framework nanosheets as a highly selective and efficient scavenger for heavy metal pollution treatment. *Chemical Engineering Journal* 2020;383:123189. DOI
47. Mon M, Lloret F, Ferrando-soria J, Martí-gastaldo C, Armentano D, Pardo E. Selective and efficient removal of mercury from aqueous media with the highly flexible arms of a BioMOF. *Angew Chem* 2016;128:11333-8. DOI PubMed
48. Fu K, Liu X, Lv C, et al. Superselective Hg(II) removal from water using a thiol-laced MOF-based sponge monolith: performance and mechanism. *Environ Sci Technol* 2022;56:2677-88. DOI PubMed
49. Nguyen PTK, Nguyen HTD, Nguyen HN, et al. New metal-organic frameworks for chemical fixation of CO_2. *ACS Appl Mater Interfaces* 2018;10:733-44. DOI PubMed

Hongliang Huang

Hongliang Huang received his B.S. degree and Ph.D. degree from Beijing University of Chemical Technology in 2009 and 2014, respectively. He joined the group of Prof. Chongli Zhong and worked as a postdoctoral fellow from 2014 to 2016. He has worked as a associate professor in Tiangong University since 2017. His research interests mainly focus on the design and synthesis of new porous materials (such as metal-organic frameworks and covalent organic frameworks) and their applications in gas separation, water treatment and catalysis.

Xinchen Kang

Xinchen Kang received his B.S. degree from Shandong University in 2011 and Ph.D. degree from Institute of Chemistry, Chinese Academy of Sciences (ICCAS) since 2016. He worked as a Royal Society research fellow in the University of Manchester from 2017 to 2020. He has worked as a professor in the group of Prof. Buxing Han in ICCAS since Jun, 2021. He is youth editorial board of *Chemical Synthesis*, youth editorial board of *Acta Physico-Chimica Sinica* and guest editor of *Symmetry*. His research fields include solution chemistry, materials chemistry and catalysis.

Buxing Han

Buxing Han received his Ph.D. degree in Physical Chemistry at Institute of Chemistry, CAS in 1988, and did postdoctoral research in Chemical Engineering at the University of Saskatchewan, Canada from 1989 to 1991. He was associate professor at Institute of Chemistry, CAS during 1991-1993, and has been a professor at the Institute since 1993. He is now the professor at Institute of Chemistry, Chinese Academy of Sciences (CAS); Academician of Chinese Academy of Sciences; Fellow of the Academy of Sciences for the Developing World (TWAS); Fellow of Royal Society of Chemistry. His research interests include physicochemical properties of green solvent systems and applications of green solvents in green chemistry, especially transformation of CO_2, biomass, and waste plastics. He is a Chief Scientist of China Innovation Think Tank; Secretary of Interdivisional Committee on Green Chemistry for Sustainable Development, (ICGCSD), Union of Pure and Applied Chemistry (IUPAC); Chairman of Green Chemistry Division, Chinese Chemical Society; President of Beijing Energy and Environment Society; Vice President of Energy Technology Industry Association of China; Former Chairman of Subcommittee on Green Chemistry of IUPAC, former Titular Member of Division III of IUPAC, and former Chairman of Thermodynamics and Thermal Analysis Committee, Chinese Chemical Society. He is an Editor-in-Chief of *The Innovation*, Associate Editors of *Green Chem.*, Associate Editor of *Chinese Sci. Bulletin*, Associate Editor of *Acta Physico-Chimica Sinica*, Associate Editor of *Chemical Journal of Chinese Universities*.

Yaguang Peng

Yaguang Peng joined the group of Prof. Chongli Zhong in Beijing University of Chemical Technology from 2013 and received his Ph.D. degree in chemical engineering and technology in 2019. He worked as a postdoctoral fellow in the group of Prof. Yadong Li in the department of chemistry, Tsinghua University from 2019 to 2021. He currently worked as a postdoctoral fellow in the group of Prof. Buxing Han and Prof. Xinchen Kang in ICCAS. His research interests mainly focus on the design and synthesis of metal-organic frameworks and their applications in adsorption, separation and CO_2 electro-reduction.

Li *et al. Chem Synth* 2022;2:16
DOI: 10.20517/cs.2022.19

Chemical Synthesis

Review

Open Access

Check for updates

Interface chemistry for sodium metal anodes/batteries: a review

Guojie Li[1,2,#], Xinyao Lou[1,#], Chengbin Peng[1], Chuntai Liu[2], Weihua Chen[1,*]

[1]College of Chemistry & Green Catalysis Center, Zhengzhou University, Zhengzhou 450001, Henan, China.
[2]National Engineering Research Center for Advanced Polymer Processing Technology, Zhengzhou University, Zhengzhou 450002, Henan, China.
[#]Authors contributed equally.

Correspondence to: Prof. Weihua Chen, College of Chemistry & Green Catalysis Center, Zhengzhou University, Zhengzhou 450001, Henan, China. E-mail: chenweih@zzu.edu.cn

How to cite this article: Li G, Lou X, Peng C, Liu C, Chen W. Interface chemistry for sodium metal anodes/batteries: a review. *Chem Synth* 2022;2:16. https://dx.doi.org/10.20517/cs.2022.19

Received: 25 Aug 2022 **First Decision:** 7 Sep 2022 **Revised:** 19 Sep 2022 **Accepted:** 22 Sep 2022 **Published:** 28 Sep 2022

Academic Editor: Bao-Lian Su **Copy Editor:** Peng-Juan Wen **Production Editor:** Peng-Juan Wen

Abstract

Sodium metal batteries (SMBs), benefiting from their low cost and high energy densities, have drawn considerable interest as large-scale energy storage devices. However, uncontrollable dendritic formation of sodium metal anodes (SMAs) caused by inhomogeneous deposition of Na^+ severely decreases the Coulombic efficiency, leads to short cycling life, and poses potential safety hazards, dragging SMBs out of practical applications. Electrolytes are attracting massive attention for not only providing ion transport channels but also exhibiting vital effects on interfacial compatibility and dendrite growth. In fact, the as-formed solid electrolyte interphase (SEI) has a great influence on the deposition and stripping process of SMAs. Moreover, Na plating process is accompanied by the generation of SEI, in which the electrolyte plays a vital role. Nevertheless, until now, the interaction among electrolyte-SEI-sodium dendrite has rarely been summarized. Herein, a fundamental understanding of sodium dendrite is concluded and the influence of the electrolyte and interface on Na^+ deposition is emphasized. Furthermore, the outlook for constructing dendrite-inhibited SMAs is suggested.

Keywords: Sodium metal anode, interface chemistry, dendrite suppression, solid electrolyte interphase, electrolytes

INTRODUCTION

In recent years, due to their low pollution and ability to regenerate, solar, geothermal, biomass, wind, and tidal power have been favored by researchers[1,2]. However, renewable energy has a short retention period, requiring strict energy storage, so the demand for high-efficiency energy storage devices is gradually increasing[3-5]. In contemporary battery technologies, owing to their excellent electrochemical properties and high energy densities, lithium-ion batteries (LIBs) have been widely used in portable electronic devices, electric vehicles, and energy storage power stations[6,7]. Nevertheless, LIBs with graphite as anode have reached their theoretical energy density, which is difficult to apply to large-scale energy storage. At the same time, the metal raw materials required by LIBs, such as lithium, cobalt, and manganese, are rare in the lithosphere, which is not conducive to expanding the production scale and lowering the cost[8]. Therefore, a new battery system is urgently needed to reduce battery cost and meet the expanding energy storage market[9-11].

With Na ranking seven most abundant and widely distributed in the Earth's crust, sodium-ion batteries (SIBs) have the edge in resource reserve, cost, energy conversion efficiency, cycle life, stability, and maintenance cost[12-16]. Sodium metal has been reckoned as an ideal anode for SIBs among the available anode materials with a high theoretical capacity of 1166 mAh g^{-1} and a low redox potential of -2.71 V (*vs.* standard hydrogen electrode)[17-19]. Na metal can be paired with high-capacity sodium-free cathodes in particular, such as sulfur (S)[20], oxygen (O_2)[21], carbon dioxide (CO_2)[22], and selenium (Se)[23-25], to achieve the high theoretical energy density. Therefore, due to these multiple advantages, sodium metal batteries (SMBs) have attracted a lot of attention from researchers and are expected to be an alternative for the next generation of high-energy batteries[26-29].

Sodium metal is in a thermodynamically unstable state in the electrolyte, and the electrode surface is inclined to form a solid electrolyte interphase (SEI) film with ion conduction and electron insulation[30,31]. The SEI film can isolate sodium metal and electrolyte to a certain extent to prevent the continuous occurrence of side reactions. However, it cannot withstand the severe volume change caused by sodium deposition/stripping during the cycling, which will lead to the formation of tree-like or moss-like dendrites after uneven deposition on the surface of sodium metal[32]. Sodium dendrites can exacerbate side reactions, cause "dead sodium" generation, reduce Coulombic efficiency (CE), and increase battery polarization. In more severe cases, dendrites will pierce the SEI, leading to short circuit[33,34]. To make things worse, the accompanying thermal runaway will cause fires and even explosions, dragging SMBs out of commercial applications. Hence, strategies to inhibit dendrite growth to achieve safe SMBs have been strongly considered during the past few decades[35,36].

By surveying the recent literature, several review papers related to dendrite-inhibited SMBs have been published in recent years[37-40]. As is known, the deposition behavior of Na^+ is closely related to the interface properties of sodium metal anodes (SMAs). Electrolytes are attracting massive attention for not only providing ion transport channels but also exhibiting vital effects on the interfacial compatibility of sodium anodes. However, until now, the interaction among electrolyte-SEI-sodium dendrite has rarely been summarized, and reviews about electrolyte regulation strategies in suppressing dendrite growth for SMBs have not been published thus far[41-43]. This review summarizes a fundamental understanding of sodium dendrite and then gathers various electrolytes, including the components, concentrations, and additives of liquid electrolytes and solid-state electrolytes technologies, to inhibit dendrite growth and the related SEI for dendrite-suppressed SMAs [Figure 1][44-52]. Finally, this review briefly presents a general conclusion and outlook for constructing high-performance and dendrite-suppressed SMBs.

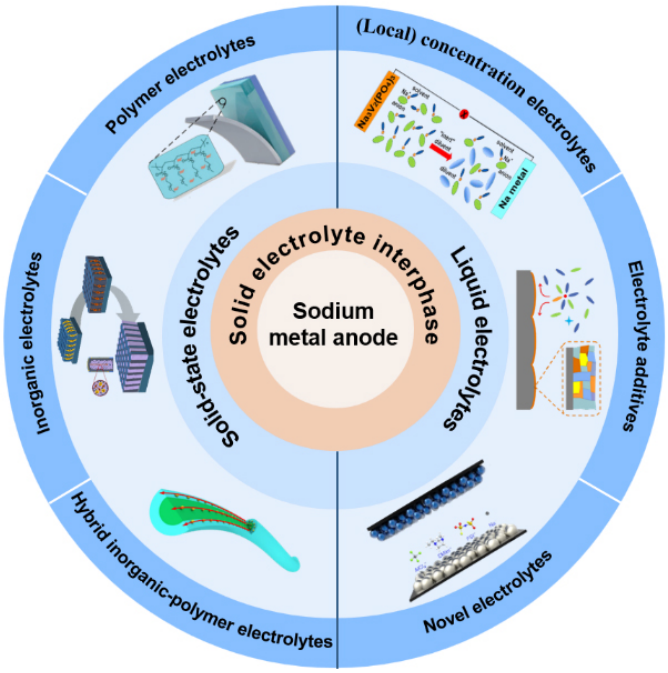

Figure 1. Summary of interface strategies towards dendrite-suppressed SMAs. SMAs: Sodium metal anodes.

UNDERSTANDING INTERFACE CHEMISTRY OF SODIUM ANODES

As is known, the existence of sodium dendrites is one of the toughest challenges for the commercial application of SMBs. It not only induces a low Coulombic efficiency and short cycling lifespan but also causes a poor safety profile for SMBs[53-55]. The generation of sodium dendrites is closely related to the formation of SEI and the resulting interfacial chemistry between SMAs and electrolytes. The nature of the SEI is believed to determine the plating/stripping behavior of sodium metals and the reversibility of batteries. In fact, electrolytes influence the formation and evolution of SEI. Therefore, controlling interfacial chemistry through electrolyte regulation plays an important role in the practical application of SMBs[56]. This section discusses a comprehensive understanding of the dendrite formation mechanisms and the interaction among electrolyte-SEI-sodium dendrite.

Formation mechanisms of sodium dendrite

In general, the deposition of Na^+ occurs during the passage of Na^+ through the SEI layer and the acquisition of electrons on the current collector, and this process is influenced by the inhomogeneous nucleation behavior[57]. During the deposition course, local electric field will induce an overpotential peak for non-homogeneous nucleation due to the uneven distribution of electric field caused by the impurities and defects in the sodium metal itself, which in turn will overcome the nucleation barrier and start the nucleation and deposition. The SEI is not sufficient to support the pressure brought by the sodium metal deposition and breaks into fragments around the deposition site to continuously expose fresh metal and generate a new SEI. Meanwhile, sodium metal tends to be deposited under the new SEI, gradually consuming sodium metal and generating dendrites. Although both sodium and lithium share many similarities, such as preferring to grow on the nucleation sites created by cracks, sodium dendrites are not just analogs of lithium dendrites[58]. The shapes of sodium dendrites are undefined but are frequently either needle or mossy structures. However, for lithium, these structures are concerned with defect catalyzed base growth conditions at low currents. In addition, they exhibit different hardness. With regard to Na, it is soft, which means it cannot penetrate separators as lithium does. As for Li, due to the greater hardness, lithium

dendrite is inclined to penetrate the SEI, thus leading to the short circuit. Furthermore, the ion radius of Na is 55% larger than Li, which will lead to different SEI forming situations, thus working on dendrites[59,60]. Besides that, the lithium dendrite growth pattern can be accounted for by Sand's time model. Nevertheless, it is difficult to explain sodium dendrite formation by using a formula, due to the lack of experimental data. Based on the current situation of SMB research, it is hard to form a continuous and complete SEI on the surface of sodium metal; sodium dendrites grow following a surface growth mechanism, i.e., they grow as particles over the entire sodium metal surface and even scatter in the pores of the diaphragm, thus causing a short circuit [Figure 2].

During the deposition process, the initial growth direction of sodium dendrites will be along the tip. In addition, dissolution of sodium dendrites is observed on the anode and, due to the electrostatic shielding effect, dissolution does not occur at the tip but preferentially at the bottom of the dendrite, where the disconnected low-density mossy electrodeposits are called "dead Na". The dead Na will quickly drift to the electrolyte surface, and the detached moss (isolated) sodium fragments will fill the electrolyte and the diaphragm, eventually short-circuiting the cell. Consequently, for sodium, owing to its softness, the short circuit can be explained by the accumulation of dead Na.

$$\frac{i_t}{i_f} = \{-\frac{1}{bC_0}\} \ln\left[e^{-bC_0} + \frac{i_f}{i_{Lf}}\left(1 - e^{-bC_0}\right)\right]^{-\frac{\alpha_c}{n}} \quad (1)$$

Thus far, lithium dendrites have been extensively studied, and models such as tip growth, root growth, and surface growth have been proposed. However, as there is no existing appropriate model for sodium dendrite, we can turn to the lithium model for insight into the influencing factors, as lithium is similar to sodium to some extent. Akolkar put forward Equation (1) (where i_t represents tip current density and i_f represents flat surface current density), which shows that the higher the i_t/i_f ratio, the higher the dendrite propagation[61]. In addition, the cathodic transfer coefficient (α_c), the bulk concentration of Li (C_0), and b parameter all function on dendrite growth. Fast dendritic growth is favored when operating near the limiting current (i_f/i_L is close to unity); however, slow but sustained dendritic growth can take place well below the limiting current density. Dendrite growth is suppressed in systems that exhibit a lower cathodic transfer coefficient[57].

The relationship between electrolyte-SEI-sodium dendrite

Electrolyte plays an important role in ion transport and affects the deposition morphology of metal anodes. Different electrolyte types have a major influence on dendrite appearance[20,47,62-69]. SEI layers will greatly affect dendrite formation. In liquid electrolytes, following the cycling of batteries, SEI layers will be easily formed, and the uneven morphology of sodium surface will contribute to the growth of dendrite[70]. The thicker SEI film exhibits better mechanical strength, conducive to inhibiting dendrite formation. Interestingly, CE will decrease because of the electrolyte consumption caused by SEI formation[71,72]. The thinner SEI cannot withstand the dendrite penetration despite showing high CE with little electrolyte consumption[73]. Therefore, the mechanical strength of SEI is important when considering the balance between CE and dendrite growth. Moreover, the component of SEI is also of importance for dendrite generation[74]. As mentioned above, during the Na plating/exfoliation process, an SEI film is produced. However, long-term, highly reversible, and non-dendritic electroplating stripping of Na anodes using diethylene glycol dimethyl ether with $NaPF_6$ electrolyte led to SEI fracture due to its poor mechanical strength. Further characterization showed that a homogeneous and dense SEI consisting of Na_2O and NaF was formed on the sodium metal surface, which was highly permeable to the solvent[17]. Homogeneity of the SEI promotes uniform Na^+ flux and non-dendritic sodium, thus keeping the SEI intact and stable during

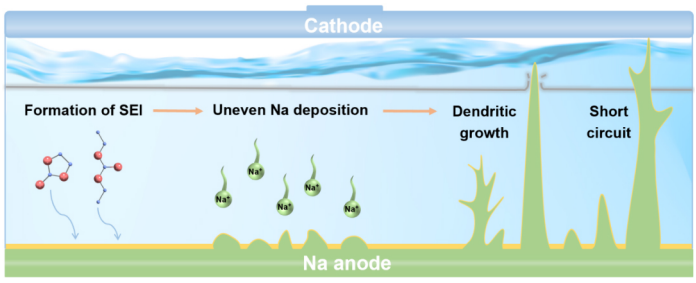

Figure 2. Formation mechanism of sodium dendrite.

cycling. Besides that, the concentration of electrolyte is worth considering. For instance, excessive NaF tends to form a more brittle SEI, which leads to CE fluctuations and dendrite growth in ether-based electrolytes. This factor is discussed in the subsequent section on high-concentration electrolytes[75]. Basically, in addition to the essential factors brought by the characteristics of SMBs, the influence of external conditions also significantly affects its growth[76]. Current density and charging capacity are the key parameters affecting dendrite morphology by influencing the formation of SEI[41,42]. Wenzel *et al.* showed that dendrites exhibit shrub-like growth with a current density of 120 μA cm^{-2}, while, when increased to 240 μA cm^{-2}, the dendrites demonstrate apparent dendritic growth[77]. It is well known that high current densities accelerate dendrite growth, but they also cause a shift from needle-like to moss-like sodium dendrites. One-dimensional needle-like dendrites are a safety hazard due to their growing length. Although three-dimensional mossy dendrites tend to grow in all directions, the lateral growth is dominant and usually results in more dead Na because the roots of sodium dendrites prefer to dissolve compared to the tips, which possess a strong electrostatic shielding effect[78]. Whichever dendrites are formed, the performance of the battery is severely affected. A further increase in current density, however, induces a further increase in the deposition overpotential, which results in a more nonuniform deposition of sodium metal. In addition to current density and capacity, temperature and internal battery pressure, referred to as the external causes, affect ion diffusion and then SEI formation, thus working on dendrite growth, which is not discussed further here because of the lack of research in SMBs.

LIQUIDE ELECTROLYTES

Liquid electrolyte is currently the most mature electrolyte system. Because of the loose and fragile SEI, with weak mechanical strength and dissolving in liquid electrolytes, unfavorable dendritic growth will emerge, leading to serious security trouble. Hence, a homogeneous, strong, and dense SEI is vital in protecting SMBs. Electrolyte additives, (local) concentrated electrolytes, and emerging novel electrolytes are regarded as some of the effective solutions in liquid electrolytes[79-81].

Electrolyte additives

Electrolyte additives are the most convenient solution to sodium dendrites. NaF, with high surface energy, possesses the strong ability to adjust surface tension and suppress dendrite growth. NaF is also intrinsically characterized by negligible solubility in most electrolytes and wide electrochemical stability windows[54]. Consequently, generated by F^-, it can enhance the mechanical strength of SEI and promote uniform distribution of Na^+. Currently, as the most extensively used additive, fluoroethylene carbonate (FEC) has been proven to be capable of promoting the formation of NaF-rich SEI and obtaining a compact deposition. However, FEC also tends to overreact with sodium, which constantly destroys and generates the SEI layer, consuming sodium and thus reducing CE. As a result, a new additive was added to the electrolyte to inhibit FEC from reacting with sodium by Zhu *et al.*[46] 1,3,2-Dioxathiolane 2,2-dioxide (DTD) and FEC were added as additives to the non-combustible electrolyte, and a stable fluoride SEI was generated in situ on the surface

of the SMAs, effectively inhibiting dendrite growth and alleviating the occurrence of side reactions [Figure 3A]. DTD additive is conducive to forming a constitutionally stable SEI layer, which enables dendrite-inhibited Na anode.

In addition to NaF additive, Li *et al.* showed that nitrofullerene [$C_{60}(NO_2)_6$] additive, exhibiting good compatibility with different electrolytes, enabled highly reversible and dendrite-free SMAs [Figure 3B][82]. Consequently, they could promote the formation of stable protective layers on SMAs and facilitate uniform Na deposition, thus effectively suppressing Na dendrite growth. Moreover, Wang *et al.* used sodium polysulfide (Na_2S_6) alone as a prepassivation agent to improve the long-term reversibility of Na anode; the concomitant stable interface could inhibit the dendrite formation[55]. However, Na_2S_6-$NaNO_3$ as co-additive had the opposite result, and the as-formed SEI with a component of sodium alkoxide (RCH_2ONa) and Na_2S gave rise to dendritic/mossy Na growth [Figure 3C]. Chen *et al.* constructed fast Na^+ diffusion SEI with different interface compositions through the interaction of sodium and tin chloride, and the results show that the interface of symbolic inorganic components had better structural stability and cycling performance [Figure 3D][83]. This provides guidance for the selection of additives for SMBs.

In addition to the above additive strategies for regulating SEI, a reasonable and feasible cationic additive strategy for stabilizing SMAs was proposed [Figure 3E][84]. Due to the electrostatic shielding effect, the electrolyte containing cationic additives gas evolution was prevented to a certain extent, and the anode appeared smooth [Figure 3F]. Through first-principles calculation and molecular dynamics simulation, three principles were proved, including electrode potential, LUMO level reduction, and binding energy with solvent. Mature cationic additive strategies provide new opportunities for the rational design of electrolytes for stable and safe SMBs.

(Local) concentration electrolytes

Salt concentration in the electrolyte has an enormous influence on improving electrochemical performance and suppressing dendrite growth. Increasing the electrolyte concentration can form a unique solvated structure and reduce the reaction between sodium and electrolyte, thereby reducing the formation of dendrites. Regarding the illustration of concentration effect, solvation structure and interfacial structure are deemed to influence the electrolyte properties as well as electrode-electrolyte interfaces that together can affect the battery performance. Figure 4A depicts two models, the superhigh concentration model and the ultralow one, which show that the former will get an anion-derived SEI and the latter will achieve a solvent-derived SEI[85]. From that perspective, Ma *et al.* used different concentrations of $NaCF_3SO_3$ dissolved in TEGDME solvent as electrolytes for Na-O_2 batteries and tested their electrochemical properties for comparison[86]. The results show that the stability of the electrolyte lowered with decreasing concentration. Thus, the stability of the Na cell was substantially improved when a saturated electrolyte was used. This is mainly due to the enhanced corrosion resistance of the sodium anode, reduced oxygen solubility, and effective inhibition of Na dendrite growth at the mercy of the high-concentration electrolyte [Figure 4B]. This work not only brings new insights to advance the development of long-life sodium-oxygen batteries but also stimulates additional studies to gain fundamental insights into the high concentration electrolytes for metal-oxygen batteries.

High-concentration electrolyte can solve the problem of dendrite growth caused by the strong reaction nature of sodium and electrolyte, but the high viscosity, excessive cost, and poor wetting of HCE also limit its application[87]. As shown in Figure 4C, by adding inert solvents such as double (2,2,2-trifluoroethyl) ether (BTFE) to the HCE, BTFE does not react with sodium metal and can form a local high-concentration electrolyte (LHCE) without changing the solvation structure[45]. LHCE not only provides high thick

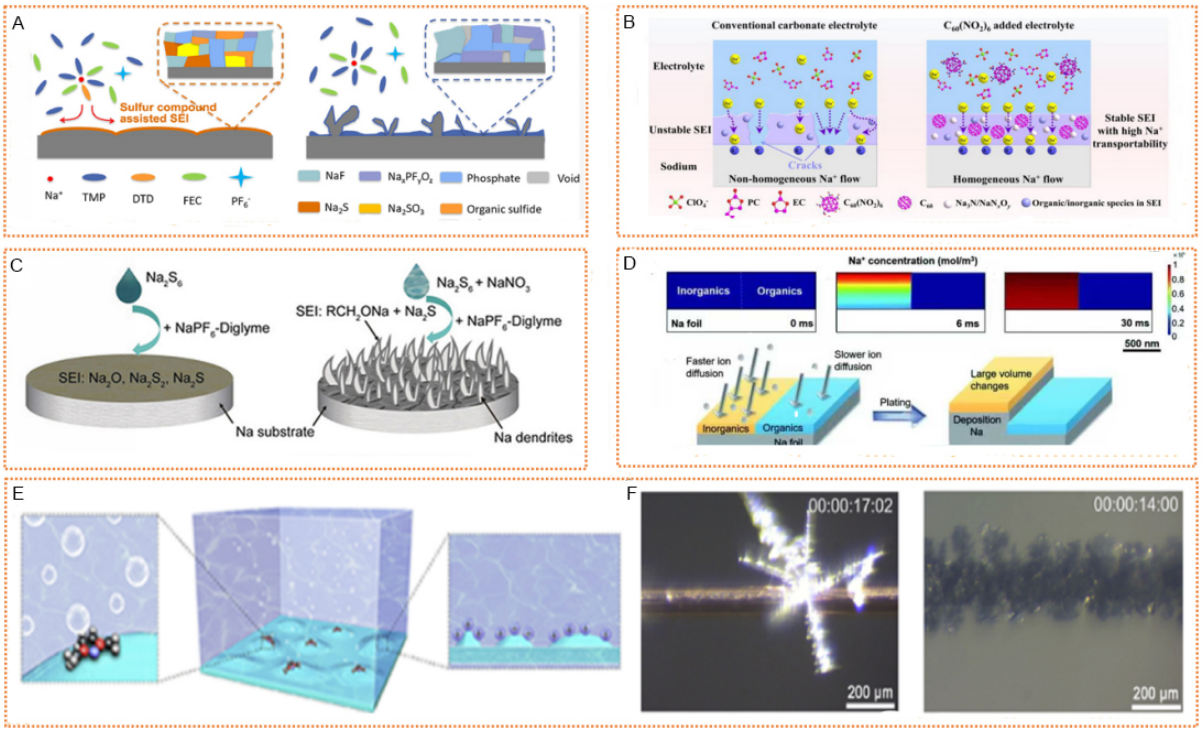

Figure 3. Electrolyte additives regulate SEI for dendrite-inhibited SMAs. (A) Diagram of SEI layer formed in TMP/FEC-E with or without DTD. Reproduced with permission from[46]. Copyright 2021, Elsevier. (B) Diagram of $C_{60}(NO_2)_6$-affected Na anode. Reproduced with permission from[82]. Copyright 2021, Elsevier. (C) Diagram of Na_2S_6 additive- and Na_2S_6-$NaNO_3$ co-additive-affected Na anode. Reproduced with permission from[55]. Copyright 2018, Wiley-VCH. (D) Simulation of Na^+ concentrations and deposition structures of Na metal anodes in the SEI layer. Reproduced with permission from[83]. Copyright 2020, The Royal Society of Chemistry. (E) Interfacial environment in the electrolyte with cation additives. (F) In situ optical microscopic observations of Na deposition on copper wire in 1.00 M $NaPF_6$ DME and 1.00 M $NaPF_6$ + 0.50 M $LiPF_6$ DME. Reproduced with permission from[84]. Copyright 2018, Cell Press. SEI: Solid electrolyte interphase; SMAs: sodium metal anodes.

electrolyte contact with metal sodium to reduce corrosion but also forms effective wetting between sodium and cathode material, providing a good interface reaction. In this study, LHCE [2.1 M NaFSI/DME-BTFE (1:2)] could achieve a high CE of > 99%, compared with other electrolytes in different concentrations. XPS analysis disclosed that more FSI anions participated in the formation of a more robust SEI layer when Na metal was cycled in either HCE or LHCE, thereby mitigating the consumption of solvent molecules during repeated Na deposition stripping processes [Figure 4D].

In addition, LHCE with a molar ratio of NaFSI:DME:OTE (1H,1H, 5H- octafluoropentyl -1,1,2, 2-tetrafluoroethyl ether) = 1:1.5:3 was used as the model electrolyte to in situ construct inorganic SEI films with gradient distribution on the surface of sodium anode [Figure 4E][88]. In the presence of OTE, the solvation configuration of the electrolyte changed from 3D network aggregation in HCE to cationic and anion solvent clusters in LHCE, which promoted more anions to enter the first solvated sheath. The overall migration mechanism of cation and anion solvent clusters in the electrolyte resulted in the enrichment of a large number of anions on the surface of Na, which promoted the gradual decomposition of FSI^- anions, thus forming the inorganic rich and gradient distribution of ultra-thin SEI, such as NaF, NaSON, Na_2S, *etc.*, which further reduced the activation energy of Na^+ transport in the SEI film. These advantages made Na||$Na_3V_2(PO_4)_3$ battery exhibit different morphology [Figure 4F-H]. This study provided new insights into developing high energy density SMBs by regulating the electrode-electrolyte interface membrane.

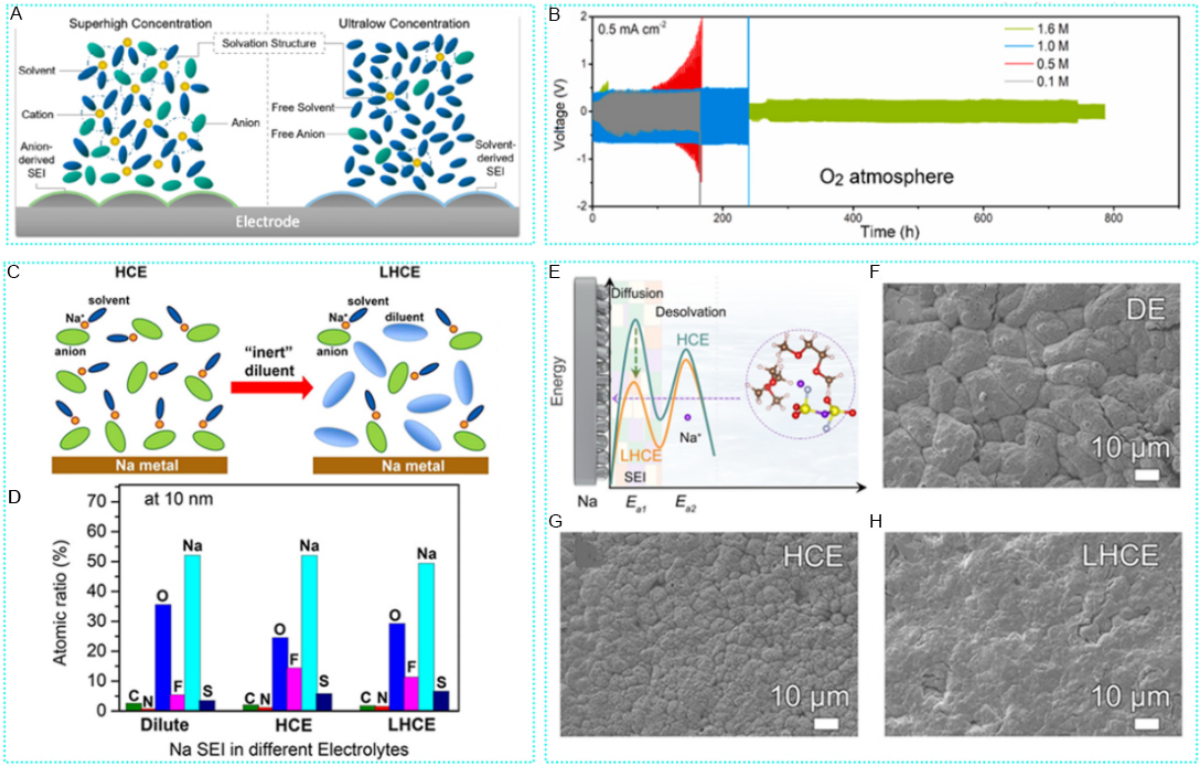

Figure 4. Local concentration electrolytes regulate SEI for dendrite-inhibited SMAs. (A) Solvation and interfacial structures of superhigh and ultralow concentrated electrolytes. Reproduced with permission from[85]. Copyright 2020, American Chemical Society. (B) Voltage profiles for Na/Na symmetric cells running in O_2 with $NaCF_3SO_3$/TEGDME electrolytes in various concentrations. Reproduced with permission from[86]. Copyright 2021, Elsevier. (C) Diagram of dilution from a HCE to a LHCE. (D) Atomic ratios of SEI layer after the 10th stripping of Na//Cu cells using dilute, HCE, and LHCE. Reproduced with permission from[45]. Copyright 2018, American Chemical Society. (E) Diagram of interface behavior Na^+ deposition. (F-H) Deposition morphology of sodium anode with different concentrations of electrolyte. (E-H) Reproduced with permission from[88]. Copyright 2021, Elsevier. SEI: Solid electrolyte interphase; SMAs: sodium metal anodes; LHCE: local high-concentration electrolyte.

Novel electrolytes

In the above discussion, we summarize the effects of additives and concentrations on the interface in the regulation of liquid electrolytes. Most of the currently available organic electrolytes form SEI with continuity and inhomogeneity, as well as more severe dendrite growth now. Hence, it is very important to regulate the interface from the composition of electrolytes (salts and solvents)[89]. As shown in Figure 5A, Sun *et al.* designed the first chloroaluminate ionic liquid electrolyte for rechargeable SMBs by adding two important additives (ethylaluminum dichloride and 1-ethyl-3-methylimidazolium bis(fluorosulfonyl)imide) to an ionic liquid consisting of $AlCl_3$/1-methyl-3-ethylimidazolium chloride/NaCl[90]. The system exhibited good inflammability and the absence of obvious dendrites. Meanwhile, they found that the formation of stable SEI is related to the existence of FSI anions, but the single presence of FSI anions is not sufficient to support metal Na anode for long-term charging and discharging cycles. Furthermore, a novel, dual electrolyte consisting of β"-alumina solid electrolyte (BASE) and an inorganic IL, Na[OTF]-Cs[TFSA], was integrated by Wang *et al.* [Figure 5B][91]. Investigations revealed IL exhibited high ionic conductivity and excellent thermal and chemical stability, making it propitious for intermediate-temperature operations. After 400 cycles, no significant change was observed in the interfacial resistance, which meant no dendrite formation. Ruiz-martínez *et al.* designed a liquid-amino electrolyte with diverse dissolved sodium salts[92]. This electrolyte had excellent properties of low flammability and high electrical conductivity. Most notably, using this electrolyte can effectively inhibit dendrite growth on the surface of SMAs, enabling highly

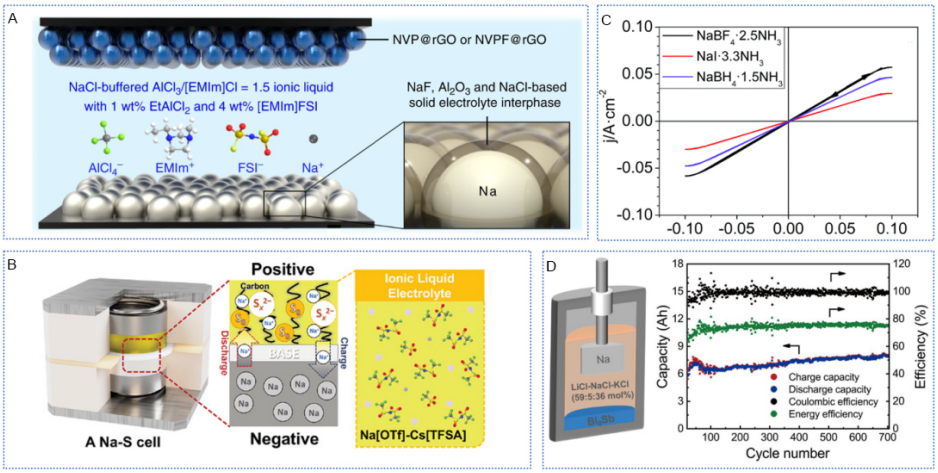

Figure 5. Novel electrolytes regulate SEI for dendrite-inhibited SMAs. (A) Diagram of the battery configuration and IL electrolyte. Reproduced with permission from[89]. Copyright 2019, Nature Publishing Group. (B) Operation mechanisms of Na-S battery using dual BASE/IL electrolyte. Operation temperature, 150 °C; IL, Na[OTF]-Cs[TFSA]. Reproduced with permission from[91]. Copyright 2021, Wiley-VCH. (C) CV for Na deposition/stripping over Na (supported on Cu) in a three-electrode cell. Reproduced with permission from[92]. Copyright 2017, The Royal Society of Chemistry. (D) Structure diagram of Na-LMBs; charge capacity, discharge capacity, Coulombic efficiency, and energy efficiency as a function of cycle number; and the theoretical capacity is 10 Ah. Reproduced with permission from[93]. Copyright 2022, Elsevier. SEI: Solid electrolyte interphase; SMAs: sodium metal anodes.

reversible plating/stripping. In addition, the same high CE and cycling stability could be achieved by sodium deposition on copper foil [Figure 5C]. Zhou *et al.* designed a new type of sodium liquid metal battery, which used low melting point ternary mixed cationic chloride molten salt LICL-NACL-KCl (59:5:36 mol%) as the electrolyte, greatly reduced the operating temperature and sodium halide content of the battery, and effectively inhibited the dissolution of SMAs in the electrolyte[93]. At the same time, the utilization rate of electrode materials was effectively improved through the construction of Bi-Sb binary alloy electrode, and the 10 Ah battery maintained a Coulomb efficiency of about 97% and ran stably for more than 700 cycles [Figure 5D]. The exploration and research of new electrolytes provide infinite possibilities for the realization of high-performance SMBs. The development of new electrolytes starts from scratch, so their development is relatively slow. In the future, new salts and solvents should be designed to regulate the interface chemistry of Na anode and thus achieve high-performance SMAs.

Table 1 shows the performance of representative batteries assembled with liquid electrolytes in the recent literature. Liquid electrolyte is the most used battery system. It has high current density and cycle life. However, its security severely limits the stable cycle for a long time. As a result, the solid-state battery is the future development trend to improve the safety performance of batteries.

SOLID-STATE ELECTROLYTES

Many safety problems emerge in liquid electrolytes, such as electrolyte volatilization and overreaction with sodium anode[101-105]. While these problems do not exist in solid-state batteries, the growth of sodium dendrite, serious interface problems between the surface of sodium and solid electrolyte, and the ion conductivity at low room temperature are all urgent problems for solid-state electrolytes. Commonly used solid-state electrolytes are mainly divided into inorganic electrolytes and polymer electrolytes[106]. Inorganic electrolytes represented by inorganic ceramics have high ionic conductivity and firm thermal stability but poor mechanical properties, and defects in inorganic materials themselves may aggravate sodium dendrite growth[107,108]. Polymer electrolytes provide an acceptable interface with their excellent flexibility, whereas low ionic conductivity and parasitic reactions with sodium make them unsuitable to SMBs[109]. Hence,

Table 1. Performance of representative batteries assembled with liquid electrolytes

Electrolyte	Current density (mA cm^{-2})	Stripping capacity (mAh cm^{-2})	Cycles hours (h)	CE (%)	Refs.
1.0 M $NaPF_6$ FEC/PC + HFE	0.5 1.0 5.0 1.0	0.5 1.0 1.0 5.0	1100 570 200 800	94.2	[44]
2.1 M NaFSI DME/BTFE	1.0 2.0	1	950 950	98.9	[45]
0.8 $NaPF_6$ FEC + DTD	0.5 1	1 5	1350 720	93.4	[46]
1 M $NaPF_6$/DGM + 0.033 M Na_2S_6	2 5	1 1	400 60	99	[55]
1.0 M NaDFOB EC/DMC	1.5	0.1	34	-	[72]
4 M NaFSI/DME + 1% SbF_3	0.5	-	1000	-	[74]
1 M $NaPF_6$ DME + 0.5M $C_{60}(NO_2)_6$	0.5 0.5 2.0	0.5 1.0 2.0	500 400 1200	99.4	[82]
0.8 M $LiPF_6$ DME + 1.0 M $NaPF_6$	0.5 2.0	0.5 2.0	300 300	99.2	[84]
1.6 M $NaCF_3SO_3$ TEGDME	0.5	2.0	800	-	[86]
1 M $NaPF_6$ FEC/DMC + DMTP	1 5	1 1	900 250	96.6	[94]
0.3 M $NaPF_6$/EC/PC + 2 wt % BSTFA	0.5	0.5	350	-	[95]
5 M NaFSI DME	0.0028	0.0014	600	99.3	[96]
1 M $NaPF_6$ DGM	0.5	1	300	99.9	[97]
0.64 M $NaBF_4$/G2	0.5 1	-	3000 2000	99.9	[98]
0.8 M $NaPF_6$ DME + 0.4 M $LiPF_6$	-	-	-	97.0	[99]
DME:NaFSI:TTE = 1:1.2:1	1	1	590	-	[100]

conventional inorganic electrolytes can be combined with polymer electrolytes to form hybrid inorganic-polymer electrolytes, which are capable of overcoming the disadvantages of polymer and inorganic electrolytes, meaning high ionic conductivity and favorable electrode-electrolyte interface. Moreover, the improved mechanical strength of hybrid inorganic-polymer electrolytes, due to inorganic binding to polymer electrolytes, can also inhibit the formation of sodium dendrite[110-112].

Polymer electrolytes

The limitations of liquid electrolytes, such as sodium dendrite growth, serious side reactions, and liquid leakage, hinder the development of SMBs. However, these safety issues will not readily happen in organic polymer electrolytes. However, low ionic conductivity is an issue for conventional polymers. Polyether, especially polyethylene oxide, has attracted extensive attention in polymer electrolytes since 1973 due to its superior coordination ability with alkali metal ions. Chen *et al.* optimized the ratio of 3-{2-[2-(2-methoxyethoxy)ethoxy]-ethoxy} methyl-3-methyloxetane (MEMO) to 3-hydroxymethyl-3-methyloxetane (HMO) monomers [Figure 6A], in which the former provides conductive suspension and the latter supplies cross-linked branched chain sites, thus forming a polyether-based hyperbranched copolymer electrolyte with both high ionic conductivity and favorable mechanical strength[113]. Furthermore, the concentration of NaTFSI plays a great role in ionic conductivity of the electrolyte, making up for its shortcomings. Similarly, as observed in Figure 6B, Yao *et al.* designed an advanced all-solid-state sodium battery (NVP@C|PEGDMA-NaFSI-SPE|Na) to achieve high ionic conductivity[49]. UV-cured novel solid polymer electrolyte displayed enhanced ionic conductivity (≈ 10^{-4} S cm^{-1} at RT) and interfacial contact. The dendrite

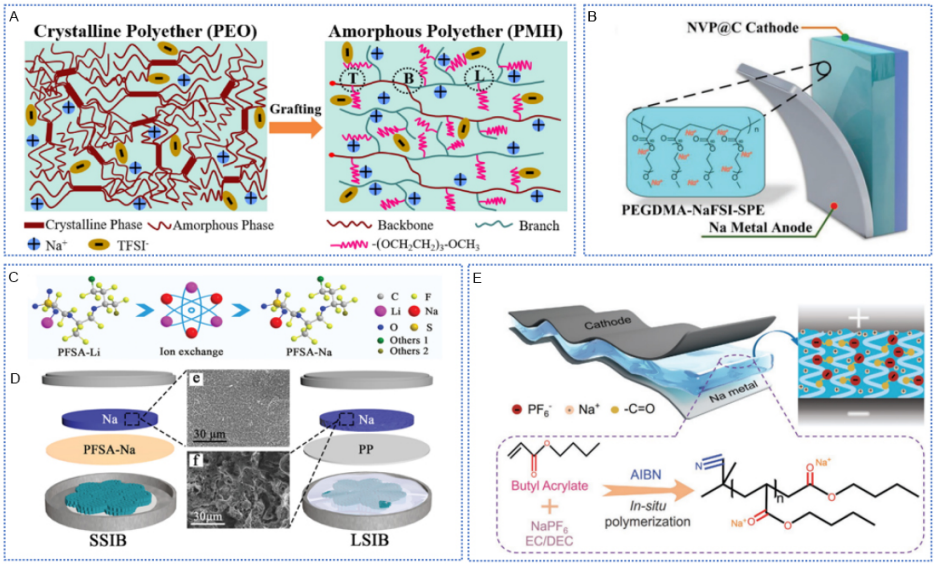

Figure 6. Polymer electrolytes regulate SEI for dendrite-inhibited SMAs. (A) Schematic conformation of PEO and PMH. Reproduced with permission from[113]. Copyright 2020, Elsevier. (B) The construction architecture of the NVP@C|PEGDMA-NaFSI-SPE|Na. Reproduced with permission from[49]. Copyright 2020, Wiley-VCH. (C) Diagram of the ionic-exchange process. (D) Surface morphology of sodium metal plates after 20 cycles in SSIB and LSIB. (C and D) Reproduced with permission from[114]. Copyright 2020, Wiley-VCH. (E) Schematic of in situ preparation process for PBA-based GPE in NVP||GPE||Na SMBs. Reproduced with permission from[120]. Copyright 2022, Wiley-VCH. SEI: Solid electrolyte interphase; SMAs: sodium metal anodes.

growth on the surface of sodium electrode was inhibited significantly. In addition, a solid-state polymer electrolyte (PFSA-Na) was fabricated by a facile ionic exchange from a raw commercial material [Figure 6C][114]. The as-prepared PFSANa not only had excellent ionic conductivity but also showed excellent resistance to low temperature. In addition, the excellent cycling performance at low temperatures indicated the practicability of the electrolyte at low temperatures. At the same time, the dendrite-free morphology also further promoted the development of SMAs [Figure 6D]. Moreover, because of the economically friendly synthetic method of PFSA-Na membranes, it can be a favorable candidate for large-scale energy storage systems.

For challenges related to the contact between anode and polymer electrolytes, Zhao *et al.* showed that an improved interface was established between a composite Na/C metal anode and the solid PEO electrolyte, which led to more homogeneous plating and stripping, reducing/suppressing dendrite formation[115]. A series of star-like hyperbranched polymers composed of a β-CD core and multiple PMMA-b-PEGMA arms were synthesized through the ATRP method, and free-standing and flexible SPE films were prepared by complexing the resultant polymers with $NaSO_3CF_3$ salt in a THF solvent and casting the resulting solution[116]. The polymer exhibited excellent ionic conductance, thermal stability, and a wide electrochemical window. This provides a new direction for the development of new and safe sodium batteries. Polymer electrolytes show excellent performance and can inhibit dendrite formation to a certain extent. This also indicates the future market prospects for polymer electrolytes.

Gel polymer electrolytes (GPEs) composed of polymer matrix and liquid electrolytes have attracted extensive attention in SMBs. The liquid parts provide high ionic conductivity and low interfacial impedance, while the polymer matrix presents excellent mechanical properties and flexibility. Unfortunately, GPEs still face the problems of unstable electrolyte interface and dendrite growth. Therefore, the design and fabrication of advanced gel electrolytes are of the utmost importance for the realization of

safe SMBs with excellent performance[117,118]. Wen *et al.* designed a new photopolymerized gel electrolyte of ETPTA-$NaClO_4$-QSSE, which exhibited unprecedented room-temperature ionic conductivity of 1.2 mS cm^{-1}, a wide electrochemical window up to 4.7 V (*vs.* Na^+/Na), and outstanding compatibility with Na metal anode[119]. Due to its enhanced interfacial stability, Na symmetric cells based on this electrolyte showed superior long-term cycling performance and morphology of dendrite-inhibited SMAs. This strategy proposed for quasi-SSE provides a new direction for the development of RT high-energy-density flexible solid-state SMBs. Besides that, Zhang *et al.* developed a poly(butyl acrylate)-based GPE with a high RT ionic conductivity of 1.6 mS cm^{-1} by in situ polymerization [Figure 6E][120]. As a result, NVP||GPE||Na full cell displayed satisfactory cycle performance and rate performance.

Considering liquid electrolytes employed in batteries give rise to safety hazards such as fire and explosions in an abnormal state, Park *et al.* devised noncombustible GPEs formed by in situ cross-combination of polypropanolactone triacrylate gel precursors[48]. Although GPEs exhibited a 3D network structure, their ionic conductivity can reach 6.3 mS cm^{-1} due to the interaction between Na^+ and carbonyl and high segmental motion of the polycaprolactone chain. The polymer network with high ionic conductivity could significantly inhibit Na dendrites by bringing in uniform Na deposition, thus improving the interface properties of Na electrode. In addition, Zheng *et al.* prepared three novel cross-linked gel tricopolymer electrolytes with different copolymers by in situ radical polymerization[121]. The GF separators with GPEs were uniform and showed outstanding integrity, whereas the one with LE manifested that a lot of small particles adhered to the fiber surface. These granules were speculated as dead Na, causing the capacity of the liquid battery to degrade or even short circuit after long cycles.

Inorganic electrolytes

The currently used inorganic SSEs are mainly divided into oxide and sulfide inorganic SSEs. For the former, the traditional oxide electrolyte exhibits high mechanical strength and good dendrite inhibition performance, but the ionic conductivity is low, and the interface contact is unstable. The latter, sulfide electrolytes, have attracted great attention these years, but the shuttling effect and instability are serious problems.

Oxide-type solid-state electrolytes

Poor interface contact is an urgent problem for inorganic solid electrolytes. Lai *et al.* demonstrated that a β”-Al_2O_3 electrolyte with a vertically porous bilayer structure [Figure 7A] could solve this issue[50]. The carbon-coated vertically porous β”-Al_2O_3 layer provided fast electronically and ionically conductive pathways, preventing sodium dendrite from penetration. In addition, β”-Al_2O_3 showed very good thermal stability, and its excellent sodium ion conductivity at high temperatures made it commonly used in high-temperature batteries. However, at room temperature, the sodium ion conductivity of the β”-Al_2O_3 is at the mercy of the content of Na_2O in materials. To make β”-Al_2O_3 exhibit acceptable sodium ion conductivity, Bay *et al.* showed that, by applying a heat treatment in an argon atmosphere to a finely polished Na-β”-alumina surface, a low interfacial resistance to sodium metal of < 10 Ω cm^2 could be achieved [Figure 7B][122]. There was a significant decrease in the interfacial resistance from 10,000s Ω cm^2 for non-heat-treated samples to 8 Ω cm^2, achieved by heat treating the Na-β”-alumina pellets at 900 °C. Therefore, the high ionic conductivity of the Na-β”-alumina ceramic at room temperature is available (1.6 mS cm^{-1}). Nevertheless, at room temperature, more issues remain to be solved, as β”-Al_2O_3 shows lower mechanical properties and more defects (crystal boundaries, pores, *etc.*) which cannot inhibit the growth of sodium dendrite. In addition, its low sodium affinity is not suitable for normal temperature SMBs.

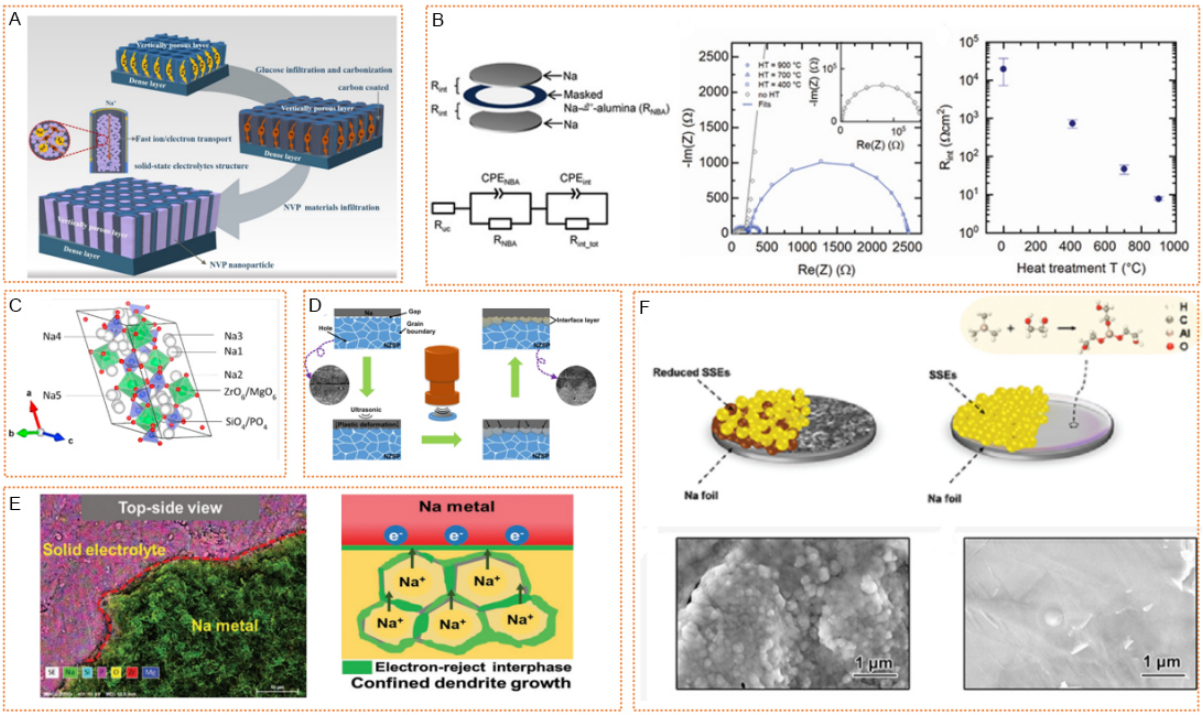

Figure 7. Inorganic electrolytes regulate SEI for dendrite-inhibited SMAs. (A) Schematic of the bilayer β''-Al_2O_3 electrolyte structure. Reproduced with permission from[50]. Copyright 2021, Elsevier. (B) Impact of heat-treatment temperature on interfacial resistance at room temperature. (left) Schematic of Na/Na-β''-alumina/Na cell and equivalent circuit for fitting the impedance spectra. (middle) Representative Nyquist plots for the different heat-treatment temperatures. Markers represent experimental data and lines represent the fitted data. (right) Interfacial resistance according to heat-treatment temperature. Reproduced with permission from[122]. Copyright 2020, Wiley-VCH. (C) Crystal structure view of $Na_{3.4}Mg_{0.1}Zr_{1.9}Si_{2.2}P_{0.8}O_{12}$. Reproduced with permission from[120]. Copyright 2021, Elsevier. (D) Diagram of the ultrasound solid welding method. Reproduced with permission from[126]. Copyright 2021, Nature Publishing Group. (E) (left) SEM-EDS mapping images of NZSP-0.2Mg against sodium metal after cycling. (right) Confined Na plating at the interface of Na/NZSP-0.2Mg. Reproduced with permission from[127]. Copyright 2021, Wiley-VCH. (F) (top) Diagram of the reactive Na/sulfide-based SSEs interface and stable Na@alucone/sulfide-based SSEs interface. Top-side SEM of the cycled Na|Na_3SbS_4|Na using (bottom left) bare Na and (bottom right) Na@mld 150 C electrodes. Reproduced with permission from[129]. Copyright 2021, Wiley-VCH. SEI: Solid electrolyte interphase; SMAs: sodium metal anodes.

NASICON is the first reported inorganic solid-state oxide electrolyte, in which $Na_3Zr_2PSi_2O_{12}$ (NZSP) is the most typical sodium superionic conductor, providing an ionic conductivity of about 10^{-4} S/cm at room temperature. Moreover, NASICON is also capable of providing high chemical and electrochemical stability, with a wide voltage window (> 5 V) for SMBs. However, the large crystal boundary impedance of the material itself makes the sodium easily grow along the crystal boundary, and the crystal boundary impedance also makes NASICON mostly exhibit poor ionic conductivity[123]. By making the graphene interface layer on the NZSP surface with CVD method, many distributed defect networks were constructed, so that the uniform deposition of metal sodium at the electrolyte and electrode interface could inhibit the growth of Na dendrite and reduce the interface impedance[124]. An integrated structure composed of dense electrolyte layer and porous sodium layer can also effectively reduce the contact resistance between electrolyte and sodium anode and effectively suppress the growth of sodium dendrite.

The dendrite suppressing ability for primitive NZSP is poor. Therefore, Weng *et al.* showed that the optimized $Na_{3.4}Mg_{0.1}Zr_{1.9}Si_{2.2}P_{0.8}O_{12}$ electrolyte was obtained by simultaneously substituting the Zr^{4+} with Mg^{2+} and P^{5+} with Si^{4+} through solid-state reaction[125]. The improved dendrite regulating performance can be explained by the monoclinic structure [Figure 7C], which forms an effective three-dimensional Na^+

transport network[125]. Furthermore, the problem of contact between Na and NZSP can be tackled by a room temperature ultrasound solid welding strategy [Figure 7D][126]. With the aid of ultrasound, an intimate bonding interface with a stable interfacial layer was constructed, effectively alleviating dendrite growth. Conversely, the grain boundary phase of a Mg^{2+}-doped NZSP conductor (denoted as NZSP-xMg) was manipulated to introduce favorable $Na_{3-2\delta}Mg_{\delta}PO_4$-dominant interphase, which facilitated its intimate contact with Na metal and worked as an electron barrier to suppress Na metal dendrite penetration into the electrolyte bulk. As shown in Figure 7E, sheet-like sodium metal was observed to adhere to the surface of NZSP-0.2Mg, and no sodium dendrites appeared[127]. The Na plating mechanism showed that, in NZSP-0.2Mg, the electron-insulted $Na_{3-2\delta}Mg_{\delta}PO_4$ was introduced to suppress electron transport through the grain boundary and helped to form desirable interphase, which ensured robust Na plating/stripping cycles constrained at the interface. In conclusion, the oxide solid-state electrolyte crystal boundary impedance is so enormous that it is necessary to improve the material density, reduce the crystal boundary impedance, usually through high-temperature annealing, and improve the solid-solid interface between the electrode and electrolyte.

Sulfide solid-state electrolytes

Sulfide plays an important role in inorganic solid electrolytes, which is generally soft in texture and obtained with high energy density and low interface resistance without high-temperature annealing. As the electrostatic effect between sulfur and sodium ions is weak, it can provide higher ion conductivity than the oxygen group. The sulfur group and the modified selenium-based solid electrolyte generally provide an ionic conductivity of 10^{-3} S cm^{-1}, which is much higher than the oxygen-based solid-state electrolyte. The reported $Na_{2.9}Sb_{0.9}W_{0.1}S_4$ showed the highest ionic conductivity and provided $4.1 \pm 0.8 \times 10^{-2}$ S cm^{-1} at room temperature. Sulfur-based solid-state electrolyte is therefore considered one of the SSEs with commercial promise. However, the high reactivity and weak electrochemical stability between sulfur solid electrolyte and sodium will lead to the decomposition of sulfur solid electrolyte, which in turn causes uneven deposition of sodium and produces sodium dendrite. Therefore, a stable interface layer is usually added to the negative pole side[128].

A molecular layer deposition (MLD) alucone film was employed on the surface of sodium, which passivated the surface of anode, effectively alleviating the growth of sodium dendrite while preventing the breakdown of Na_3SbS_4, a solid electrolyte. However, for sulfide-based electrolytes, an inherent problem is that metallic sodium reacts thermodynamically with most thiophosphates to form poor ionic conducting products. Although substitution of P can improve electrochemical performance, those elements that contribute to improved ionic conductivity and chemical stability (As, Sb, *etc.*) have redox activity, which directly leads to the decomposition of electrolytes in SMB. Therefore, Zhang *et al.* used alucone films deposited on Na foil to separate Na metal and sulfide electrolytes (as shown in Figure 7F)[129]. In the absence of MLD coating, continuous protruding particles appeared on the surface of the exposed Na metal electrode, indicating the growth of Na dendrites. In contrast, Na@mld 150 C had a flat and smooth surface, showed evidence of limiting Na dendrites and was in close contact with the Na_3SbS_4 electrolyte. Inserting CPEO, an electrolyte membrane between sodium and Na_3SbS_4, prevents electron transport from reducing solid-state electrolyte surface defects, thus forming a uniform surface on sodium metal surface and inhibiting dendrite growth.

Hybrid inorganic-polymer electrolytes

Solid electrolytes, considered as promising electrolytes which exhibit much less danger than liquid electrolytes in SMBs, cannot contact thoroughly with the anode/cathode. Modification of inorganic electrolytes can enhance the ion conductivity at room temperature and suppress dendrite growth through coating. Nonetheless, inorganic electrolytes are costly and usually not stable enough in air, thus are not conducive to the development of commercialization. Correspondingly, polymer electrolytes generally

exhibit strong flexibility, are inexpensive, easy to prepare, and are more likely to form a tight electrode-electrolyte interface with them.

Inorganic fillers are introduced into polymer electrolytes to form hybrid inorganic-polymer electrolytes. The hydroxyl and functional groups with other characteristics are brought into hybrid electrolytes, such as oxygen vacancy available with Lewis acids and Lewis bases on the polymer chain or sodium salt formation interaction, which transforms the crystallinity of polymers, increases freed Na^+ concentration, improves stability and mechanical modulus of polymer electrolytes, *etc.* It is expected to solve the above key problems of low ionic conductivity and mechanical property.

Different materials have been used in the hybrid electrolyte system, including 0D nanoparticles, 1D nanowires, 2D layered materials, and 3D continuous packing structures[130-135]. Nano-sized NZSP powders were first prepared by Niu *et al.* with a sol-gel method[136]. As shown in Figure 8A, there are many pores in the cathode without succinonitrile (SN), and the interface contact between the cathode and solid electrolyte is poor, which hinders the transport of Na^+ at the cathode and electrolyte-cathode interface. The addition of SN is conducive to the formation of a compact and stable contact interface between nanocomposite cathode and solid electrolyte, improves ion transport, and increases battery cycle life. As shown in Figure 8B, a composite electrolyte with sandwich heterostructure was designed, and the electrochemical window was widened to 5 V[51]. A continuous interface can be formed between the 3D interconnected NZSP and the polymer matrix, facilitating rapid diffusion of sodium ions. The integrated 3D structure is permeated by PAN or PEO. The porous side filled with PAN can withstand oxidation at high voltage, while the porous side filled with PEO can withstand Na metal reduction at low voltage. The battery composed of $Na_3V_2(PO_4)_2F_3$ showed excellent electrochemical performance towards a high-voltage solid-state battery. The combination of inorganic ceramic filler and organic polymer matrix is an effective method to improve the safety of hybrid electrolyte. However, increasing the amount of ceramic filler reduces flexibility and thus increases the interfacial resistance[137]. Ran *et al.* proposed a gradient composite electrolyte (GCE), which used Sc and GE doped NZSP as filler and PEO as matrix[138]. In Figure 8C, an enhanced conduction pathway is formed around the ceramic filler in NZSP-PEO CE (blue area). This region is called the space charge region and is driven by the different free energy densities of the region from the inner layer to the outer surface. In such CE, the ceramic filler concentration must be greater than the percolation threshold to ensure a highly conductive pathway for interconnection. Matios *et al.* formulated a reactivity-guided strategy for the synthesis of hybrid SPEs with optimized compositions of polyester PPC, ceramic NASICON, and PEO host to simultaneously improve ionic conductivity, interfacial impedance, electrochemical stability, and mechanical properties[139].

A low-cost and cross-linked gel-polymer electrolyte of poly(methyl methacrylate) (PMMA) was compounded, enabling dendrite suppression and excellent cycling stability[117]. In addition to organic cross-linked polymers, Lei *et al.* developed a blended inorganic ionic conductor/GPE composite electrolyte, where a β/β”-Al_2O_3 nanowire (AN) membrane possessing 78.1% β”-phase was tightly wrapped by PVDF-HFP-based GPE, effectively inhibiting the growth of Na dendrite and successive side reactions of the Na metal anode [Figure 8D][47]. This study for the first time proved the efficient inorganic solid electrolyte ion conductor/polymer composite gel transmission behavior of sodium ions with inorganic ion conductor in its solid-liquid mixture of sodium ion transport mechanism, and illustrated the high efficient inorganic ion conductor matrix composite gel electrolyte for building an important highly stable solid SMB system. It provides a universal strategy for achieving high energy density, long life, and high safety of SMBs [Figure 8E].

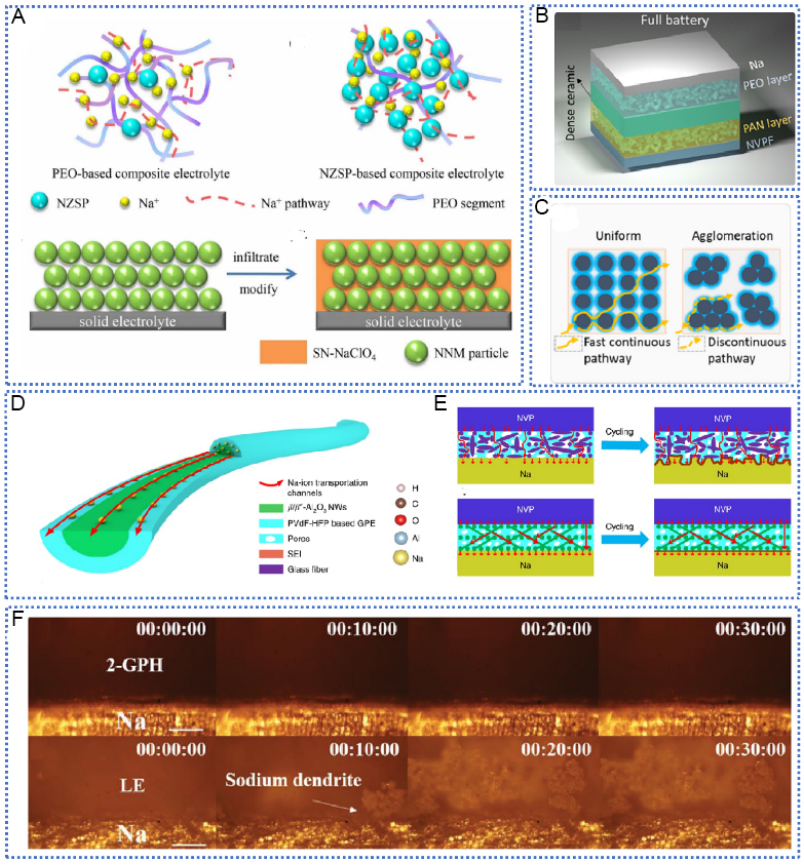

Figure 8. Hybrid inorganic-polymer electrolytes regulate SEI for dendrite-inhibited SMAs. (A) Proposed Na^+ transport model schematic in the composite electrolytes and illustration of the cathodes. Reproduced with permission from[136]. Copyright 2020, Elsevier. (B) Schematic representation of composite electrolyte. Reproduced with permission from[51]. Copyright 2021, Elsevier. (C) Schematic of ion pathway in NZSP-PEO CE. Reproduced with permission from[137]. Copyright 2021, American Chemical Society. (D) Structure of ANS-GPE composite electrolyte and mechanism of sodium ion transport. (E) Schematic of NVP/Na batteries using ANs-GPE and GFs-GPE electrolytes. (D and E) Reproduced with permission from[47]. Copyright 2016, Nature Publishing Group. (F) Optical microscope images of pristine Na and its morphologies after 100 h plating/deposition when coupled with 2-GPH GPE and LE. Reproduced with permission from[142]. Copyright 2020, Wiley-VCH. SEI: Solid electrolyte interphase; SMAs: sodium metal anodes.

Different materials can be mixed into gels to enhance mechanical strength and form an excellent interfacial matrix on the anode. As observed in Figure 8F, doping graphene oxide (GO) into PVDF-HFP generates many amorphous regions during the gel electrolyte generation to enhance sodium ion conductivity and form a uniform and smooth surface[140]. Meanwhile, the large number of oxygen-containing groups provided by GO can effectively anchor the sodium ions in the electrolyte and promote rapid and uniform sodium ion transport. Moreover, the strong H-F hydrogen bond between GO and PH can significantly increase Young's modulus of the gel electrolyte and effectively inhibit the growth of sodium dendrites. As a result, uniform sodium deposition and ultra-long reversible sodium plating/exfoliation at high current density (5 mA cm^{-2}) are achieved. Furthermore, the photoinitiator benzophenone (BP) and nanometer filler HKUST-1 were imported into the PEO matrix, thus acquiring a composite electrolyte by UV curing[141]. For PHGE (PEO + 5.0 wt.% HKUST-1 gel electrolyte), comparatively coarse surfaces could be noticed even after many cycles. The addition of HKUST-1 convincingly fixed the anions in the battery, stabilized the interface, facilitated the even deposition of Li/Na, and significantly improved the cyclic stability of symmetrical batteries, leading to uniform Na deposition and high sodium transport.

With the progress of gel polymer, novel electrolytes are being developed all the time. Wang *et al.* showed that, due to the existence of loose and multilayered structure of the $Ti_3C_2T_x$ MXene filler, the electrochemical properties of the battery were greatly enhanced, as the filler could expand the porosity of the polymer films and augment the contact sites of sodium ions[65]. After 300 cycles, lichen-like sodium dendrites were viewed on the Na anode with GPE-0 (no $Ti_3C_2T_x$). In contrast, no pronounced dendrites were noticed on the one with GPE-8, while the sodium ions were evenly deposited on its anode. Although gel electrolyte can inhibit the growth of dendrites to a certain extent, the liquid electrolyte it contains may also pose a safety hazard. Moreover, gel electrolytes generally need to be operated at higher temperatures, so cells that can cycle stably at RT are yet to be developed. In addition to GO and MXene, some 2D materials (BN, clay, *etc.*) have also been used as electrolytes in battery systems to improve ionic conductivity and inhibit dendrite growth[141,142]. Hamisu *et al.* fabricated an hBN-SPSU(Na)/PPEGMA hybrid electrolyte based on polysulfone-sodium sulfonate [SPSU(Na)] blended with poly(polyethylene glycol methacrylate) (PPEGMA) using nano-sized hexagonal boron nitride (nano-hBN) as filler[142]. Homogeneous dispersion of hBN not only improves the mechanical properties of polymer electrolytes but also enhances ionic conductivity. The addition of new 2D materials provides a new idea for the preparation of high-performance electrolytes. Through the hybrid effect, solid electrolytes present high ionic conductivity, wide stable potential windows, excellent mechanical properties, and good interface binding ability, thus meeting the requirements of practical application of solid batteries.

Table 2 presents the performance of representative batteries assembled with solid electrolytes in the recent literature. Solid electrolytes have high mechanical properties, wide electrochemical windows, and excellent thermal stability. They can also inhibit dendrite growth and promote the development of metal battery commercialization. However, due to their poor interfacial contact and low working current density, it is still necessary to spend a lot of energy to develop high-performance solid electrolytes systems.

In conclusion, we have discussed each of types of electrolytes above. The ideal electrolyte should have high ionic conductance, high interfacial stability, wide electrochemical window, thermal stability, low cost, and long life. However, different electrolytes show diverse properties. Liquid electrolyte additives can directly or indirectly participate in the construction of SEI layer to effectively inhibit the growth of sodium dendrite, but different kinds of additives may cause the battery internal reaction to be too complex, which is not conducive to the study of the electrode surface reaction; High-concentration electrolyte is an improvement of liquid electrolyte, which can solve the problem of sodium dendrite and prevent the excessive reaction of metal sodium and electrolyte, but the ion transmission speed and cost caused by high-concentration electrolyte density are important reasons for the difficulty of its commercialization; Novel electrolytes provide infinite possibilities for the development of high-performance batteries. The solid-state electrolyte is the hotspot and focus of research; Polymer electrolytes can provide excellent flexibility thus forming an acceptable contact with the anode; Inorganic solid-state electrolytes can confine the growth of dendrite by strategies such as doping; Hybrid solidstate electrolytes can effectively use the properties of the first two. Nevertheless, whatever the type of the electrolyte is, interfacial chemistry between SMAs and electrolytes plays a vital role in regulating the Na plating/stripping behavior and improving the cycling performance of SMBs. This shows that there is still a lot of space for the progress of SMBs.

CONCLUSIONS AND OUTLOOK

Sodium batteries, as an important supplement to LIBs, can effectively alleviate the dilemma of energy storage, and SMBs receive more attention because of their high energy density. Nevertheless, the safety problems of dendrite growth seriously hinder the development of sodium batteries. We provide a fundamental discussion on sodium dendrite and then summarize the study advances on suppressed

Table 2. Performance of representative batteries assembled with solid electrolytes

Material	Ionic conductivity (mS cm^{-1})	Na^+ transference number	Electrochemical window (V)	Current density (mA cm^{-2})	Cycles hours (h)	Refs.
β/β″-Al_2O_3 ANs + PVdF-HFP	1.07	0.37	-	0.5	300	[47]
8 wt % PCL-TA + 15 vol % TMP	6.3	-	4.5	0.5	400	[48]
PSTB + PVCA	0.1	0.88	4.5	0.1 0.25 0.5 1	620	[62]
PVDF-HFP/PMMA + 8wt %$Ti_3C_2T_x$ MXene	3.28	0.558	5.25	0.5	300	[65]
PFSA-Na	0.159	-	4.7	0.5	300	[114]
ETPTA-QSSE	1.2	0.62	4.7	0.1	1000	[119]
PBA	1.6	0.39	4	0.2	900	[120]
MADEMP-AEDEP-EA	3.37	0. 52	4.9	0.2	700	[121]
HKUST-1/PEO	0.6	3.48	5.17	0.2	1000	[122]
GO/NASICON	0.6	-	-	0.5	1000	[124]
NZSP-xMg	0.15	0.95	-	0.3	7000	[127]
NZSP/PEO	0.04	-	4.7	0.2	300	[136]
PEO-PN	0.12	0.61	5.2	0.1	1000	[138]
GO + PVDF-HFP	2.3	0.82	4.7	5	400	[140]
AlF_3/NASICON	0.024	-	-	0.15 0.25	150 150	[143]
BTO/NZSP	0.96	-	4.4	0.1 0.2 0.3	1000 1000 1000	[144]
NBO/NASICON	1	-	6	0.3	600	[145]
$Na_3Zr_2Si_2PO_{12}$	0.85	-	4.3	0.1	1000	[146]
SnO_x/Sn + NASICON	0.59	-	3	0.1	1500	[147]
NaPTAB + PVDF-HFP	0.94	0.91	5.2	0.05	100	[148]
NaTFSI/PEO 80 °C	0.41	0.16	4.66	0.1	1000	[149]
octa-POSS/PEG/$NaClO_4$	0.45	0.23	4.5	0.1 0.5	5100 3550	[150]
NZSP/PVDF-HFP	0.1	0.63	4.4	0.2	400	[151]
$NaClO_4$/PEGDA/PEG	0.08	0.83	4.8	-	-	[152]
EPTA	5.33	0.42	5.5	1	800	[153]
PEO/PMMA/PVDF-HFP	2.02	-	4.9	0.25	600	[154]

dendrite from the perspective of electrolytes and related SEI, including the component and the concentration of liquid electrolytes, solid-state electrolytes, and gel electrolytes. The related issues of SMAs and the strategies regulated by electrolytes and SEI are summarized in Figure 9. This provides a direction for us to inhibit dendrite growth through electrolytes regulation and SEI strategies in the future.

At present, despite great efforts implemented by researchers to surmount SMA issues, there are still a lot of unknown things about Na anode interface chemistry, including the Na ion nucleation mechanism on electrode surface, growth behavior of Na, the Na stripping mechanism, the dynamic evolution mechanism of SEI, the interaction mechanism between SEI and Na anode, the physical and chemical properties of SEI, and the state of SEI in the liquid environment. Thus, how to thoroughly characterize the existing crucial issues is an urgent challenge to be solved in future research.

Insight into the mechanism of dendrite formation. As a world-class problem in LMBs, dendrite has perplexed many researchers, as there does not exist a perfect description of its growth. Nevertheless, for SMBs, there is

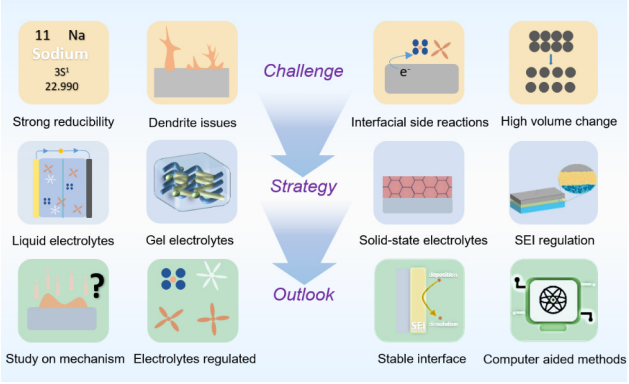

Figure 9. Conclusion and outlook of sodium metal anodes.

not even a proposed model at present. Therefore, the formation model of sodium dendrite is urgent to put forward, which lies in more advanced characterization techniques to reveal the in-depth mechanism.

Exploring advanced electrolyte additives. Electrolyte additives can optimize the physical structure and chemical composition of SEI, facilitate the even deposition of sodium ions, and realize the dendrite-free metallic sodium anode.

Developing novel functional electrolytes. For liquid electrolytes, novel functional salts and solvents need to be explored and designed, with a focus on enhancing CE and settling safety issues. In terms of solid electrolytes, new synthesis methods and preparation technologies need to be explored to realize high ionic conductivity and a broad electrochemical window of electrolytes.

Delving into the influence of SEI on dendrite. Currently, most research on SEI focuses on the battery performance. However, the overall dendrite suppression is inseparable from the construction of SEI. Hence, the study of the inhibitory effect of SEI on dendrite should be given great importance, e.g. the impact of different chemical components in SEI and the influence of the balance between thickness and uniformity on dendrite.

Clarify the relationship among electrolyte, SEI, and dendrite. The structural characteristics of electrolyte, SEI, and dendrite need to be studied by advanced characterization methods, and the relationship among them should be elucidated. This provides a more effective way to achieve a dendrite-free sodium anode through electrolyte regulation and SEI strategies in the future.

Emerging computer-aided methods. The design and development of electrolytes and the influencing factors of SEI components on dendrites are very complex. It is a rather time-consuming and costly process to explore through experiments. As a result, mechanism exploration can be combined with emerging computational science such as machine learning and large data analysis to predict the possible mechanism for sodium dendrite and SEI, thus saving labor cost and contributing to technological development.

Combining advanced characterization with theoretical simulations. Advanced characterization techniques should be combined with theoretical simulation to explore Na metal deposition/stripping behavior and the mechanism of SEI formation.

DECLARATIONS

Authors' contributions

Prepared and revised the manuscript: Li G, Lou X
Revised the manuscript: Peng C, Liu C
Designed and revised the manuscript: Chen W
All authors contributed to the discussion and preparation of the manuscript.

Availability of data and materials

Not applicable.

Financial support and sponsorship

This review was supported by the National Natural Science Foundation of China (22279121, U1804129), China Postdoctoral Science Foundation (Grant No. 2022M712863), Basic Discipline Top Student Training Program 2.0 of Ministry of Education, Zhongyuan Youth Talent Support Program of Henan Province, Joint Fund of Scientific and Technological Research and Development Program of Henan Province, and Zhengzhou University.

Conflicts of interest

All authors declared that there are no conflicts of interest.

Ethical approval and consent to participate

Not applicable.

Consent for publication

Not applicable.

REFERENCES

1. Ge J, Fan L, Rao AM, Zhou J, Lu B. Surface-substituted Prussian blue analogue cathode for sustainable potassium-ion batteries. *Nat Sustain* 2022;5:225-34. DOI
2. Song K, Liu C, Mi L, Chou S, Chen W, Shen C. Recent progress on the alloy-based anode for sodium-ion batteries and potassium-ion batteries. *Small* 2021;17:e1903194. DOI PubMed
3. Wan Y, Song K, Chen W, et al. Ultra-high initial coulombic efficiency induced by interface engineering enables rapid, stable sodium storage. *Angew Chem Int Ed Engl* 2021;60:11481-6. DOI PubMed
4. Leng K, Li G, Guo J, et al. A safe polyzwitterionic hydrogel electrolyte for long-life quasi-solid state zinc metal batteries. *Adv Funct Mater* 2020;30:2001317. DOI
5. Zhang C, Liu S, Li G, Zhang C, Liu X, Luo J. Incorporating ionic paths into 3D conducting scaffolds for high volumetric and areal capacity, high rate lithium-metal anodes. *Adv Mater* 2018:e1801328. DOI PubMed
6. Li G, Guan X, Wang A, Wang C, Luo J. Cations and anions regulation through zwitterionic gel electrolytes for stable lithium metal anodes. *Energy Storage Mater* 2020;24:574-8. DOI
7. Wang R, Zheng J, Feng X, et al. Highly [010]-oriented, gradient Co-doped $LiMnPO_4$ with enhanced cycling stability as cathode for Li-ion batteries. *J Solid State Electrochem* 2020;24:511-9. DOI
8. Yang K, Zhang X, Song K, et al. Se-C bond and reversible SEI in facile synthesized $SnSe_2$3D carbon induced stable anode for sodium-ion batteries. *Electrochimica Acta* 2020;337:135783. DOI
9. Hwang JY, Myung ST, Sun YK. Sodium-ion batteries: present and future. *Chem Soc Rev* 2017;46:3529-614. DOI PubMed
10. Åvall G, Mindemark J, Brandell D, Johansson P. Sodium-ion battery electrolytes: modeling and simulations. *Adv Energy Mater* 2018;8:1703036. DOI
11. Zhang J, Song K, Mi L, et al. Bimetal synergistic effect induced high reversibility of conversion-type $Ni@NiCo_2S_4$ as a free-standing anode for sodium ion batteries. *J Phys Chem Lett* 2020;11:1435-42. DOI PubMed
12. Chen L, Song K, Shi J, et al. PAANa-induced ductile SEI of bare micro-sized FeS enables high sodium-ion storage performance. *Sci*

China Mater 2021;64:105-14. DOI
13. Ma B, Bai P. Fast charging limits of ideally stable metal anodes in liquid electrolytes. *Adv Eng Mater* 2022;12:2102967. DOI
14. Zhao Y, Liu H, Meng X, Liu A, Chen Y, Ma T. A cross-linked tin oxide/polymer composite gel electrolyte with adjustable porosity for enhanced sodium ion batteries. *Chem Energ J* 2022;431:133922. DOI
15. Zhou S, Lan J, Song K, Zhang Z, Shi J, Chen W. SnS/SnS_2/rGO heterostructure with fast kinetics enables compact sodium ion storage. *FlatChem* 2021;28:100259. DOI
16. Miao RJ, Cao XG, Wang WG, Zhang HY. Influence of Bi_2O_3 additive on the electrochemical performance of $Na_{3.1}Y_{0.1}Zr_{1.9}Si_2PO_{12}$ inorganic solid electrolyte. *Ceram Int* 2021;47:17455-62. DOI
17. Das SK, Lau S, Archer LA. Sodium-oxygen batteries: a new class of metal-air batteries. *J Mater Chem A* 2014;2:12623. DOI
18. Manthiram A, Yu X. Ambient temperature sodium-sulfur batteries. *Small* 2015;11:2108-14. DOI PubMed
19. Zhang D, Li B, Wang S, Yang S. Simultaneous formation of artificial SEI film and 3D host for stable metallic sodium anodes. *ACS Appl Mater Interfaces* 2017;9:40265-72. DOI PubMed
20. Wu J, Liu J, Lu Z, et al. Non-flammable electrolyte for dendrite-free sodium-sulfur battery. *Energy Storage Mater* 2019;23:8-16. DOI
21. Zhao S, Li L, Li F, Chou S. Recent progress on understanding and constructing reliable Na anode for aprotic Na-O_2 batteries: a mini review. *Electrochem commun* 2020;118:106797. DOI
22. Tong Z, Wang S, Fang M, et al. Na-CO_2 battery with NASICON-structured solid-state electrolyte. *Nano Energy* 2021;85:105972. DOI
23. Ding J, Zhou H, Zhang H, Tong L, Mitlin D. Selenium impregnated monolithic carbons as free-standing cathodes for high volumetric energy lithium and sodium metal batteries. *Adv Energy Mater* 2018;8:1701918. DOI
24. Pham VH, Boscoboinik JA, Stacchiola DJ, et al. Selenium-sulfur (SeS) fast charging cathode for sodium and lithium metal batteries. *Energy Storage Mater* 2019;20:71-9. DOI
25. Wang Y, Wang Y, Wang Y, et al. Developments and perspectives on emerging high-energy-density sodium-metal batteries. *Chem* 2019;5:2547-70. DOI
26. Wang Y, Jiang R, Liu Y, et al. Enhanced sodium metal/electrolyte interface by a localized high-concentration electrolyte for sodium metal batteries: first-principles calculations and experimental studies. *ACS Appl Energy Mater* 2021;4:7376-84. DOI
27. Yu Q, Lu Q, Qi X, et al. Liquid electrolyte immobilized in compact polymer matrix for stable sodium metal anodes. *Energy Storage Mater* 2019;23:610-6. DOI
28. Xu X, Li Y, Cheng J, et al. Composite solid electrolyte of Na_3PS_4-PEO for all-solid-state SnS_2/Na batteries with excellent interfacial compatibility between electrolyte and Na metal. *J Energ Chem* 2020;41:73-8. DOI
29. Mittal N, Tien S, Lizundia E, Niederberger M. Hierarchical nanocellulose-based gel polymer electrolytes for stable na electrodeposition in sodium ion batteries. *Small* 2022:e2107183. DOI PubMed
30. Bao C, Wang B, Liu P, et al. Solid electrolyte interphases on sodium metal anodes. *Adv Funct Mater* 2020;30:2004891. DOI
31. Yao G, Zhang X, Yan Y, et al. Facile synthesis of hierarchical $Na_2Fe(SO_4)_2$@rGO/C as high-voltage cathode for energy density-enhanced sodium-ion batteries. *J Energ Chem* 2020;50:387-94. DOI
32. Ponrouch A, Monti D, Boschin A, Steen B, Johansson P, Palacín MR. Non-aqueous electrolytes for sodium-ion batteries. *J Mater Chem A* 2015;3:22-42. DOI PubMed
33. Li Y, Arnold W, Halacoglu S, Jasinski JB, Druffel T, Wang H. Phase-transition interlayer enables high-performance solid-state sodium batteries with sulfide solid electrolyte. *Adv Funct Mater* 2021;31:2101636. DOI
34. Wei S, Choudhury S, Xu J, Nath P, Tu Z, Archer LA. Highly stable sodium batteries enabled by functional ionic polymer membranes. *Adv Mater* 2017;29:1605512. DOI PubMed
35. Manohar C, Raj K A, Kar M, Forsyth M, Macfarlane DR, Mitra S. Stability enhancing ionic liquid hybrid electrolyte for NVP@C cathode based sodium batteries. *Sustainable Energy Fuels* 2018;2:566-76. DOI
36. Mishra K, Yadav N, Hashmi SA. Recent progress in electrode and electrolyte materials for flexible sodium-ion batteries. *J Mater Chem A* 2020;8:22507-43. DOI
37. Wang T, Hua Y, Xu Z, Yu JS. Recent advanced development of artificial interphase engineering for stable sodium metal anodes. *Small* 2022;18:e2102250. DOI PubMed
38. Lee J, Kim J, Kim S, Jo C, Lee J. A review on recent approaches for designing the SEI layer on sodium metal anodes. *Mater Adv* 2020;1:3143-66. DOI
39. Zhao C, Lu Y, Yue J, et al. Advanced Na metal anodes. *J Energ Chem* 2018;27:1584-96. DOI
40. Ma C, Xu T, Wang Y. Advanced carbon nanostructures for future high performance sodium metal anodes. *Energy Storage Mater* 2020;25:811-26. DOI
41. Fan L, Li X. Recent advances in effective protection of sodium metal anode. *Nano Energy* 2018;53:630-42. DOI
42. Matios E, Wang H, Wang C, Li W. Enabling safe sodium metal batteries by solid electrolyte interphase engineering: a review. *Ind Eng Chem Res* 2019;58:9758-80. DOI
43. Zhao C, Liu L, Qi X, et al. Solid-state sodium batteries. *Adv Energy Mater* 2018;8:1703012. DOI
44. Zheng X, Gu Z, Liu X, et al. Bridging the immiscibility of an all-fluoride fire extinguishant with highly-fluorinated electrolytes toward safe sodium metal batteries. *Energy Environ Sci* 2020;13:1788-98. DOI
45. Zheng J, Chen S, Zhao W, Song J, Engelhard MH, Zhang J. Extremely stable sodium metal batteries enabled by localized high-

concentration electrolytes. *ACS Energy Lett* 2018;3:315-21. DOI

46. Zhu M, Li L, Zhang Y, et al. An in-situ formed stable interface layer for high-performance sodium metal anode in a non-flammable electrolyte. *Energy Storage Mater* 2021;42:145-53. DOI
47. Lei D, He YB, Huang H, et al. Cross-linked beta alumina nanowires with compact gel polymer electrolyte coating for ultra-stable sodium metal battery. *Nat Commun* 2019;10:4244. DOI PubMed PMC
48. Park T, Park M, Ban A, Lee Y, Kim D. Nonflammable gel polymer electrolyte with ion-conductive polyester networks for sodium metal cells with excellent cycling stability and enhanced safety. *ACS Appl Energy Mater* 2021;4:10153-62. DOI
49. Yao Y, Wei Z, Wang H, et al. Toward high energy density all solid-state sodium batteries with excellent flexibility. *Adv Energy Mater* 2020;10:1903698. DOI
50. Lai H, Li Y, Wang J, Li W, Wu X, Wen Z. Design of solid-state sodium-ion batteries with high mass-loading cathode by porous-dense bilayer electrolyte. *Journal of Materiomics* 2021;7:1352-7. DOI
51. Ran L, Li M, Cooper E, et al. Enhanced safety and performance of high-voltage solid-state sodium battery through trilayer, multifunctional electrolyte design. *Energy Storage Mater* 2021;41:8-13. DOI
52. Zhang Z, Zhang Q, Ren C, et al. A ceramic/polymer composite solid electrolyte for sodium batteries. *J Mater Chem A* 2016;4:15823-8. DOI
53. Hong Y, Li N, Chen H, Wang P, Song W, Fang D. In operando observation of chemical and mechanical stability of Li and Na dendrites under quasi-zero electrochemical field. *Energy Storage Mater* 2018;11:118-26. DOI
54. Han M, Zhu C, Ma T, Pan Z, Tao Z, Chen J. In situ atomic force microscopy study of nano-micro sodium deposition in ester-based electrolytes. *Chem Commun (Camb)* 2018;54:2381-4. DOI PubMed
55. Wang H, Wang C, Matios E, Li W. Facile stabilization of the sodium metal anode with additives: unexpected key role of sodium polysulfide and adverse effect of sodium nitrate. *Angew Chem Int Ed Engl* 2018;57:7734-7. DOI PubMed
56. Hu J, Wang H, Wang S, et al. Electrochemical deposition mechanism of sodium and potassium. *Energy Storage Mater* 2021;36:91-8. DOI
57. Zheng X, Bommier C, Luo W, Jiang L, Hao Y, Huang Y. Sodium metal anodes for room-temperature sodium-ion batteries: applications, challenges and solutions. *Energy Storage Mater* 2019;16:6-23. DOI
58. Gaissmaier D, van den Borg M, Fantauzzi D, Jacob T. Microscopic properties of Na and Li-a first principle study of metal battery anode materials. *ChemSusChem* 2020;13:771-83. DOI PubMed PMC
59. Medenbach L, Bender CL, Haas R, et al. Origins of dendrite formation in sodium-oxygen batteries and possible countermeasures. *Energy Technol* 2017;5:2265-74. DOI
60. Rodriguez R, Loeffler KE, Nathan SS, et al. In situ optical imaging of sodium electrodeposition: effects of fluoroethylene carbonate. *ACS Energy Lett* 2017;2:2051-7. DOI
61. Akolkar R. Mathematical model of the dendritic growth during lithium electrodeposition. *J Power Sources* 2013;232:23-8. DOI
62. Park MS, Woo HS, Heo JM, et al. Thermoplastic polyurethane elastomer-based gel polymer electrolytes for sodium-metal cells with enhanced cycling performance. *ChemSusChem* 2019;12:4645-54. DOI PubMed
63. Gu Y, Wang WW, Li YJ, et al. Designable ultra-smooth ultra-thin solid-electrolyte interphases of three alkali metal anodes. *Nat Commun* 2018;9:1339. DOI PubMed PMC
64. Sun B, Xiong P, Maitra U, et al. Design strategies to enable the efficient use of sodium metal anodes in high-energy batteries. *Adv Mater* 2020;32:e1903891. DOI PubMed
65. Wang X, Wang X, Chen J, Zhao Y, Mao Z, Wang D. Durable sodium battery composed of conductive Ti_3C_2Tx MXene modified gel polymer electrolyte. *Solid State Ionics* 2021;365:115655. DOI
66. Gao H, Xin S, Xue L, Goodenough JB. Stabilizing a high-energy-density rechargeable sodium battery with a solid electrolyte. *Chem* 2018;4:833-44. DOI
67. Wang H, Matios E, Luo J, Li W. Combining theories and experiments to understand the sodium nucleation behavior towards safe sodium metal batteries. *Chem Soc Rev* 2020;49:3783-805. DOI PubMed
68. Rees GJ, Spencer Jolly D, Ning Z, Marrow TJ, Pavlovskaya GE, Bruce PG. Imaging sodium dendrite growth in all-solid-state sodium batteries using ^{23}Na T_2-weighted magnetic resonance imaging. *Angew Chem Int Ed Engl* 2021;60:2110-5. DOI
69. Wang X, Chen J, Mao Z, Wang D. In situ construction of a stable interface induced by the SnS_2 ultra-thin layer for dendrite restriction in a solid-state sodium metal battery. *J Mater Chem A* 2021;9:16039-45. DOI
70. Yi Q, Lu Y, Sun X, Zhang H, Yu H, Sun C. Fluorinated ether based electrolyte enabling sodium-metal batteries with exceptional cycling stability. *ACS Appl Mater Interfaces* 2019;11:46965-72. DOI PubMed
71. Wang T, Yang K, Shi J, et al. Simple synthesis of sandwich-like $SnSe_2$/rGO as high initial coulombic efficiency and high stability anode for sodium-ion batteries. *J Energ Chem* 2020;46:71-7. DOI
72. Gao L, Chen J, Liu Y, Yamauchi Y, Huang Z, Kong X. Revealing the chemistry of an anode-passivating electrolyte salt for high rate and stable sodium metal batteries. *J Mater Chem A* 2018;6:12012-7. DOI
73. Xu Y, Sun H, Ma C, Gai J, Wan Y, Chen W. Pre-sodiation strategy for superior sodium storage batteries. *Chin J Chem Eng* 2021;39:261-8. DOI
74. Fang W, Jiang H, Zheng Y, et al. A bilayer interface formed in high concentration electrolyte with SbF_3 additive for long-cycle and high-rate sodium metal battery. *J Power Sources* 2020;455:227956. DOI
75. Lei Y, Du G, Qi Y, Niu Y, Bao S, Xu M. Gelation of organic liquid electrolyte to achieve superior sodium-ion full-cells. *J Colloid*

Interface Sci 2021;599:190-7. DOI PubMed

76. Xu M, Li Y, Ihsan-ul-haq M, et al. NaF-rich solid electrolyte interphase for dendrite-free sodium metal batteries. *Energy Storage Mater* 2022;44:477-86. DOI
77. Wenzel S, Leichtweiss T, Krüger D, Sann J, Janek J. Interphase formation on lithium solid electrolytes - an in situ approach to study interfacial reactions by photoelectron spectroscopy. *Solid State Ionics* 2015;278:98-105. DOI
78. Binder M, Mandl M, Zaubitzer S, et al. Sodium cyclopentadienide as a new type of electrolyte for sodium batteries. *ChemElectroChem* 2021;8:365-9. DOI
79. Ge C, Wang L, Xue L, et al. Synthesis of novel organic-ligand-doped sodium bis(oxalate)-borate complexes with tailored thermal stability and enhanced ion conductivity for sodium ion batteries. *J Power Sources* 2014;248:77-82. DOI
80. Voropaeva D, Novikova S, Kulova T, Yaroslavtsev A. Solvation and sodium conductivity of nonaqueous polymer electrolytes based on Nafion-117 membranes and polar aprotic solvents. *Solid State Ionics* 2018;324:28-32. DOI
81. Xu X, Zhou D, Qin X, et al. A room-temperature sodium-sulfur battery with high capacity and stable cycling performance. *Nat Commun* 2018;9:3870. DOI PubMed PMC
82. Li P, Jiang Z, Huang X, Lu X, Xie J, Cheng S. Nitrofullerene as an electrolyte-compatible additive for high-performance sodium metal batteries. *Nano Energy* 2021;89:106396. DOI
83. Chen Q, He H, Hou Z, et al. Building an artificial solid electrolyte interphase with high-uniformity and fast ion diffusion for ultralong-life sodium metal anodes. *J Mater Chem A* 2020;8:16232-7. DOI
84. Chen X, Shen X, Hou T, Zhang R, Peng H, Zhang Q. Ion-solvent chemistry-inspired cation-additive strategy to stabilize electrolytes for sodium-metal batteries. *Chem* 2020;6:2242-56. DOI
85. Hu Y, Lu Y. The mystery of electrolyte concentration: from superhigh to ultralow. *ACS Energy Lett* 2020;5:3633-6. DOI
86. Ma J, Zhang W, Wang X, et al. Revealing the mechanism of saturated ether electrolyte for improving the long-cycling stability of Na-O_2 batteries. *Nano Energy* 2021;84:105927. DOI
87. Wang H, Tong Z, Yang R, et al. Electrochemically stable sodium metal-tellurium/carbon nanorods batteries. *Adv Energy Mater* 2019;9:1903046. DOI
88. Zhou X, Zhang Q, Zhu Z, Cai Y, Li H, Li F. Anion-reinforced solvation for a gradient inorganic-rich interphase enables high-rate and stable sodium batteries. *Angew Chem Int Ed Engl* 2022;61:e202205045. DOI PubMed
89. Forsyth M, Yoon H, Chen F, et al. Novel Na^+ ion diffusion mechanism in mixed organic-inorganic ionic liquid electrolyte leading to high Na^+ transference number and stable, high rate electrochemical cycling of sodium cells. *J Phys Chem C* 2016;120:4276-86. DOI
90. Sun H, Zhu G, Xu X, et al. A safe and non-flammable sodium metal battery based on an ionic liquid electrolyte. *Nat Commun* 2019;10:3302. DOI PubMed PMC
91. Wang D, Hwang J, Chen C, Kubota K, Matsumoto K, Hagiwara R. A β”-Alumina/inorganic ionic liquid dual electrolyte for intermediate-temperature sodium-sulfur batteries. *Adv Funct Materials* 2021;31:2105524. DOI
92. Ruiz-martínez D, Kovacs A, Gómez R. Development of novel inorganic electrolytes for room temperature rechargeable sodium metal batteries. *Energy Environ Sci* 2017;10:1936-41. DOI
93. Zhou H, Li H, Gong Q, et al. A sodium liquid metal battery based on the multi-cationic electrolyte for grid energy storage. *Energy Storage Mater* 2022;50:572-9. DOI
94. Liu X, Zheng X, Deng Y, et al. Implanting a fire-extinguishing alkyl in sodium metal battery electrolytes via a functional molecule. *Adv Funct Materials* 2022;32:2109378. DOI
95. Jiang R, Hong L, Liu Y, et al. An acetamide additive stabilizing ultra-low concentration electrolyte for long-cycling and high-rate sodium metal battery. *Energy Storage Mater* 2021;42:370-9. DOI
96. Shi Q, Zhong Y, Wu M, Wang H, Wang H. High-performance sodium metal anodes enabled by a bifunctional potassium salt. *Angew Chem Int Ed Engl* 2018;57:9069-72. DOI PubMed
97. Lee J, Lee Y, Lee J, et al. Ultraconcentrated sodium bis(fluorosulfonyl)imide-based electrolytes for high-performance sodium metal batteries. *ACS Appl Mater Interfaces* 2017;9:3723-32. DOI PubMed
98. Seh ZW, Sun J, Sun Y, Cui Y. A Highly reversible room-temperature sodium metal anode. *ACS Cent Sci* 2015;1:449-55. DOI PubMed PMC
99. Wang S, Chen Y, Jie Y, et al. Stable sodium metal batteries via manipulation of electrolyte solvation structure. *Small Methods* 2020;4:1900856. DOI
100. Zhang Q, Lu Y, Miao L, et al. An alternative to lithium metal anodes: non-dendritic and highly reversible sodium metal anodes for Li-Na hybrid batteries. *Angew Chem Int Ed Engl* 2018;57:14796-800. DOI PubMed
101. Lee B, Paek E, Mitlin D, Lee SW. Sodium metal anodes: emerging solutions to dendrite growth. *Chem Rev* 2019;119:5416-60. DOI PubMed
102. He J, Bhargav A, Shin W, Manthiram A. Stable dendrite-free sodium-sulfur batteries enabled by a localized high-concentration electrolyte. *J Am Chem Soc* 2021;143:20241-8. DOI PubMed
103. Chen F, Wang X, Armand M, Forsyth M. Cationic polymer-in-salt electrolytes for fast metal ion conduction and solid-state battery applications. *Nat Mater* 2022. DOI PubMed
104. Lu Z, Yang H, Guo Y, et al. Electrolyte sieving chemistry in suppressing gas evolution of sodium-metal batteries. *Angew Chem Int Ed Engl* 2022;61:e202206340. DOI PubMed
105. Wang X, Zhang C, Sawczyk M, et al. Ultra-stable all-solid-state sodium metal batteries enabled by perfluoropolyether-based

electrolytes. *Nat Mater* 2022;21:1057-65. DOI PubMed

106. Zhu X, Zhao R, Deng W, Ai X, Yang H, Cao Y. An all-solid-state and all-organic sodium-ion battery based on redox-active polymers and plastic crystal electrolyte. *Electrochimica Acta* 2015;178:55-9. DOI
107. Babu B, Enke M, Prykhodska S, Lex-Balducci A, Schubert US, Balducci A. New diglyme-based gel polymer electrolytes for na-based energy storage devices. *ChemSusChem* 2021;14:4836-45. DOI PubMed PMC
108. Yu X, Xue L, Goodenough JB, Manthiram A. Ambient-temperature all-solid-state sodium batteries with a laminated composite electrolyte. *Adv Funct Mater* 2021;31:2002144. DOI
109. Zheng J, Yang Y, Li W, Feng X, Chen W, Zhao Y. Novel flame retardant rigid spirocyclic biphosphate based copolymer gel electrolytes for sodium ion batteries with excellent high-temperature performance. *J Mater Chem A* 2020;8:22962-8. DOI
110. Bitner-Michalska A, Nolis GM, Żukowska G, et al. Fluorine-free electrolytes for all-solid sodium-ion batteries based on percyano-substituted organic salts. *Sci Rep* 2017;7:40036. DOI PubMed PMC
111. Gao H, Xue L, Xin S, Park K, Goodenough JB. A plastic-crystal electrolyte interphase for all-solid-state sodium batteries. *Angew Chem Int Ed Engl* 2017;56:5541-5. DOI PubMed
112. Makhlooghiazad F, Nti F, Sun J, et al. Composite electrolytes based on electrospun PVDF and ionic plastic crystal matrices for Na-metal battery applications. *J Phys Mater* 2021;4:034003. DOI
113. Chen G, Ye L, Zhang K, et al. Hyperbranched polyether boosting ionic conductivity of polymer electrolytes for all-solid-state sodium ion batteries. *Chem Eng J* 2020;394:124885. DOI
114. Du G, Tao M, Li J, et al. Low-operating temperature, high-rate and durable solid-state sodium-ion battery based on polymer electrolyte and prussian blue cathode. *Adv Energy Mater* 2020;10:1903351. DOI
115. Zhao C, Liu L, Lu Y, Wagemaker M, Chen L, Hu YS. Revealing an interconnected interfacial layer in solid-state polymer sodium batteries. *Angew Chem Int Ed Engl* 2019;58:17026-32. DOI PubMed
116. Chen S, Feng F, Yin Y, Che H, Liao X, Ma Z. A solid polymer electrolyte based on star-like hyperbranched β-cyclodextrin for all-solid-state sodium batteries. *J Power Sources* 2018;399:363-71. DOI
117. Gao H, Zhou W, Park K, Goodenough JB. A sodium-ion battery with a low-cost cross-linked gel-polymer electrolyte. *Adv Energy Mater* 2016;6:1600467. DOI
118. Xiong W, Tu Z, Yin Z, Zhang X, Hu X, Wu Y. Supported ionic liquid gel membranes enhanced by ionization modification for sodium metal batteries. *ACS Sustainable Chem Eng* 2021;9:12100-8. DOI
119. Wen P, Lu P, Shi X, et al. Photopolymerized gel electrolyte with unprecedented room-temperature ionic conductivity for high-energy-density solid-state sodium metal batteries. *Adv Energy Mater* 2021;11:2002930. DOI
120. Zhang W, Zhang J, Liu X, et al. In-situ polymerized gel polymer electrolytes with high room-temperature ionic conductivity and regulated Na^+ solvation structure for sodium metal batteries. *Adv Funct Materials* 2022;32:2201205. DOI
121. Zheng J, Sun Y, Li W, Feng X, Chen W, Zhao Y. Effects of comonomers on the performance of stable phosphonate-based gel terpolymer electrolytes for sodium-ion batteries with ultralong cycling stability. *ACS Appl Mater Interfaces* 2021;13:25024-35. DOI PubMed
122. Bay M, Wang M, Grissa R, Heinz MVF, Sakamoto J, Battaglia C. Sodium plating from Na-β"-alumina ceramics at room temperature, paving the way for fast-charging all-solid-state batteries. *Adv Energy Mater* 2020;10:1902899. DOI
123. Wu J, Zhang R, Fu Q, et al. Inorganic solid electrolytes for all-solid-state sodium batteries: fundamentals and strategies for battery optimization. *Adv Funct Mater* 2021;31:2008165. DOI
124. Matios E, Wang H, Wang C, et al. Graphene regulated ceramic electrolyte for solid-state sodium metal battery with superior electrochemical stability. *ACS Appl Mater Interfaces* 2019;11:5064-72. DOI PubMed
125. Weng W, Liu G, Shen L, Yao X. High ionic conductivity and stable phase $Na_{11.5}Sn_2Sb_{0.5}Ti_{0.5}S_{12}$ for all-solid-state sodium batteries. *J Power Sources* 2021;512:230485. DOI
126. Wang X, Chen J, Wang D, Mao Z. Improving the alkali metal electrode/inorganic solid electrolyte contact via room-temperature ultrasound solid welding. *Nat Commun* 2021;12:7109. DOI PubMed PMC
127. Wang C, Sun Z, Zhao Y, et al. Grain boundary design of solid electrolyte actualizing stable all-solid-state sodium batteries. *Small* 2021;17:e2103819. DOI PubMed
128. Quérel E, Seymour ID, Cavallaro A, Ma Q, Tietz F, Aguadero A. The role of NaSICON surface chemistry in stabilizing fast-charging Na metal solid-state batteries. *J Phys Energy* 2021;3:044007. DOI
129. Zhang S, Zhao Y, Zhao F, et al. Gradiently sodiated alucone as an interfacial stabilizing strategy for solid-state na metal batteries. *Adv Funct Mater* 2020;30:2001118. DOI
130. Johari NSM, Jonderian A, Jia S, et al. High-throughput development of Na_2ZnSiO_4-based hybrid electrolytes for sodium-ion batteries. *J Power Sources* 2022;541:231706. DOI
131. Nsm J, Sbrs A, Ahmad N. Sodium-ion nanoionic hybrid solid electrolyte: extended study on enhanced electrical and electrochemical properties. *Solid State Ionics* 2022;377:115882. DOI
132. Zhang T, Li J, Li X, et al. A silica-reinforced composite electrolyte with greatly enhanced interfacial lithium-ion transfer kinetics for high-performance lithium metal batteries. *Adv Mater* 2022:e2205575. DOI PubMed
133. Zhang C, Wang A, Zhang J, Guan X, Tang W, Luo J. 2D materials for lithium/sodium metal anodes. *Adv Energy Mater* 2018;8:1802833. DOI
134. Tang W, Tang S, Zhang C, et al. Simultaneously enhancing the thermal stability, mechanical modulus, and electrochemical

performance of solid polymer electrolytes by incorporating 2D sheets. *Adv Energy Mater* 2018;8:1800866. DOI

135. He F, Tang W, Zhang X, Deng L, Luo J. High energy density solid state lithium metal batteries enabled by sub-5 μm solid polymer electrolytes. *Adv Mater* 2021;33:e2105329. DOI PubMed
136. Niu W, Chen L, Liu Y, Fan L. All-solid-state sodium batteries enabled by flexible composite electrolytes and plastic-crystal interphase. *Chem Eng J* 2020;384:123233. DOI
137. Zhou Y, Xiao Z, Han D, et al. Approaching practically accessible and environmentally adaptive sodium metal batteries with high loading cathodes through in situ interlock interface. *Adv Funct Materials* 2022;32:2111314. DOI
138. Ran L, Tao S, Gentle I, et al. Stable interfaces in a sodium metal-free, solid-state sodium-ion battery with gradient composite electrolyte. *ACS Appl Mater Interfaces* 2021;13:39355-62. DOI PubMed
139. Matios E, Wang H, Luo J, et al. Reactivity-guided formulation of composite solid polymer electrolytes for superior sodium metal batteries. *J Mater Chem A* 2021;9:18632-43. DOI
140. Luo C, Shen T, Ji H, et al. Mechanically robust gel polymer electrolyte for an ultrastable sodium metal battery. *Small* 2020;16:e1906208. DOI PubMed
141. Zhang Z, Huang Y, Li C, Li X. Metal-organic framework-supported poly(ethylene oxide) composite gel polymer electrolytes for high-performance lithium/sodium metal batteries. *ACS Appl Mater Interfaces* 2021;13:37262-72. DOI PubMed
142. Hamisu A, Çelik SÜ. Polymer composite electrolyte of SPSU(Na)/PPEGMA/hBN for sodium-ion batteries. *Polymers and Polymer Composites* 2019;27:419-28. DOI
143. Miao X, Di H, Ge X, et al. AlF3-modified anode-electrolyte interface for effective Na dendrites restriction in NASICON-based solid-state electrolyte. *Energy Storage Mater* 2020;30:170-8. DOI
144. Sun Z, Zhao Y, Ni Q, et al. Solid-state Na metal batteries with superior cycling stability enabled by ferroelectric enhanced Na/$Na_3Zr_2Si_2PO_{12}$ interface. *Small* 2022;18:e2200716. DOI
145. Zhao Y, Wang C, Dai Y, Jin H. Homogeneous Na^+ transfer dynamic at Na/$Na_3Zr_2Si_2PO_{12}$ interface for all solid-state sodium metal batteries. *Nano Energy* 2021;88:106293. DOI
146. Wang C, Jin H, Zhao Y. Surface potential regulation realizing stable sodium/$Na_3Zr_2Si_2PO_{12}$ interface for room-temperature sodium metal batteries. *Small* 2021;17:e2100974. DOI
147. Yang J, Xu H, Wu J, et al. Improving Na/$Na_3Zr_2Si_2PO_{12}$ interface via SnO_x/Sn film for high-performance solid-state sodium metal batteries. *Small Methods* 2021;5:e2100339. DOI
148. Yang L, Jiang Y, Liang X, et al. Novel sodium-poly(tartaric acid)borate-based single-ion conducting polymer electrolyte for sodium-metal batteries. *ACS Appl Energy Mater* 2020;3:10053-60. DOI
149. Qi X, Ma Q, Liu L, et al. Sodium bis(fluorosulfonyl)imide/poly(ethylene oxide) polymer electrolytes for sodium-ion batteries. *ChemElectroChem* 2016;3:1741-5. DOI
150. Zheng Y, Pan Q, Clites M, Byles BW, Pomerantseva E, Li CY. High-capacity all-solid-state sodium metal battery with hybrid polymer electrolytes. *Adv Energy Mater* 2018;8:1801885. DOI
151. Ling W, Fu N, Yue J, et al. A flexible solid electrolyte with multilayer structure for sodium metal batteries. *Adv Energy Mater* 2020;10:1903966. DOI
152. Luo C, Li Q, Shen D, Zheng R, Huang D, Chen Y. Enhanced interfacial kinetics and fast Na^+ conduction of hybrid solid polymer electrolytes for all-solid-state batteries. *Energy Storage Mater* 2021;43:463-70. DOI
153. Xu X, Lin K, Zhou D, et al. Quasi-solid-state dual-ion sodium metal batteries for low-cost energy storage. *Chem* 2020;6:902-18. DOI
154. Shi J, Xiong H, Yang Y, Shao H. Nano-sized oxide filled composite PEO/PMMA/P(VDF-HFP) gel polymer electrolyte for rechargeable lithium and sodium batteries. *Solid State Ionics* 2018;326:136-44. DOI

AUTHOR INSTRUCTIONS

1. Submission Overview

Before you decide to publish with *Chemical Synthesis*, please read the following items carefully and make sure that you are well aware of Editorial Policies and the following requirements.

1.1 Topic Suitability

The topic of the manuscript must fit the scope of the journal. Please refer to Aims and Scope for more information.

1.2 Open Access and Copyright

The journal adopts Gold Open Access publishing model and distributes content under the Creative Commons Attribution 4.0 International License. Copyright is retained by authors. Please make sure that you are well aware of these policies.

1.3 Publication Fees

Chemical Synthesis is an open access journal. When a paper is accepted for publication, authors are required to pay Article Processing Charges (APCs) to cover its editorial and production costs. The APC for each submission is $600. There are no additional charges based on color, length, figures, or other elements. For more details, please refer to OAE Publication Fees.

1.4 Language Editing

All submissions are required to be presented clearly and cohesively in good English. Authors whose first language is not English are advised to have their manuscripts checked or edited by a native English speaker before submission to ensure the high quality of expression. A well-organized manuscript in good English would make the peer review even the whole editorial handling more smoothly and efficiently.
If needed, authors are recommended to consider the language editing services provided by Charlesworth to ensure that the manuscript is written in correct scientific English before submission. Authors who publish with OAE journals enjoy a special discount for the services of Charlesworth via the following two ways.

Submit your manuscripts directly at http://www.charlesworthauthorservices.com/~OAE;
Open the link http://www.charlesworthauthorservices.com/, and enter Promotion Code “OAE” when you submit.

1.5 Work Funded by the National Institutes of Health

If an accepted manuscript was funded by National Institutes of Health (NIH), the authors may inform Editors of the NIH funding number. The Editors are able to deposit the paper to the NIH Manuscript Submission System on behalf of the authors.

2. Submission Preparation

2.1 Cover Letter

A cover letter is required to be submitted accompanying each manuscript. It should be concise and explain why the study is significant, why it fits the scope of the journal, and why it would be attractive to readers, etc.
Here is a guideline of a cover letter for authors’ consideration:
In the first paragraph: include the title and type (e.g., Original Article, Review, Case Report, etc.) of the manuscript, a brief on the background of the study, the question the author sought out to answer and why;
In the second paragraph: concisely explain what was done, the main findings and why they are significant;
In the third paragraph: indicate why the manuscript fits the Aims and Scope of the journal, and why it would be attractive to readers;
In the fourth paragraph: confirm that the manuscript has not been published elsewhere and not under consideration of any other journal. All authors have approved the manuscript and agreed on its submission to the journal. Journal’s specific requirements have been met if any.
If the manuscript is contributed to a Special Issue, please also mention it in the cover letter.
If the manuscript was presented partly or entirely in a conference, the author should clearly state the background information of the event, including the conference name, time and place in the cover letter.

2.2 Types of Manuscripts

The journal publishes Research Article, Review Article, Short Communication, Feature Article, Commentary, Editorial, News, Research Highlight, Perspective, *etc*. For more details about paper type, please refer to the following table.

Manuscript Type	Definition	Abstract	Keywords	Main Text Structure
Research Article	A Research Article is a seminal and insightful research study and showcases that often involves modern techniques or methodologies. Authors should justify that their work are of novel findings.	The abstract should state briefly the purpose of the research, the principal results and major conclusions. No more than 250 words.	3-6 keywords.	The main content should include four sections: Introduction, Experimental, Results and discussion, and Conclusions.
Review Article	A Review Article should be an authoritative, well balanced and critical survey of recent progresses in an attractive or a fundamental chemical research field.	Unstructured abstract. No more than 250 words.	3-6 keywords.	The main text may consist of several sections with unfixed section titles. We suggest that the author include an "Introduction" section at the beginning, several sections with unfixed titles in the middle part, and a "Conclusion and outlook" section in the end. Corresponding authors are requested to provide a short biography (up to 200 words) and headshot for inclusion at the end of the published article.
Short Communication	Short Communications are for the urgent publication of a research which is of outstanding significance and interest to experts in the field and also to general chemistry readership. Authors should write in a clear and concise way to demonstrate the necessity of an urgent publication.	Unstructured abstract. No more than 150 words.	3-6 keywords.	The short Communication is a one body text with maximum 4 items (figures and tables) and 12 references.
Feature Article	A Feature Article is not a typical review. Feature article should highlight the author's contribution to a key field with a balanced discussion of related work from the field. A Feature Article should not, in principle, contain original research.	Unstructured abstract. No more than 250 words.	3-6 keywords.	The main text may consist of several sections with unfixed section titles. We suggest that the author include an "Introduction" section at the beginning, several sections with unfixed titles in the middle part, and a "Conclusion and outlook" section in the end.
Commentary	A Commentary is to provide comments on a newly published article or an alternative viewpoint on a certain topic.	Unstructured abstract. No more than 250 words.	3-6 keywords.	/
Editorial	An Editorial can be a comment about an important event in the world related or not to chemistry or a particular discovery in chemistry, needing a particular attention of chemistry community.	None required.	None required	/
News	A News comments an important event in the world related or not to chemistry, or a particular discovery in chemistry, needing a particular attention of chemistry community.	None required.	None required	/
Research Highlight	A Research Highlight article is peer-reviewed paper and highlights work recently published in the journal or in a recent issue of another journal.	None required.	3-6 keywords.	/
Perspective	A Perspective provides personal points of view on the state-of-the-art of a specific area of knowledge and its future prospects.	Unstructured abstract. No more than 150 words.	3-6 keywords.	/

2.3 Manuscript Structure

2.3.1 Front Matter

2.3.1.1 Title

The title of the manuscript should be concise, specific and relevant, with no more than 16 words if possible. When gene or protein names are included, the abbreviated name rather than full name should be used.

2.3.1.2 Authors and Affiliations

Authors' full names should be listed. The initials of middle names can be provided. Institutional addresses and email addresses for all authors should be listed. At least one author should be designated as corresponding author. In addition, corresponding authors are suggested to provide their Open Researcher and Contributor ID upon submission. Please note that any change to authorship is not allowed after manuscript acceptance.

2.3.1.3 Highlights

Highlights are mandatory because they can help increase the discoverability of your article through search engines. They consist of a short collection of bullet points that capture the novel results of your research as well as new methods that were used during the study (if any). They should be submitted in a separate editable file in the online submission system. Please use 'Highlights' in the file name and include 3 to 5 bullet points (maximum 85 characters per bullet point, including spaces).

2.3.1.4 Abstract

The abstract should be a single paragraph with word limitation and specific structure requirements (for more details please refer to Types of Manuscripts). It usually describes the main objective(s) of the study, explains how the study was done, including any model organisms used, without methodological detail, and summarizes the most important results and their significance. The abstract must be an objective representation of the study: it is not allowed to contain results which are not presented and substantiated in the manuscript, or exaggerate the main conclusions. Citations should not be included in the abstract.

2.3.1.5 Graphical Abstract

The graphical abstract is essential as this can catch first view of your publication by readers. We recommend you to submit an eye-catching figure. It should summarize the content of the article in a concise graphical form. It is recommended to use it because this can make online articles get more attention. The graphic abstract should be submitted as a separate document in the online submission system. Please provide an image with a minimum of 531 × 1,328 pixels (h × w) or proportionally more. The image should be readable at a size of 5 × 13 cm using a regular screen resolution of 96 dpi. Preferred file types: tiff, psd, AI, jpeg and eps files.

2.3.1.6 Keywords

Three to six keywords should be provided, which are specific to the article, yet reasonably common within the subject discipline.

2.3.2 Main Text

Manuscripts of different types are structured with different sections of content. Please refer to Types of Manuscripts to make sure which sections should be included in the manuscripts.

2.3.2.1 Introduction

The introduction should contain background that puts the manuscript into context, allow readers to understand why the study is important, include a brief review of key literature, and conclude with a brief statement of the overall aim of the work and a comment about whether that aim was achieved. Relevant controversies or disagreements in the field should be introduced as well.

2.3.2.2 Experimental

Experimental should contain sufficient details to allow others to fully replicate the study. New methods and protocols should be described in detail while well-established methods can be briefly described or appropriately cited. Experimental participants selected, the drugs and chemicals used, the statistical methods taken, and the computer software used should be identified precisely. Statistical terms, abbreviations, and all symbols used should be defined clearly. Protocol documents for clinical trials, observational studies, and other non-laboratory investigations may be uploaded as supplementary materials.

2.3.2.3 Results and Discussion

This section should contain the findings of the study and discuss the implications of the findings in context of existing research and highlight limitations of the study. Future research directions may also be mentioned. Results of statistical analysis should also be included either as text or as tables or figures if appropriate. Authors should emphasize and summarize only the most important observations. Data on all primary and secondary outcomes identified in the section Methods should also be provided. Extra or supplementary materials and technical details can be placed in supplementary documents.

2.3.2.4 Conclusions

It should state clearly the main conclusions and include the explanation of their relevance or importance to the field.

2.3.3 Back Matter

2.3.3.1 Acknowledgments

Anyone who contributed towards the article but does not meet the criteria for authorship, including those who provided professional writing services or materials, should be acknowledged. Authors should obtain permission to acknowledge from all those mentioned in the Acknowledgments section. This section is not added if the author does not have anyone to acknowledge.

2.3.3.2 Authors' Contributions

Each author is expected to have made substantial contributions to the conception or design of the work, or the acquisition, analysis, or interpretation of data, or the creation of new software used in the work, or have drafted the work or substantively revised it.

Please use Surname and Initial of Forename to refer to an author's contribution. For example: made substantial contributions to conception and design of the study and performed data analysis and interpretation: Salas H, Castaneda WV; performed data acquisition, as well as provided administrative, technical, and material support: Castillo N, Young V.

If an article is single-authored, please include "The author contributed solely to the article." in this section.

2.3.3.3 Availability of Data and Materials

In order to maintain the integrity, transparency and reproducibility of research records, authors should include this section in their manuscripts, detailing where the data supporting their findings can be found. Data can be deposited into data repositories or published as supplementary information in the journal. Authors who cannot share their data should state that the data will not be shared and explain it. If a manuscript does not involve such issue, please state "Not applicable." in this section.

2.3.3.4 Financial Support and Sponsorship

All sources of funding for the study reported should be declared. The role of the funding body in the experiment design, collection, analysis and interpretation of data, and writing of the manuscript should be declared. Any relevant grant numbers and the link of funder's website should be provided if any. If the study is not involved with this issue, state "None." in this section.

2.3.3.5 Conflicts of Interest

Authors must declare any potential conflicts of interest that may be perceived as inappropriately influencing the representation or interpretation of reported research results. If there are no conflicts of interest, please state "All authors declared that there are no conflicts of interest." in this section. Some authors may be bound by confidentiality agreements. In such cases, in place of itemized disclosures, we will require authors to state "All authors declare that they are bound by confidentiality agreements that prevent them from disclosing their conflicts of interest in this work.". If authors are unsure whether conflicts of interest exist, please refer to the "Conflicts of Interest" of *Chemical Synthesis* Editorial Policies for a full explanation.

2.3.3.6 Ethical Approval and Consent to Participate

Research involving human subjects, human material or human data must be performed in accordance with the Declaration of Helsinki and approved by an appropriate ethics committee. An informed consent to participate in the study should also be obtained from participants, or their parents or legal guardians for children under 16. A statement detailing the name of the ethics committee (including the reference number where appropriate) and the informed consent obtained must appear in the manuscripts reporting such research.

Studies involving animals and cell lines must include a statement on ethical approval. More information is available at Editorial Policies.

If the manuscript does not involve such issue, please state "Not applicable." in this section.

2.3.3.7 Consent for Publication

Manuscripts containing individual details, images or videos, must obtain consent for publication from that person, or in the case of children, their parents or legal guardians. If the person has died, consent for publication must be obtained from the next of kin of the participant. Manuscripts must include a statement that a written informed consent for publication was obtained. Authors do not have to submit such content accompanying the manuscript. However, these documents must be available if requested. If the manuscript does not involve this issue, state "Not applicable." in this section.

2.3.3.8 Copyright

Authors retain copyright of their works through a Creative Commons Attribution 4.0 International License that clearly states how readers can copy, distribute, and use their attributed research, free of charge. A declaration "© The Author(s)

2022." will be added to each article. Authors are required to sign License to Publish before formal publication.

2.3.3.9 References

References should be numbered in order of appearance at the end of manuscripts. In the text, reference numbers should be placed in square brackets and the corresponding references are cited thereafter. If the number of authors is less than or equal to six, we require to list all authors' names. If the number of authors is more than six, only the first three authors' names are required to be listed in the references, other authors' names should be omitted and replaced with "et al.". Abbreviations of the journals should be provided on the basis of Index Medicus. Information from manuscripts accepted but not published should be cited in the text as "Unpublished material" with written permission from the source.

References should be described as follows, depending on the types of works:

Types	Examples
Journal articles by individual authors	Weaver DL, Ashikaga T, Krag DN, et al. Effect of occult metastases on survival in node-negative breast cancer. *N Engl J Med* 2011;364:412-21. [PMID: 21247310 DOI: 10.1056/NEJMoa1008108]
Organization as author	Diabetes Prevention Program Research Group. Hypertension, insulin, and proinsulin in participants with impaired glucose tolerance. *Hypertension* 2002;40:679-86. [PMID: 12411462]
Both personal authors and organization as author	Vallancien G, Emberton M, Harving N, van Moorselaar RJ; Alf-One Study Group. Sexual dysfunction in 1,274 European men suffering from lower urinary tract symptoms. *J Urol* 2003;169:2257-61. [PMID: 12771764 DOI: 10.1097/01.ju.0000067940.76090.73]
Journal articles not in English	Zhang X, Xiong H, Ji TY, Zhang YH, Wang Y. Case report of anti-N-methyl-D-aspartate receptor encephalitis in child. *J Appl Clin Pediatr* 2012;27:1903-7. (in Chinese)
Journal articles ahead of print	Odibo AO. Falling stillbirth and neonatal mortality rates in twin gestation: not a reason for complacency. BJOG 2018; Epub ahead of print [PMID: 30461178 DOI: 10.1111/1471-0528.15541]
Books	Sherlock S, Dooley J. Diseases of the liver and billiary system. 9th ed. Oxford: Blackwell Sci Pub; 1993. pp. 258-96.
Book chapters	Meltzer PS, Kallioniemi A, Trent JM. Chromosome alterations in human solid tumors. In: Vogelstein B, Kinzler KW, editors. The genetic basis of human cancer. New York: McGraw-Hill; 2002. pp. 93-113.
Online resource	FDA News Release. FDA approval brings first gene therapy to the United States. Available from: https://www.fda.gov/NewsEvents/Newsroom/PressAnnouncements/ucm574058.htm. [Last accessed on 30 Oct 2017]
Conference proceedings	Harnden P, Joffe JK, Jones WG, editors. Germ cell tumours V. Proceedings of the 5th Germ Cell Tumour Conference; 2001 Sep 13-15; Leeds, UK. New York: Springer; 2002.
Conference paper	Christensen S, Oppacher F. An analysis of Koza's computational effort statistic for genetic programming. In: Foster JA, Lutton E, Miller J, Ryan C, Tettamanzi AG, editors. Genetic programming. EuroGP 2002: Proceedings of the 5th European Conference on Genetic Programming; 2002 Apr 3-5; Kinsdale, Ireland. Berlin: Springer; 2002. pp. 182-91.
Unpublished material	Tian D, Araki H, Stahl E, Bergelson J, Kreitman M. Signature of balancing selection in Arabidopsis. *Proc Natl Acad Sci U S A*. Forthcoming 2002.

For other types of references, please refer to U.S. National Library of Medicine.
The journal also recommends that authors prepare references with a bibliography software package, such as EndNote to avoid typing mistakes and duplicated references.

2.3.3.10 Supplementary Materials

Additional data and information can be uploaded as Supplementary Materials to accompany the manuscripts. The supplementary materials will also be available to the referees as part of the peer-review process. Any file format is acceptable, such as data sheet (word, excel, csv, cdx, fasta, pdf or zip files), presentation (PowerPoint, pdf or zip files), image (cdx, eps, jpeg, pdf, png or tiff), table (word, excel, csv or pdf), audio (mp3, wav or wma) or video (avi, divx, flv, mov, mp4, mpeg, mpg or wmv). All information should be clearly presented. Supplementary materials should be cited in the main text in numeric order (e.g., Supplementary Figure 1, Supplementary Figure 2, Supplementary Table 1, Supplementary Table 2, etc.). The style of supplementary figures or tables complies with the same requirements on figures or tables in main text. Videos and audios should be prepared in English, and limited to a size of 500 MB or a duration of 3 minutes.

2.4 Manuscript Format

2.4.1 File Format

Manuscript files can be in DOC and DOCX formats and should not be locked or protected.

2.4.2 Length

There are no restrictions on paper length, number of figures, or amount of supporting documents. Authors are encouraged to present and discuss their findings concisely.

2.4.3 Language

Manuscripts must be written in English.

2.4.4 Multimedia Files

The journal supports manuscripts with multimedia files. The requirements are listed as follows:
Videos or audio files are only acceptable in English. The presentation and introduction should be easy to understand. The frames should be clear, and the speech speed should be moderate.
A brief overview of the video or audio files should be given in the manuscript text.
The video or audio files should be limited to a size of up to 500 MB.
Please use professional software to produce high-quality video files, to facilitate acceptance and publication along with the submitted article. Upload the videos in mp4, wmv, or rm format (preferably mp4) and audio files in mp3 or wav format.

2.4.5 Figures

Figures should be cited in numeric order (e.g., Figure 1, Figure 2) and placed after the paragraph where it is first cited;
Figures can be submitted in format of tiff, psd, AI or jpeg, with resolution of 300-600 dpi;
Figure caption is placed under the Figure;
Diagrams with describing words (including, flow chart, coordinate diagram, bar chart, line chart, and scatter diagram, *etc.*) should be editable in word, excel or powerpoint format. Non-English information should be avoided;
Labels, numbers, letters, arrows, and symbols in figure should be clear, of uniform size, and contrast with the background;
Symbols, arrows, numbers, or letters used to identify parts of the illustrations must be identified and explained in the legend;
Internal scale (magnification) should be explained and the staining method in photomicrographs should be identified;
All non-standard abbreviations should be explained in the legend;
Permission for use of copyrighted materials from other sources, including re-published, adapted, modified, or partial figures and images from the internet, must be obtained. It is authors' responsibility to acquire the licenses, to follow any citation instruction requested by third-party rights holders, and cover any supplementary charges.

2.4.6 Tables

Tables should be cited in numeric order and placed after the paragraph where it is first cited;
The table caption should be placed above the table and labeled sequentially (e.g., Table 1, Table 2);
Tables should be provided in editable form like DOC or DOCX format (picture is not allowed);
Abbreviations and symbols used in table should be explained in footnote;
Explanatory matter should also be placed in footnotes;
Permission for use of copyrighted materials from other sources, including re-published, adapted, modified, or partial tables from the internet, must be obtained. It is authors' responsibility to acquire the licenses, to follow any citation instruction requested by third-party rights holders, and cover any supplementary charges.

2.4.7 Abbreviations

Abbreviations should be defined upon first appearance in the abstract, main text, and in figure or table captions and used consistently thereafter. Non-standard abbreviations are not allowed unless they appear at least three times in the text. Commonly-used abbreviations, such as DNA, RNA, ATP, *etc*., can be used directly without definition. Abbreviations in titles and keywords should be avoided, except for the ones which are widely used.

2.4.8 Italics

General italic words like *vs*., *et al., etc*., *in vivo*, *in vitro*; *t* test, *F* test, *U* test; related coefficient as *r*, sample number as *n*, and probability as *P*; names of genses; names of bacteria and biology species in Latin.

2.4.9 Units

SI Units should be used. Imperial, US customary and other units should be converted to SI units whenever possible. There is a space between the number and the unit (i.e., 23 mL). Hour, minute, second should be written as h, min, s.

2.4.10 Numbers

Numbers appearing at the beginning of sentences should be expressed in English. When there are two or more numbers in a paragraph, they should be expressed as Arabic numerals; when there is only one number in a paragraph, number < 10 should be expressed in English and number > 10 should be expressed as Arabic numerals. 12345678 should be written as 12,345,678.

2.4.11 Equations

Equations should be editable and not appear in a picture format. Authors are advised to use either the Microsoft Equation Editor or the MathType for display and inline equations.

2.5 Submission Link

Submit an article via https://oaemesas.com/login?JournalId=cs.

www.oaepublish.com

Chemical Synthesis
(*CS*)
Los Angeles Office
245 E Main Street ste122, Alhambra,
CA 91801, USA
E-mail: editorialoffice@chesynjournal.com
Website: www.chesynjournal.com